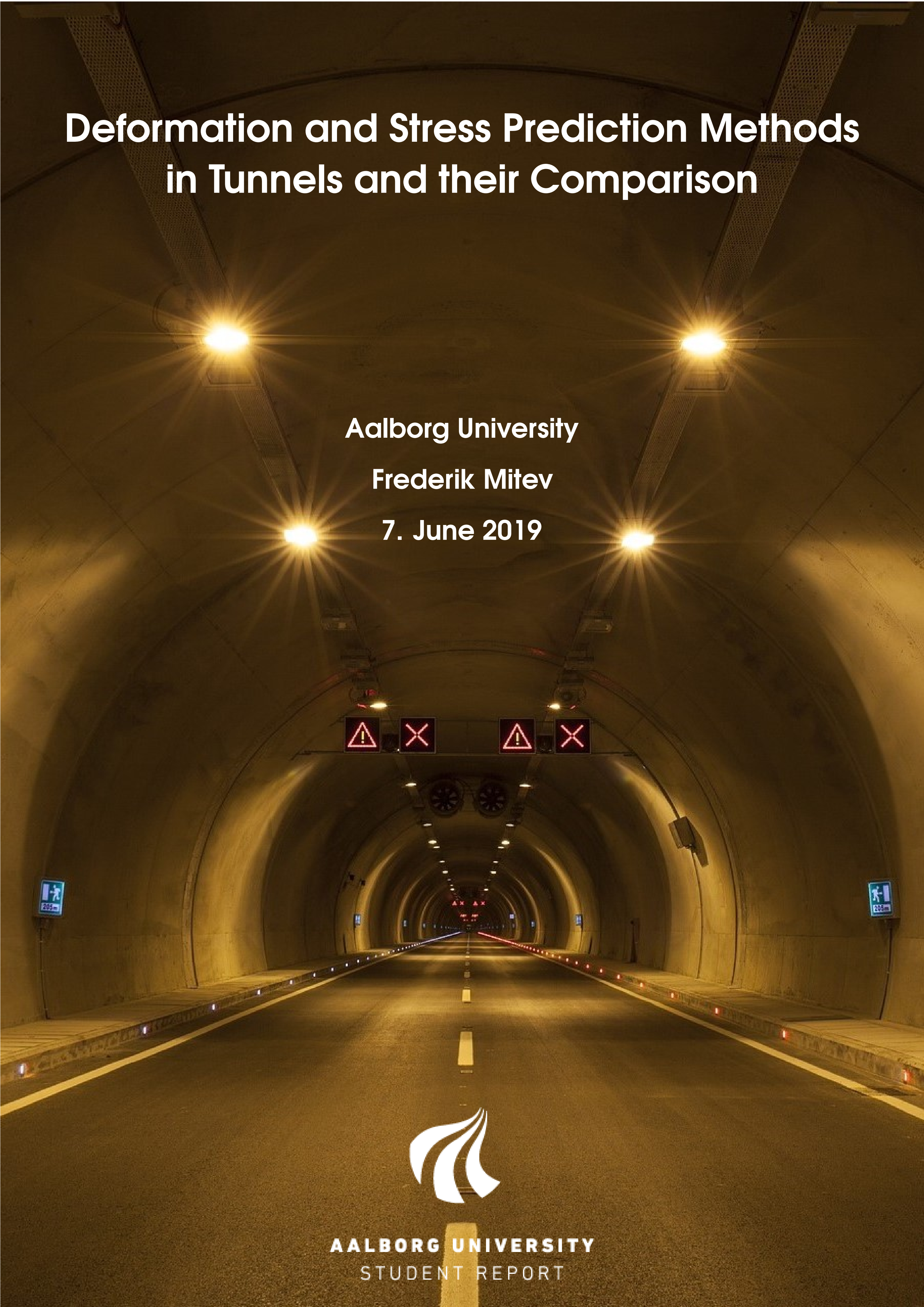

Deformation and Stress Prediction Methods in Tunnels and their Comparison

Aalborg University

Frederik Mitev

7. June 2019

AALBORG UNIVERSITY

STUDENT REPORT

AALBORG UNIVERSITY
STUDENT REPORT

School of Engineering and Science
Structural and Civil Engineering
Thomas Manns Vej 23
9220 Aalborg Øst
www.civil.aau.dk

Title:

Master Thesis

Semester:

MSc. 4th semester

Semester theme:

Deformation and Stress Prediction Methods in Tunnels and their Comparison

Project period:

4. February 2019 - 7. June 2019

Author:

Frederik Mitev

Supervisor:

Lars Bo Ibsen

Pages: 126
Submission date: 7. June 2019

Readers guide

In the present report, several terms and expressions, which are considered commonly accepted in the field of structural and tunnel engineering, will be used. Hence, it is expected that the reader has a basic understanding in subjects and topics related to structural and tunnel engineering, in order to comprehend all parts of the presented report thoroughly.

Where sources are used, specific references will be given. These will be indicated in active cases by surname(s), year of publication, whereas in passive cases these are indicated as [surname(s), year of publication].

Figures, tables and expressions are consecutively numbered with respect to the chapter in which they are presented, which means that e.g. third figure of chapter six is named figure 6.3. The specification of the name and number will appear just below figures and tables, whereas the numbering of expressions will appear close to the right-margin of the page. Figures without references are composed by the authors of the report.

If numbers higher than a thousand appear in the text, these are separated by a space, which means that the output for six million and two-hundred thousand will be displayed as 6 200 000. Regarding mathematical notation, { } refers to vectors and [ ] to matrices.

The content of the report is split into two parts, consisting of a main part followed by appendices. In the first part, the most important concerns, approaches and findings are presented. The appendices presents details assessed to be of less importance, which for instance could be trivial or repetitive content, material that is assessed to be of minor significance for the aim of the project or figures which contents are summarised in the form of a table in the main part. The appendices are named starting from the letter A and so on.

A few abbreviations will be used throughout the report, which are important for the understanding of the content. These are shown in table 1, presented below:

Abbreviation	Definition
ADECO-RS	Analysis of Controlled Deformation in Rocks and Soils
CCM	Convergence Confinement Method
EPB	Earth Pressure Balance
FRC	Fibre Reinforced Concrete
GCC	Ground Characteristic Curve
LDP	Longitudinal Displacement Profile
NATM	New Austrian Tunnelling Method
RMR	Rock Mass Rating
RQD	Rock Quality Designation
RSR	Rock Structure Rating
SCC	Support Characteristic Curve
TBM	Tunnel Boring Machine

Table 1: Abbreviations used in the report

Abstract

In this report a brief introduction to tunnel engineering is presented with different tunneling methods, support techniques and concepts all being presented. The main focus of the report however, mainly lies on the different methods of calculations of the deformations and stresses in tunnels. Analytical solutions are presented and evaluated and numerical models are established, for all geotechnical sections of the tunnel Višňové. Pressure theories, deformation theories based on soil loosening, or so called loosening zones along with convergence confinement method are among the analysed analytical methods. A 3D and 2D FEM model was created and calculated in the PLAXIS. All of these results have then been compared to the actual measurements on site, gathered during the excavation of the tunnel. Subsequent back-analysis of the numerical models was performed.

The results show that the analytical methods can be used as guidance and verification of the numerical model, but care needs to be taken when applying them to different geological conditions. The most accurate analytical method was found to be the Convergence Confinement Method, modelling the displacements fairly well compared to the FE model. The Hoek-Brown material model was found to be under predicting deformations and therefore to be a dangerous model. The results from analytical and numerical solutions on the other hand, deviate to some extent from the measured displacements on site.

Contents

II Appendix

List of Figures

List of Tables

Main Report

1. Introduction

The aim of this section is to familiarise the reader with the brief summary of the history of tunneling and to introduce the basic concepts of tunnel wall stabilisation. Furthermore a short description of tunnel types and tunneling methods used throughout time is presented. The structure on which the subsequent analysis and comparison will be carried out on, Tunnel Višňové, is presented.

Tunnelling is an essential part of civil engineering. To design modern tunnels vast knowledge, not just the on-site geological conditions are needed, but also all the different methods of design, different support systems, rock mass and soil behaviours and numerous other parts of the tunnel design which have become a standard. The aim of this report is to guide the reader through most of the basic and essential parts of tunneling in rock, from types of tunnels all the way to 3D modelling of a given tunnel. Different support systems, their design according to rock mass classification systems and analytical relationships will be introduced. Comparisons between the analytical and numerical solutions of a tunnel profile in sample geological conditions will be presented as well. These would be then compared to real measurements provided in the tunnel by geotechnical monitoring. Using back analysis, the soil parameters of each section will be optimised to reflect the real-time measurements, whilst this is performed with two different soil models. However, as with any theme it is necessary to start from the beginning in order to understand the development a bit better.

1.1 History

Tunnelling, just like many other fields of civil engineering, have a long history throughout which they have developed into the structures we know them as today. From the begging of time humanity most probably sought to enlarge caves through digging. A first well known tunnel however, was constructed in Babylon between 2180 and 2160 BC under the Euphrates river which was 900 m long. Passage ways for water and for people have since then been tunnelled using simple tools all over the world, with good examples from the Roman Empire or by the Ancient Greeks.

Figure 1.1: A 600 m roman tunnel “La Bot” which was an aqueduct to supply a thermal bath [www.asolo.it]

An advancement came only after Alfred Nobel discovered dynamite in 1867 and allowed for the first tunnels to be dug using explosives. Most of the notable tunnels have been constructed through cut and cover techniques or explosives. A large number of the tunnels which are dug these days are using cyclic methods, whether it is the so called New Austrian Tunnelling Method (NATM) which started to be popular and gained international recognition around the 1960s [Karakus and Fowell, 2004] or method using Analysis of Controlled Deformation in Rocks and Soils otherwise knows as ADECO-RS, a method similar to NATM developed in Italy . Great examples are the 24.5 km Lærdal Tunnel or the first Gotthard Tunnel.

In 1952 however, a Tunnel Boring Machine (from here only TBM) machine was developed and used for the first time in South Dakotas Oahe Dam project. This development allowed the tunnel engineers to tunnel through tougher terrain and more unfavourable hydro-geological conditions than they could with the use of explosives. Thanks to this tunnels such as the Channel Tunnel between England and France or more recently the Gotthard Base Tunnel was accomplished. The TBM method or the continuous method, is gaining popularity [Krishnan, 2000], however in modern times, both techniques are being used and the tunnelling method is chosen according to the predicted conditions and the use of the tunnel.

1.2 Types of tunnels

There are many different types of tunnels in the world that were or are being built today. They are separated according to many categories, however for the sake of this report and its delimitation, they will be divided according to: use, tunnelling method, depth and geological conditions.

1.2.1 Use

The use of the tunnel is one of the basic classifications in tunneling. The two major categories would be transport and mining. Obviously transport tunneling developed from and thanks to the mining industry, but the differences between them grew rather large throughout history. The dimensions of a mining tunnel are fairly small, as only small trains for excavated material and miners pass through the tunnels. Since the main use of the tunnel is to find earthly materials, the walls of the tunnel are minimally supported, what is allowed thanks to the small cross-section.

Traffic tunnels on the other hand have a large variations of profiles and cross-section sizes, and hence they are divided further. There are numerous transport tunnels that are distinguished. Road, railway, pedestrian and hydro-power (water transport) tunnels are most common today. The designated use of a tunnel has effect on the profile, support systems, additional structures (emergency niches, tunnel connections, etc.) and numerous other parts. Railway tunnels for example require a different profile as train traffic needs less extra space unlike cars in road tunnels. The structure of the transport tunnels however, remains mostly the same. Most developed countries create tunnels with 2 linings, primary and secondary, an example of which can be seen on a road tunnel Korbel'ka in figure 1.2 below.

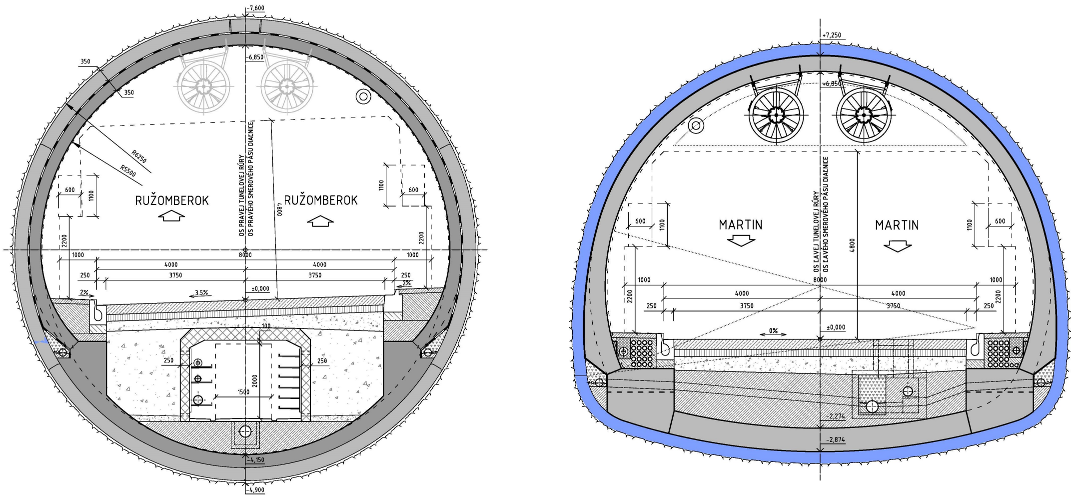

Figure 1.2: A sample tunnel cross-section for a TBM (left) and for a NATM (right) tunnel

1.2.2 Tunnelling Method

NATM and TBM tunneling is the most common in modern times. The two methods affect the profile shape and also the primary lining of the tunnel. The lining within a continuous tunneling (TBM) is precast, while cyclic tunneling uses shotcrete with reinforcement meshes or fibres. The profile shape also changes, what in turn changes also the stresses not just around the tunnel in the rock mass but also in the linings. Both of these methods have advantages and disadvantages that can constitute a thesis on their own, therefore only a brief summary and description of the two methods are described in this paper.

1.2.3 Depth and Geological Conditions

The depth and the geology of a tunnel determine the failure mechanisms and the critical delimitation. For example a shallow tunnel with a small overburden has a different failure mechanisms than a deep tunnel in hard rock with a high overburden. It has to deal with the possibility of a chimney-like failure [Kirsch, 2009], and very critical are also deformations on the surface, as most of the time these tunnels are driven under urban zones which are to be left untouched. Moderate to deep tunnels on the other hand, deal with much higher pressures and a stress-field change driven failures are most common. These differences make a very large difference in the design process and a very clear separation is made between these two categories.

1.3 Analysed Tunnel Višňové

Comparison of force and deformation predictions using analytical and numerical methods has to be performed on a set structure. Tunnel Višňové has been chosen for this report as the basis of comparison. It is a 2 lane road tunnel on the crucial highway D1 in Slovakia, connecting Bratislava and Košice, more precisely Lietavská Lúčka and Dubová Skala. It is located in the Malá Fatra (Small Fatra) mountains, in the range with altitudes of 800 - 1300 meters above sea level (MASL). This means that it is a moderate to deep tunnel.

Figure 1.3: Map of Slovakia with the location of the Višňové tunnel indicated with the blue dot

Each of the two tunnels shafts is 7500 m long and it is currently being excavated using NATM. Construction started with pilot tunnels being driven from both sides of the tunnel in 1998. One was using NATM, however the other pilot tunnel from the eastern portal was excavated using a TBM. To this day this is the only use of a TBM machine in Slovakia. Excavation of the full profile due to political reasons started only in 2014.

Figure 1.4: Inside of Višňové in February 2017. Credit:Renáta Jaloviarová, Pravda

The considered part of the massive in which the tunnel is excavated, consists mainly of Variscan granitoids. As to perform a reliable analysis, all of the numerous quasi-homogeneous sections the tunnel goes through have to be analysed. All of the quasi-homogeneous sections are be described in chapter 3. For each of the sections, analytical and numerical models will be performed and analysed. Analytical methods in this report correspond to the most common techniques of estimating tunnel deformations and stresses throughout history some of which are used in today's tunneling industry. Numerical models represent the most modern tools for tunnel engineers, but even these are subject to simplifications. This report is no different and the delimitations and simplifications of the model are presented in chapter 6.

2. Tunnel engineering

The aim of this chapter is to familiarise the reader with the main concepts in modern tunneling and the general structure of a tunnel. A more in depth explanation of tunneling methods, tunnel overburden and support systems are given.

2.1 Tunnel Structure

Although there are a lot of different types of road tunnels in the world, the structure remains usually the same. The tunnel excavation is done at the face or the heading. The upper part of the tunnel then becomes the crown and the bottom the invert, while the the two are connected through tunnel sides or walls. Primary lining is installed just behind the unsupported length, where this is just a temporary support. On top of the primary, the secondary lining is installed, which is the final lining which provides support for the whole lifespan of the tunnel. Between the two linings hydro-insulation is usually placed to inhibit inflow of water into the tunnel.

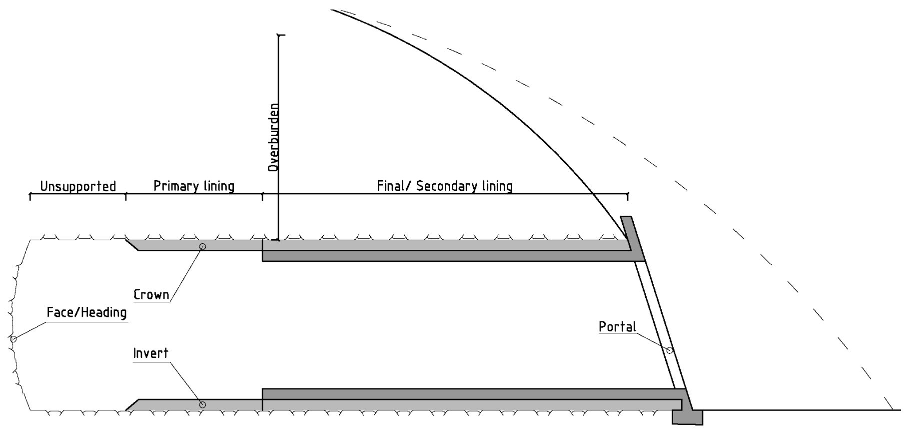

Figure 2.1: Typical structure of a tunnel with two linings

The overburden is a term heavily discussed in the later chapters of this report. It is the depth at which the tunnel is buried in or the height of rock mass that acts on the tunnel. The overburden depends on the shallowness of the tunnel. This phenomena is explained section 2.3.

2.2 Tunnelling methods and profiles

Each of the aforementioned methods have their specifications and differences. These lie within supports, profile shape, tunneling rate and flexibility and many other parameters.

2.2.1 NATM

The New Austrian Tunnelling Method is a type of cyclic tunneling. This means that the tunneling is done in batches, with the procedure shown in figure 2.2 repeating over and over again once (or if circumstances allow twice) per day. It uses either blasting or digging machinery to loosen the rock massif. After the heading has been blasted/excavated and the loose rock is transported out of the tunnel, installation of the supports can begin. Steel meshes are installed and shotcrete (dry or wet, both are used) is applied. This is what is called the primary lining of a tunnel. In recent times however, fibre reinforced concrete (FRC) is becoming popular, and the need for steel mesh reinforcement is somewhat declining, as FRC concrete can achieve comparable strength capacity to the mesh-reinforced concrete [Vojkan and Jakob, 2008].

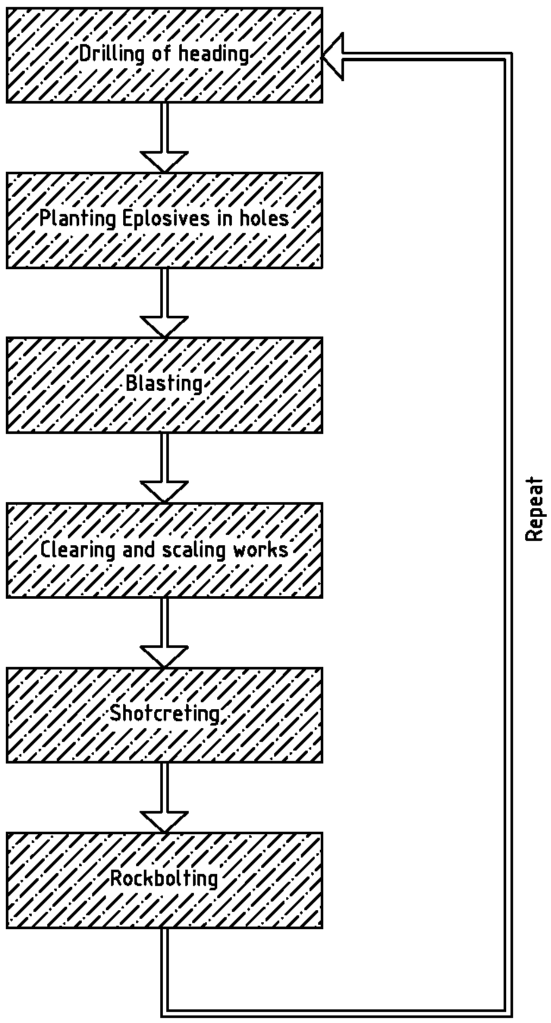

Figure 2.2: Generalised procedure of NATM tunneling

Once the shotcrete is set, Rock bolts can be installed. These can have different lengths and types, which are determined according to the support class of the tunnel section. Rock bolts are discussed in a bit more detail in later sections.

 

Figure 2.3: Drilling of the tunnel face for explosives in NATM (left)[*Tunneling Online* n.d.] and application of the primary lining using shotcrete on a steel reinforcement mesh [*Dr. Sauer and Partners* n.d.]

NATM distinguishes itself from ADECO-RS, which is another cyclic tunneling method, with the division of the heading into smaller sections, depending on the complexity of the geology, and therefore allow more time for the tunnel walls to be unsupported and the deformations in them to converge, so the rock mass can "lose some steam" (lower the pressure in the rock mass). ADECO-RS on the other hand excavates the whole heading at the same time and provides stiff supports right after excavation [Černá Vydrová, 2015], so minimum deformations are allowed .

2.2.2 TBM

Tunnelling using a TBM is just like ADECO-RS excavating the full heading at once, nonetheless it is a continuous method, meaning the excavation is ongoing during the whole time of operation (24 hours a day) while simultaneously the excavated material is transported out of the tunnel and the primary lining is installed on the walls. This is all thanks to the TBM which is capable of completing all these tasks at a much higher rate than NATM or ADECO-RS can. The structure of a typical TBM consists of a cutter-head, which excavates the heading. Behind it is the back end, which is made up of conveyor belts for transporting of rubble, equipment to install prefabricated concrete segments as primary lining, ventilation and many more [Oslo-Navet, 2015]. There are however many different TBMs in the world, each one with a different additional equipment to help with the specific geology of the tunnel. Most common equipment is a shield, which protects the inside of the TBM from falling loosened rock segments and from underground water inflow. There are not just single shields, but mixed shields, allowing the TBM to tackle a changing geology. Another additional equipment commonly installed to help cope with high water pressure at the heading is either a Earth Pressure Balance (from here only EPB) or a Slurry-Support [Tunnelling, 2000]. Both, work on the principle of balancing the earth and the groundwater pressure at the heading behind the cutter-head, although in different manners. A single shield TBM can be seen on figure 2.4 below:

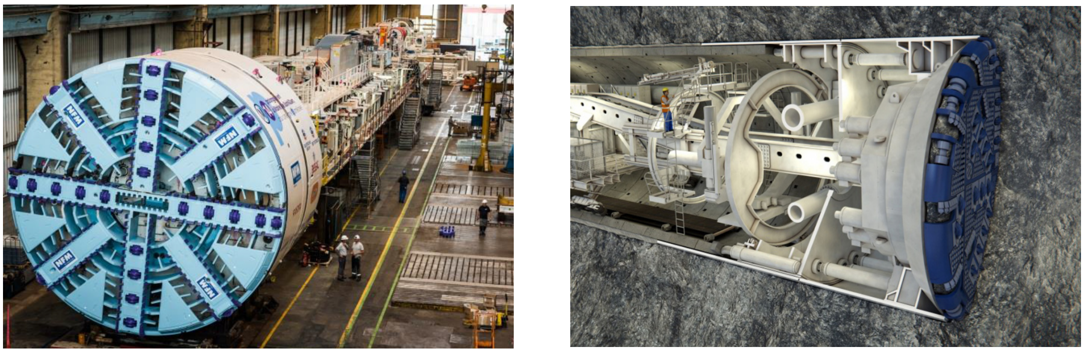

Figure 2.4: TBM with a shield

Due to the above listed reasons, one can see why TBM tunneling is a large part of tunneling in modern days and is expanding from the west into developing countries as well.

2.3 Depth of a tunnel

The depth at which the tunnel is built is also a way of categorising them. As explained previously, shallow tunnels have their differences in comparison to deep or moderately deep tunnels, that is from rock mechanics point of view, all the way to the supports and tunneling methods, and precautions that need to be taken during excavations. Nonetheless, the biggest difference the depth makes is the material in which the tunnels are built. Shallow tunnels usually deal with soils, such as clay and sand, while moderate to deep tunnels are driven through rock. These materials obviously have different parameters and mechanics which prompts adjustments.

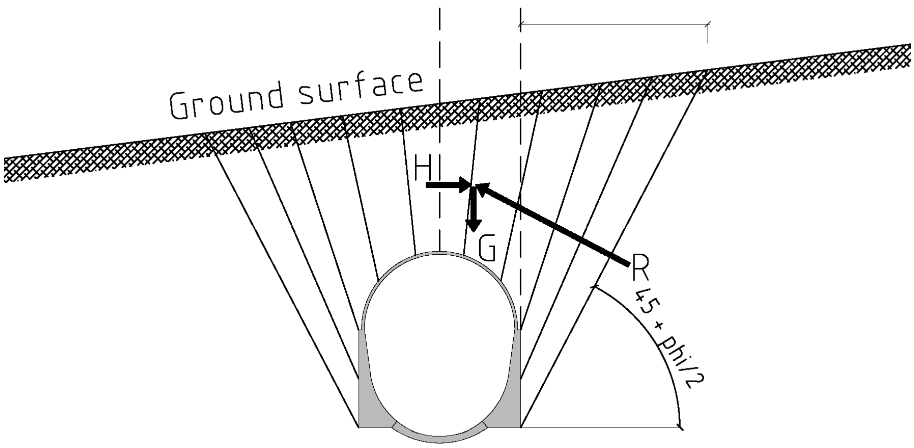

Figure 2.5: Overburden in shallow tunnels according to Suquet

Shallow tunnels assume an expected overburden, where the entire soil mass is assumed to act on the tunnel, with only some reductions or changes to the zone of soil, depending on the theory used. This causes a collapse mechanism of a chimney effect through slip lines, a so called "method of slices", which is very similar to the ground structures' silo theory [Anagnostou, 2007]. This chimney failure, swelling or dipping of soil at ground level, which can affect structures above the tunnel are some of the main concerns in shallow tunneling. Either way the failure/plastic zone is linked to the ground. Due to these conditions there are additional support works that need to be done during tunneling, which in deep tunnels would be used only in very unfavourable rock. These consist of micro-pile umbrellas and forepoling in the crown, alongside stabilisation and reinforcement of the face [Tun and Singal, 2016], in order to prevent the soil from back-filling the tunnel and face collapse.

Moderate and deep tunnels on the other hand have a different assumption of the overburden acting on the tunnel. The assumption that the entire rock mass above the tunnel acts on the tunnel is not valid anymore, as the rock mass is self load bearing, therefore some of the mass can be neglected. The exact shape depends on the analytical theory used, but generally it is assumed to look as is shown in figure 2.7 [Szechy, 1973]. The depth also plays a role in the failure mechanisms, as in deeper tunnels the failure/plastic zone moves from the tunnel sides into the invert. The exact shape of the failure zone and its location in respect to the tunnel placement depend on the geology and tunnel geometry. These failure mechanisms and assumed overburdens will be analysed in the later chapters of this report for a given structure.

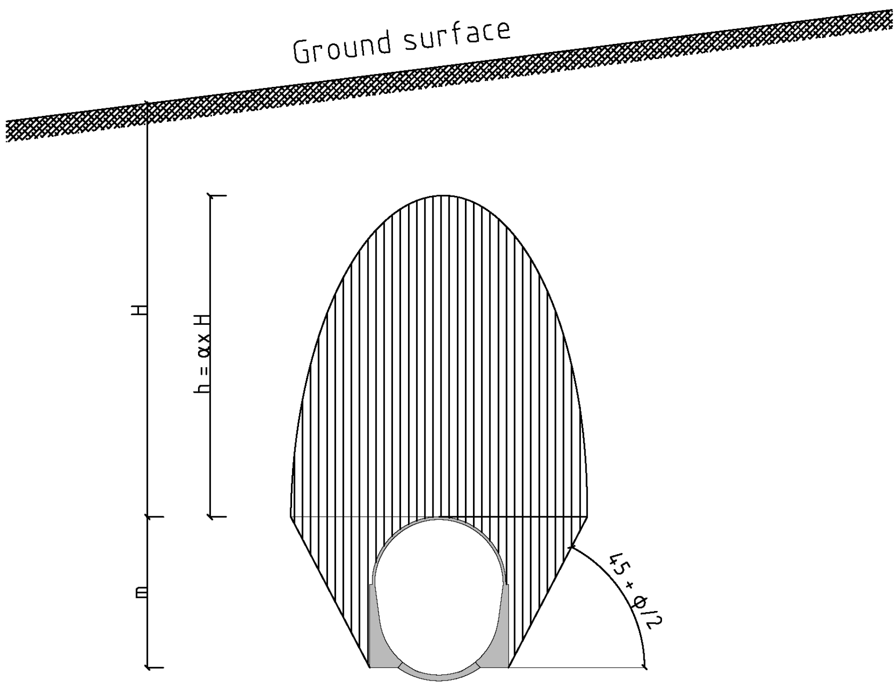

Figure 2.6: Overburden in deep tunnels according to Bierbäumer

2.4 Support systems

Throughout history a lot of different tunnel wall stabilisation techniques were used. Some were more effective than others. Early on wood was used to support the tunnel walls through frames that were closely packed together. As the steel industry developed, steel beams and sheets were being used and are still used today, though in a slightly different manner. In modern tunneling concrete is the main material of choice when it comes to reinforcement, thanks to its inflammable properties.

The main idea of supporting the tunnel is that the structural elements carry the least and the rock mass carries as much load as possible. This is achieved through allowance of the rock mass to deform. As it deforms, it releases the load on the structure that would be installed, and hence makes the rock mass more stable and allows the moments in the lining to redistribute, making the main load of the lining axial load [AASHTO, 2010]. An attempt at estimation of the time at which the supports should be installed and what types should be used was made by numerous scientists. A good visualisation of the tunnel deformations and support systems is presented by the Fenner-Pacher curves, first derived in 1964. Section 5.5 deals with Fenner-Pacher curves in more detail.

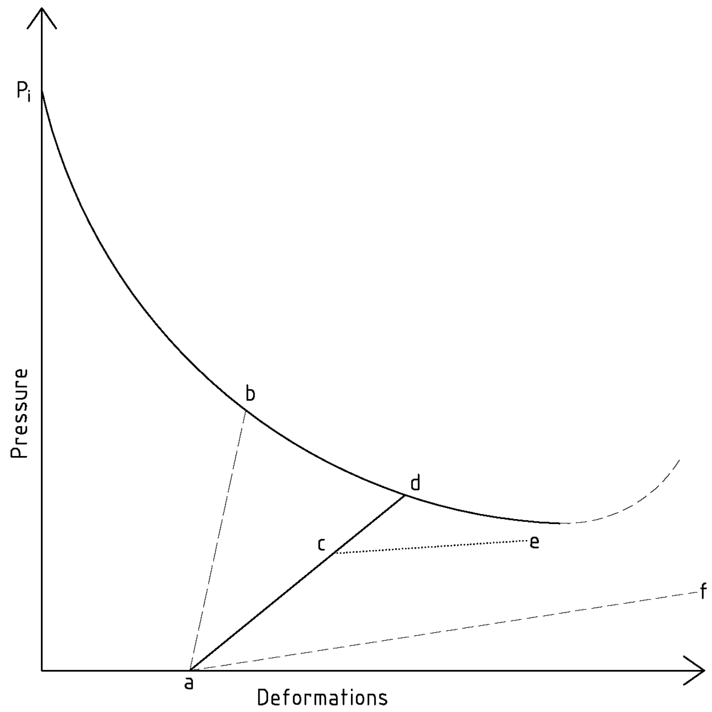

Figure 2.7: Example of a Fenner Pacher curve with different support curves. Curved line represents the tunnel wall deformations, line a-b represents overly conservative support bearing a lot of load, line a-c-d represent the most optimal support, lines a-c-e and a-f represent supports at which failure happens

To allow for this, modern support systems are usually divided into two parts or phases, primary and secondary linings. Primary lining is installed shortly after excavation to ensure safe working conditions, to prevent rock fall and rock bursts, water ingress and complete closing of the tunnel. Secondary reinforcement is installed when the deformations of the primary reinforcement have stalled, and in ensures the load bearing capacity of the tunnel throughout its lifespan, fire protection and smooth air-flow inside the tunnel [J. Kim et al., 2015].

As secondary lining is just a concrete segment with steel reinforcement, it largely remains unchanged in respect to the geology or profile of the tunnel. From a structural point of view, only the thickness and the reinforcement ratio change. Primary lining or temporary reinforcement on the other hand, can consist of numerous systems used in conjunction which are described below. Amongst the most common used in Slovak tunnels are shotcrete and Rock Bolts.

2.4.1 Shotcrete and TBM segments

The fundamental part of a primary lining in NATM tunneling is shotcrete or blasted concrete. First a reinforcement mesh is installed on the newly excavated tunnel walls, onto which a layer of concrete is sprayed. In modern tunnels sometimes FRC is used rather than a steel mesh and concrete for time and economical savings. The concrete can be either dry mix or wet mix, both having their advantages and disadvantages. However both are applied onto a cleaned and slightly wetted surface, with no loose rocks, to produce the best results [Patel R. and Patel, 2013]. In the end however the result is the same, with the concrete lining acting as a ring supporting the surrounding rock mass. The thickness of the layer depends on the geological and hydrogeological conditions in that given section of the tunnel. In some circumstances there is no need for shotcrete like in strong non-jointed rock mass without faults. On the other side of the spectrum lies a heavily weather rock mass, swelling or squeezing rock, which require up to 35cm of shotcrete on given sections (highest reinforcement category used in Slovakia).

The same purpose of a primary lining as shotcrete is achieved by TBM segments, which are used in TBM driven tunnels. After installation of the segments are grouted, closing off the space between the rock mass and the concrete elements. Once the primary lining is applied, Rock Bolts can be drilled into the rock mass.

2.4.2 Rock bolts

The main role of a Rock Bolt is to stabilise the newly excavated tunnel. More precisely they are to prevent any movement of rock wedges or blocks, and the rock mass near to, or at the tunnel walls. In other words, it is a reinforcement system that transfers the load from the potentially unstable region near an excavation, to a stable region beyond the depth of instability [G. Thompson and Villaescusa, 2014]. Furthermore the frictional force between the layers is increased. The bolt should be long enough to reach undamaged rock, in order to transfer the load from the rock wedges into the healthy rock. The bolts are designed to work in tension, but also to resist shear forces. The bolt length is anywhere between 2 to 6 meters, depending on the geology of the tunnel section, as so to guarantee the connection to healthy rock. A bolt can be designed based on one or more design basis studied by Haberknicht in 1984. Figure 2.8 below shows a Rock Bolt designed based on suspension [Chen, 1994]. Nailing effect, beam building and arch building effects are another 3 bases.

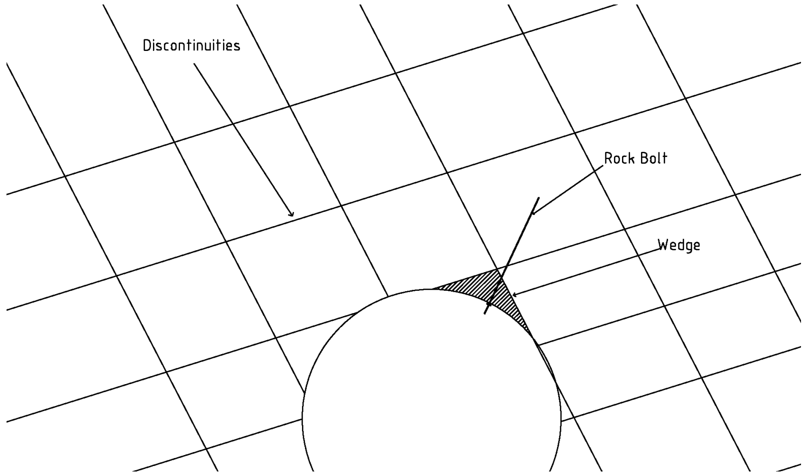

Figure 2.8: Example of a Rock Bolt holding a loose rock wedge in place

Once again there are different types of bolts, however some of the structure remains the same. A rock bolt consists of a straight steel rod, which has an anchor, chemical or mechanical, at one end, and a face plate with a nut on the other. Once the hole is drilled the entire setup is inserted and tightened to the required force. Depending on the use the bolts can be grouted or not, for permanent and temporary use respectively.

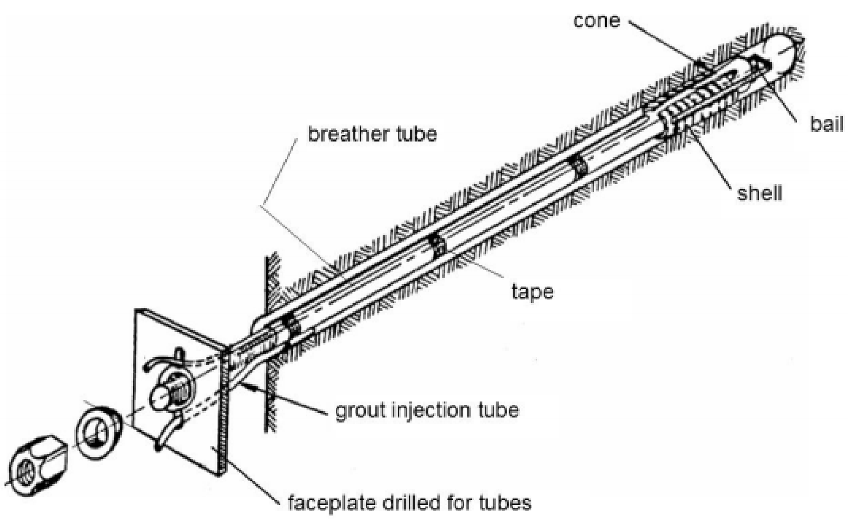

Figure 2.9: Structure of a Rock bolt with expansion anchor [E. Hoek, 2006]

Self drilling Rock Bolts have also been developed, and are commonly being used in sand, clay or soft to medium fractured rock. They consist of a hollow steel rod, that is then grouted on the inside and outside. As the process is faster than conventional bolts, they have grown into a widely used Rock Bolt category. In Slovakia self drilling IBO bolts, "Swellex" anchors and mechanical anchor SN (grouted and non-grouted) are mostly used.

2.4.3 Lattice girders

To move away from the bulky and inflexible H beams, lattice girders were developed and widely used since the 70s [Komselis C., 2005]. A lattice girder is an important primary tunnel support for NATM, and it has become increasingly popular due to its simple installation process and structural benefits [H. J. Kim et al., 2018]. Lattice girders have the following functions:

- Immediate support in the area of the working face over the length of the leading excavated section
- Template when applying the shotcrete and excavating the next section.
- Part of the reinforcement of the shotcrete lining.
- Supports for rods and plates, which provide advance support for the next excavated section.

Figure 2.10: Installation of lattice girders at tunnel crown with shotcrete cover from [Baumann and Betzle, 1984]

The main advantages of lattice girders over conventional steel arch supports are, on the one hand, a low weight per metre length of girder and, on the other, a more efficient bond with the shotcrete. In Slovakia lattice girders are systematically being used and incorporated into tunnel linings, however they are regarded to have a secondary use compared to rock bolts and shotcrete, as they provide mostly only immediate support [S. Kim et al., 2012].

2.4.4 Other methods

Other methods of reinforcing the tunnel excavation is in the form of face reinforcement. As during NATM tunneling it can occur that very unfavourable geology is encountered that would cause face collapse or crown collapse after the blasting and before the primary lining can be applied. In such cases face reinforcements must be used. These usually consist of micro-pile umbrellas and face bolts or forepoling, of which the later is most common in Europe [Date, J Mair, and Soga, 2008].

Micro-pile umbrellas are a set of piles, usually circular hollow steel sections, that are drilled into the future crown of the tunnel and subsequently grouted on the inside and outside. They are at a slight angle as shown in figure 2.11, to not change the tunnel profile. This umbrella stabilises the crown, decreases the deformations [B. Thanh Le, 2012] and allows for a better force transfers to the tunnel side wall, which prevents crown collapse during excavation. In this manner tunnel workers are able to work safely under the newly excavated crown without risk of partial of full collapse.

In difficult rock masses, not just the crown has to be reinforced during excavation. The face needs to be reinforced by slim bolts or injections, that prevent the rock or soil from the new face from collapsing after blasting. For loose soils grouting is injected into the soil ahead of the face of the tunnel [Zhang, Fang, and Lou, 2014], the load from the injected grout consolidated the soil, and therefore prevents face collapse. In other situations bolts or anchors may be used to stabilise the soil through redistribution of stresses. These bolts can be steel of even polyurethane. There are however many other face stabilisation techniques like soil freezing which is used usually in shallow tunnels to minimise deformations and stabilise the tunnel face [Afshani and Akagi, 2015]. This technique has been used in number of projects including the construction of the Copenhagen metro.

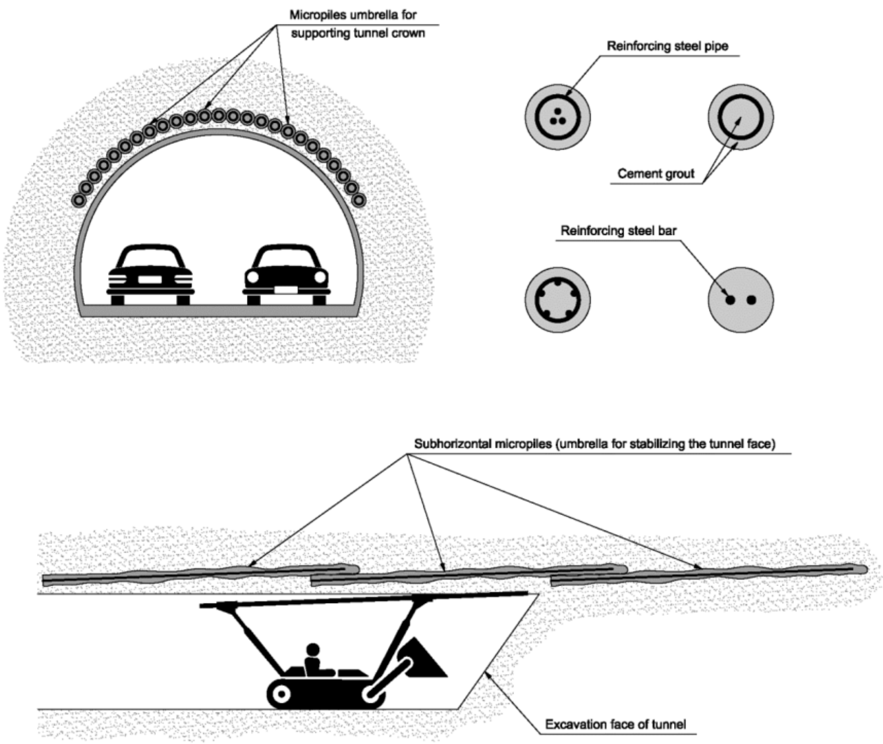

Figure 2.11: Installation of Micropile umbrellas in the tunnel crown from [Pastor et al., 2016]

Although there are many sections of the tunneling field which can be looked at, the report will solely focus on the previously mentioned Višňové tunnel in order to delimit the work. Therefore some of these techniques described above are not included and serve merely an educational purpose of widening overall tunneling knowledge. The tunnel will be therefore described to the reader in more detail in the upcoming chapter.

3. Tunnel Višňové

The aim of this chapter is to introduce tunnel Višňové which is in construction and to be finished in 2020. Geological and Hydro-geological conditions will be described and the structure of the tunnel will be summed up. The section of concern will be presented. The subsequent measurements of deformations of the linings to be compared with calculations in later chapters will be shown.

The structure analysed throughout this report is the Tunnel Višňové. It is part of the largest infrastructure project currently ongoing in Slovakia. The highway D1 connecting the capital, Bratislava, with the 2^{nd} largest city, Košice, on the east of the country, is almost complete. The remaining sections of this project to be built are a number of tunnels, of which Višňové is a part of.

3.1 Geology

The area of a tunnel of this length obviously has varying geology, unlike smaller projects dealing with only one homogeneous section of soil. Therefore it is necessary to first understand the global geology of the region and then the massive through which the tunnel is excavated. Based on a detailed geotechnical investigation, can the geotechnical zones be created where the rock or soil have similar properties, to simplify the design and constructions. From the laboratory and in-situ tests the individual rock properties are determined.

3.1.1 Natural Conditions and Geological structure of massive

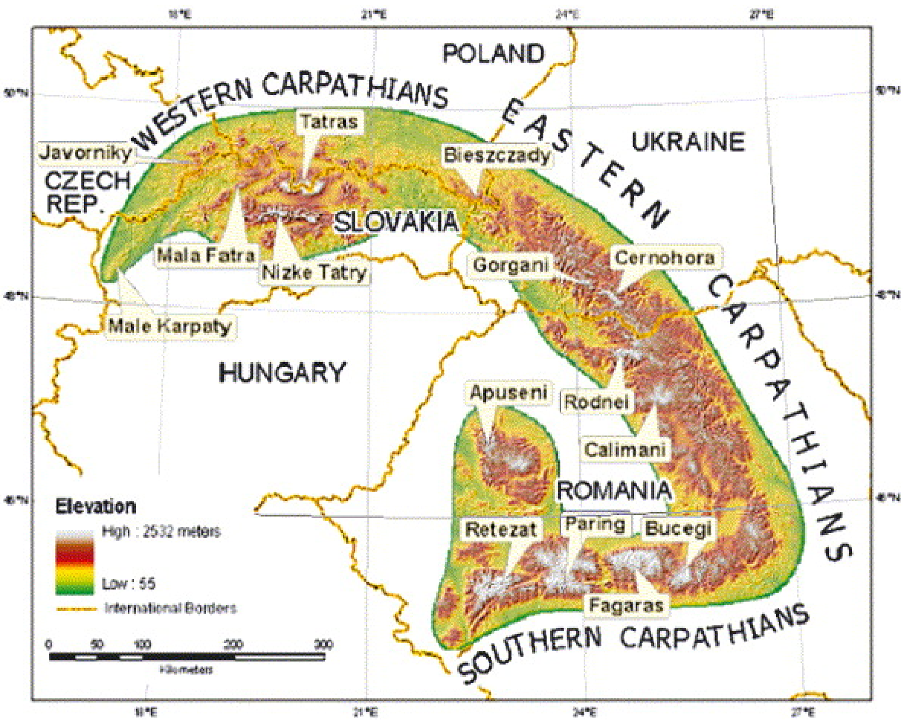

Figure 3.1: Map of the Carpathian mountain range from ENCYCLOPÆDIA BRITANNICA

As mentioned the tunnel Višňové is located in the Malá Fatra mountains with altitudes of 800-1300 MASL. The Malá Fatra mountains belong to the nappe-fold formation of the Fatra-Tatra Area, which is part of the Western Carpathians, the second longest European mountain range, extending from Slovakia to Romania.

Figure 3.2: Flysch formation in the Inner Western Carpathians

The Carpathian mountains occupy a region once covered by smaller oceans. The mountain range was formed through oceanic plates subducting below each other. This causes the external part of the northern section of the Carpathians to be composed of mainly Flysch (Carpathian Flysch belt), which was formed by the uppermost sedimentary rocks on the ocean floor, to be scraped off during the subducting process. This Flysch formation causes sequential alterations of different sedimentary rocks from the heavier breccias and conglomerates deposited in deep-turbulent flow, to shallow-water deposits like shale and sandstone.

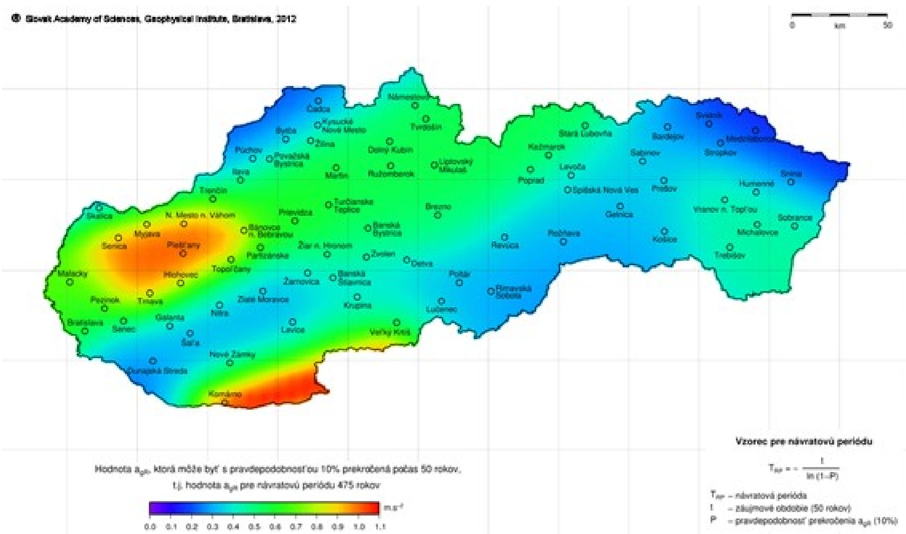

Figure 3.3: The Seismic map of Slovakia with a 475-year return period produced by GFÚ SAV,2012

The internal zones of the Western Carpathians are made of Variscan Granitoids. These have formed in different conditions and different times [Broska and Uher, 1994], be it through S-type magmatism or I-type plutonism. In the Western Carpathians S-type granitoids, derived from meta-sedimentary sources with Alminium rich characteristics, occur most frequently. This results in a mineral assemblage of Al-,Fe, Ti-rich biotite and muscovite.

The area in which the tunnel is located is in the seismic hazard zone with reference peak acceleration of $a_{gR} = 0,63\ m.s^{-2}$ for a 475-year return period, as can be seen from figure 3.3 above. Nonetheless, in this report, seismicity is not taken into account.

3.1.2 Engineering geological properties of basic rock types

The conditions predicted at the tunnel were interpreted based on engineering geology, map on the level of exploratory gallery, performed laboratory tests and analysing the rock mass samples. The massive consists mainly of the so-called crystallinicum rock types, mainly biotite granitoids with porphyric granites, with local veins of lamprophyre. At the eastern portal of the tunnel following rocks types were discovered.

Gkn	tectonic melange
BrGtp	mylonite granitoid (schist)
brmylGn, brmylGtp	Granitopid blastomylonit (schist)
Gz,Gn,Gtp	granitoid mainly tonalite
bGn	biotite granodiorite
pGn,pGtp	porphyritic granitoids, locally turns to pegmatite
hGn, hGtp	hybrid granitoids
MGN, MGtp	migmatic granitoids
L	lamprophyre
ktGtp	cataclastic granitoids

Table 3.1: Rock types identified at the tunnel site in the eastern portal

The whole massive and its heterogeneity is bound to the tectonic evolution, which changes its geotechnical properties. The weakest rock types are located in mylonite and cataclastic fault zones. The following risks have been identified in the crystallinicum and the cataclastic fault zones.

Crystallinicum	Cataclastic
Small block fall/wedge failure	Sudden change of quality
Loosening ground	Time consuming driving through these zones
Instability in zones on Kalkirite	sudden water ingress with possible suffosion
Suffosion within zones of water ingress	Water pressure
Alteration of rock types(weak, rigid)	Low strength of rock
	Low strength of rock
	Overbreaks due to excavation

Table 3.2: Identified risks in the different zones

3.1.3 Rock mass properties and hydro-geological properties

Based on the laboratory and in-situ tests the rock mass was divided into 7 types, 1, 2, 3, 4, 5, 6a and 6b. The most unfavourable types are 5, 6a and 6b, which consist of tectonically deformed and weathered rock and cataclastic fault rock. For each type geotechnical properties were derived and form the basis of geotechnical sections. The parameters needed for analytical and numerical modelling of the rock mass, for the Mohr-Coulomb and Hoek-Brown failure criteria described in Appendix B, are presented in table 3.3 below. Rock mass parameters RQD, RMR, QTS and GSI are rock mass classification methods described in the upcoming chapter 4.

Rock type property	**GA1**	**GA2**	**GA3**	**GA4**	**GA5**
Overburden [m]	655	520	360	300	300
RQD	70-100	60-85	40-80	35-75	30-70
RMR	81-100	61-80	41-60	21-40	20
QTS	>84	68-84	54-68	40-54	40
GSI	60-70	50-65	40-55	30-45	25-35
E [MPa]	6 000	5 000	2 000	1 700	1 400
E_{rm} [KPa]	25 000	17 000	9 000	4 400	1 500
ν [-]	0.13	0.15	0.17	0.19	0.21
γ [kN/m^3]	27.1	27.1	27.1	26.9	26.8
ϕ [°]	55	53	47	44	42
ψ [°]	0.33	0.32	0.28	0.26	0.25
c [kPa]	1 150	1 000	800	700	550
σ_c [MPa]	120	100	80	70	50
m_i [MPa]	32	30	27	22	18
D [MPa]	0	0	0	0	0

Table 3.3: Geotechnical properties of all geotechnical sections, needed for a Mohr-Coulomb and Hoek-Brown material models along with rock mass classification indices

During the excavation of the exploratory gallery the groundwater flow was 15-100 $l.s^{-1}$. Once breakthrough was achieved the flow stabilised at 150-220 $l.s^{-1}$. Only a minor risk of water ingress was predicted. Only a 10 $l.s^{-1}$ groundwater flow is predicted in the crystallinicum.

3.1.4 Interpretation of geotechnical monitoring

As geotechnical monitoring was carried out throughout the excavation of the tunnel, and some of the excavation was carried out already, feedback from the site was available. The face survey revealed all of the rock types described above confirming the predictions. The spacing of the rock was approximately 20-60 cm to 2 m, usually with a rigid filling. In tectonic fault zones the rock is weathered, damp, with soft filling of the joints.

Rock type 6a was encountered almost in the exact place it was predicted to be in. The values of RMR reached an average of 35 points, which was somewhat higher than expected. The displacements reached up to 60 mm.

Figure 3.4: Tunnel face showing rock type 6a

Values of RMR for the other rock types (GA1-GA5) reached 43-61 points, with a 53 point average. Recorded displacements were recorded within a 5-22 mm range for weak rock, and average of 10 mm in the rest of the excavation. The rock was competent, unweathered to slightly weathered.

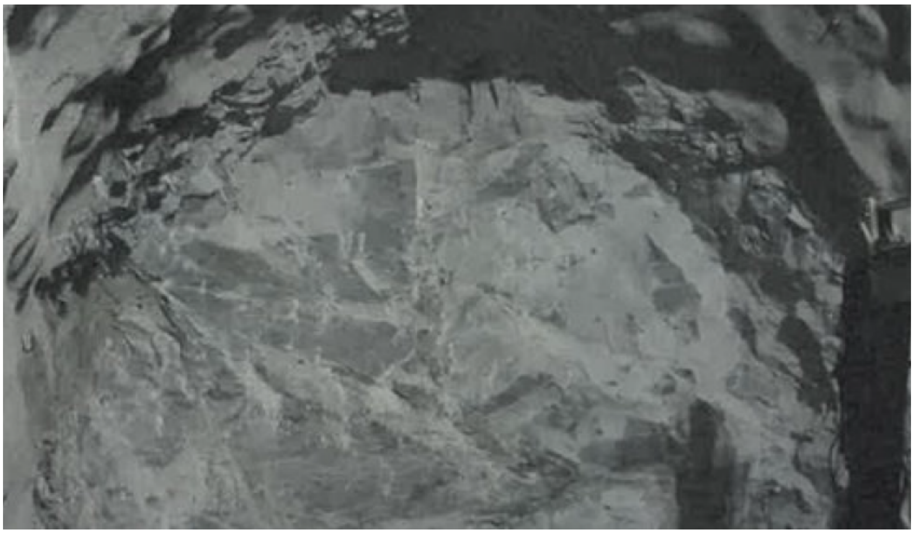

Figure 3.5: Tunnel face showing rock type GA1

3.2 Structure

In the tunnel structure, few things remain the same throughout, no matter the support class. Mainly it is the gabarit, or in other words the space that must be kept clear for movement of traffic. The gabarit cannot be changed (unless it is enlarged in areas of niches), therefore the excavated profile must allow for the change of lining thickness. According to the geology in the given section, a support class is established with all the necessary supporting structures (i.e. shotcrete, Rock Bolts, etc.).

In tunnel Višňové, as mention previously, there are 7 rock mass or geotechnical sections, each one corresponding to a support class, hence 7 support classes were identified. As to delimit this paper, it is necessary to focus only on 5 sections, namely GA1-5 and its respective support class, for the analyses in later chapters. For this purpose support classes A2/1p, A2/2p, A2/3p, B1/1p and B2/1p are introduced. Each support class has its own geometry and specification as in regard to structure, which are described in tables 3.5, 3.6 and 3.7 and shown in figures 3.6 and 3.7. Which support class used in which geotechnical section is explained in table 3.4 below.

Geotechnical section	**Support Class**
GA1	A2/1p
GA2	A2/2p
GA3	A2/3p
GA4	B1/1p
GA5	B2/1p

Table 3.4: Definition of support classes use within geotechnical sections

The general shape of the profile can be seen on the figure 3.6 and 3.7 below.

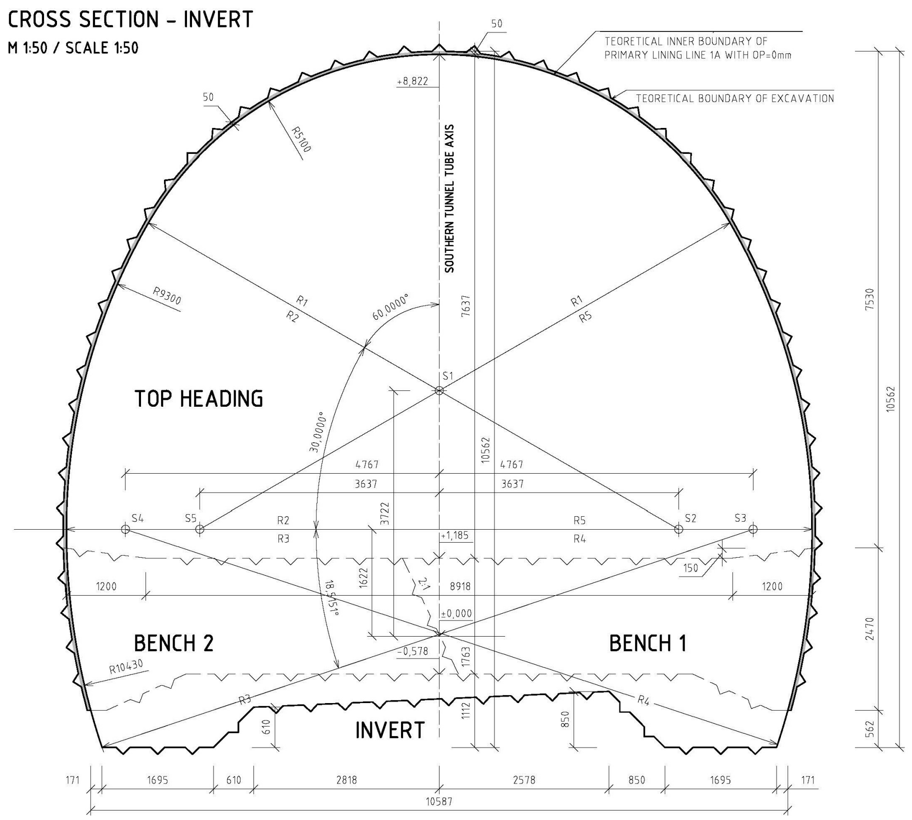

Figure 3.6: The normal profile of Tunnel Višňové without invert in geotechnical sections GA1-3

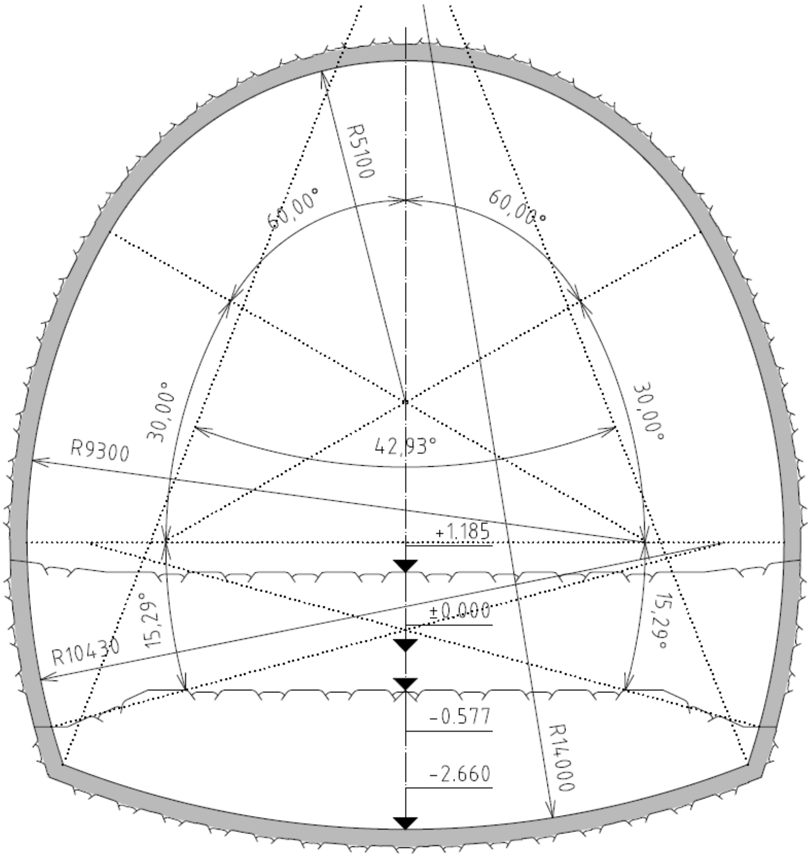

Figure 3.7: The normal profile of Tunnel Višňové without invert in geotechnical sections GA4-5

The material properties of the linings and the other supporting structures, along with the tunnel dimensions are the following:

Dimension	**Without Invert**	**With Invert**
Width [m]	11.3	11.3
Height [m]	9.8	11.5
Thickness of lining [cm]	5.0 - 15.0	20.0 - 25.0
Rock Bolt length [m]	4.0	4.0 - 6.0

Table 3.5: Tunnel and support dimensions in all support classes depending on whether the profile contains an invert or not

It should be noted that geotechnical sections GA1 to GA3 are without an invert, while the others are with an invert.

Material property	Shotcrete C30 (FRC)
σ_c (uniaxial) [MPa]	30
γ $[kN/m^3]$	25
E_c [MPa]	33 000
ν [-]	0.2

Table 3.6: Material properties of shotcrete (fibre reinforced concrete) used in all support classes

Material property	Rock Bolts
Ultimate load [kN]	200

Table 3.7: Material properties of all Rock Bolts (Swellex,grouted or self-drilled) used in all support classes

3.3 Geotechnical monitoring

As the primary lining in the entire tunnel was completed, a geotechnical monitoring was carried out on the displacements of the tunnel, before the secondary lining could be installed. In NATM tunneling this monitoring is an inseparable part of the construction process. It consists of numerous combinations of measurement types. Typically, 3D displacement measurement (in the tunnel and if required on the surface), extensometers, inclinometers, strain gauges, piezometers, tilt meters, hose water levels, and invert probes are used to observe the system behaviour in underground structures. Additional instrumentation and tools, such as compass-clinometer or digital face mapping techniques may be required [ÖGG, 2014]. In Višňové mostly the absolute 3D displacement monitoring system was used. A group of reflective targets were installed from which the total station reads their spatial position in the global coordinate system. The measurements gathered from this method, will be compared to the analytical and numerical solutions in later chapters.

3.3.1 Warning states

For the needs of geotechnical monitoring, a behaviour of deformations and stresses of the tunnel construction and the rock mass surrounding it, has to be defined. These are the so called warning states. A warning state in the deformations of the tunnel lining and surrounding rock mass, is a qualitative change of behaviour from their previous behaviour, which forces certain measures to be taken. These measures are based on the KAV method (observation method), and are to keep the deformation and stress behaviour within the expected limits. The warning states are usually divided into 4 or 5 categories and are either exact or empirically deduced [Ministerstvo dopravy, 2016]. For the construction of Tunnel Višňové, 5 categories were established in accordance to Slovak norms. Each one is based on certain criteria which varies according to the standards of the country. In this case the categories were set up based on the expected and actual displacement measurements. The categories and their respective basis are explained in figure 3.8 below:

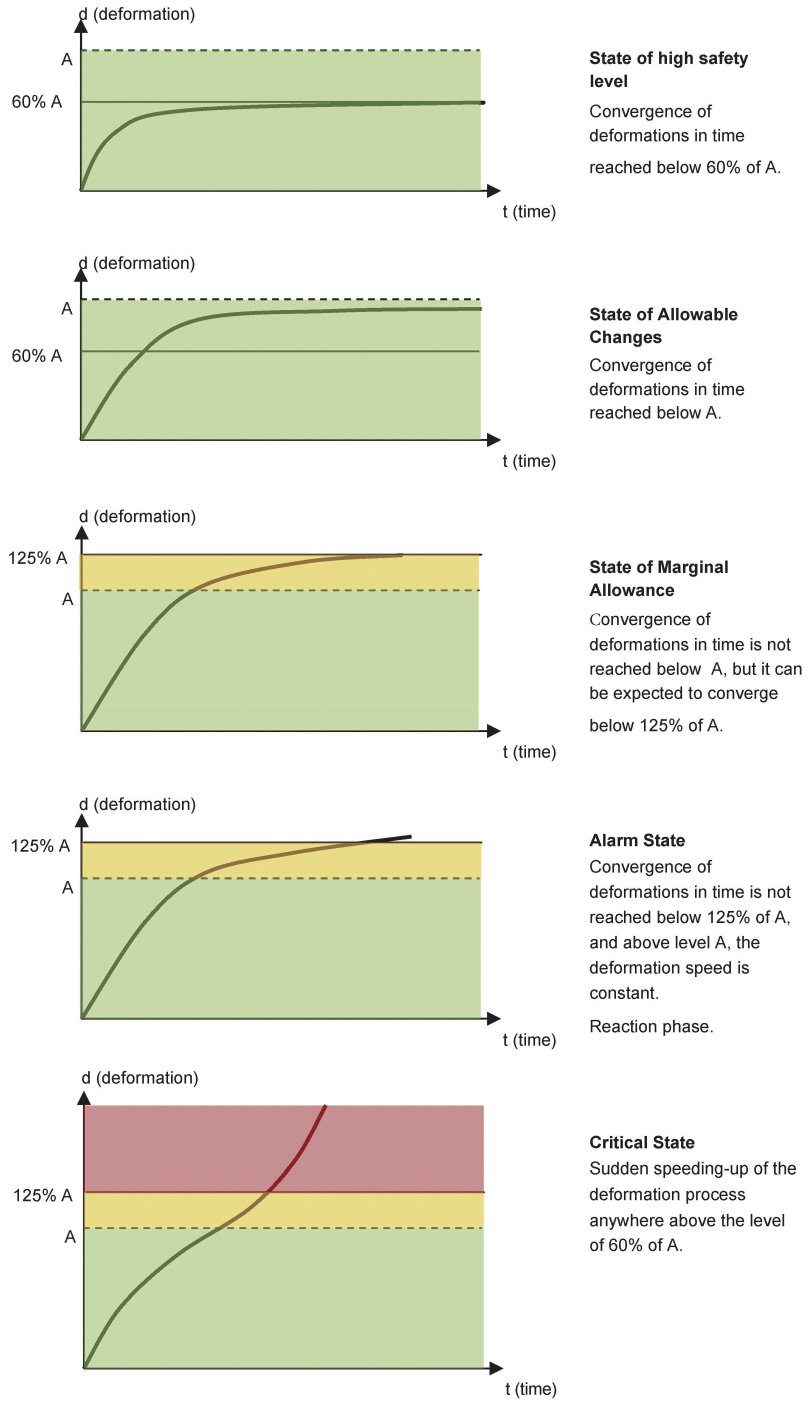

Figure 3.8: The warning states established during design process of Tunnel Višňové

First 3 categories are within the limits and are acceptable. Once the deformations reach beyond 125% then stabilisation measures are taken. The last, Critical state, is a stage at which risk not only to the tunnel structure, but also the risk of loss of life in the tunnel, and damage to adjacent structures is present in high levels. In tunnel Višňové a wide variety of readings from the monitoring were recorded.

3.3.2 Measurements

The performed geotechnical monitoring in the geotechnical sections of interest, namely GA1 - GA5, consisted of only deformation measurements, and not the formerly mentioned inclinometers, pressure gauges and other such equipment. The deformations were measured roughly every 25 m in 5 points. One point in the crown and two in the tunnel wall on each side, as can be seen on the figure below.

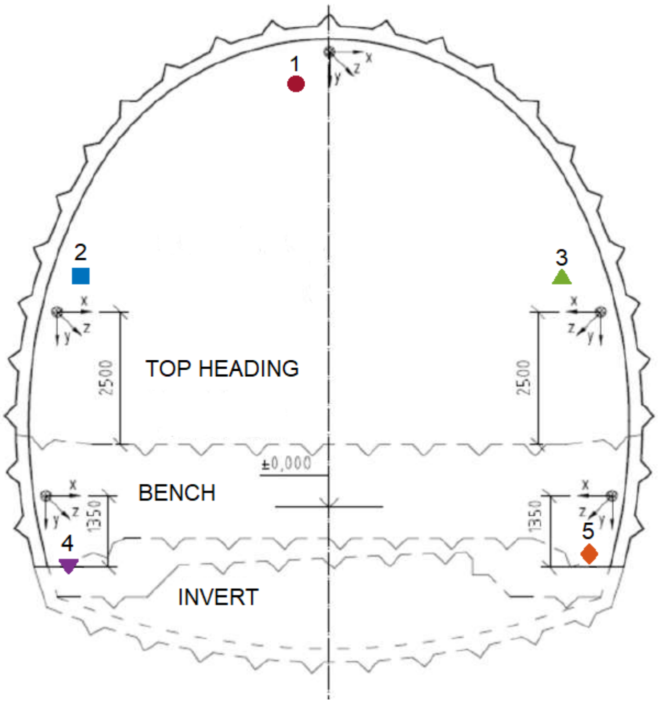

Figure 3.9: Location of the measurements in the tunnel profile, for all geotechnical sections

All of the measured displacements of the 5 points for each stationing for section GA1 - GA5 were plotted and analysed. An example of such plot can be see on figure 3.10 below.

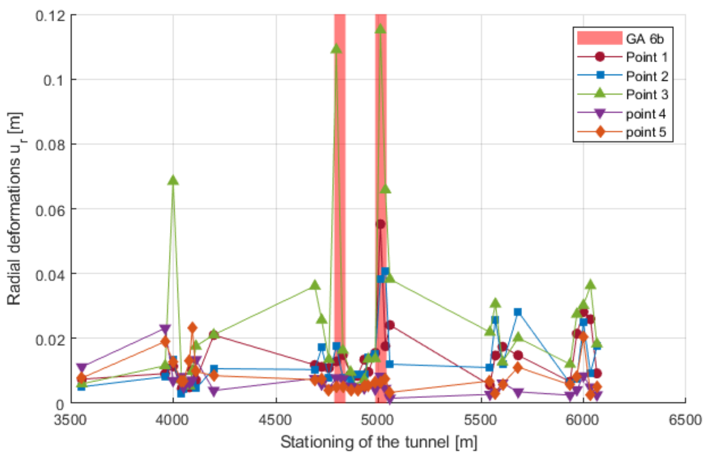

Figure 3.10: Location of the measurements in the tunnel profile, for all geotechnical sections

The analysis consists of matching the data plot to the geological investigation (presented in figure 3.11), carried out prior to the tunnel construction, or elimination on inconsistent outliers. Matching analysis compares the measured data to the geological sections predicted. If a fairly good correlation can be established, as is the case in the majority of the time and can be seen in figures 3.10 and 3.11, the measurements can be subsequently filtered out and disregarded.

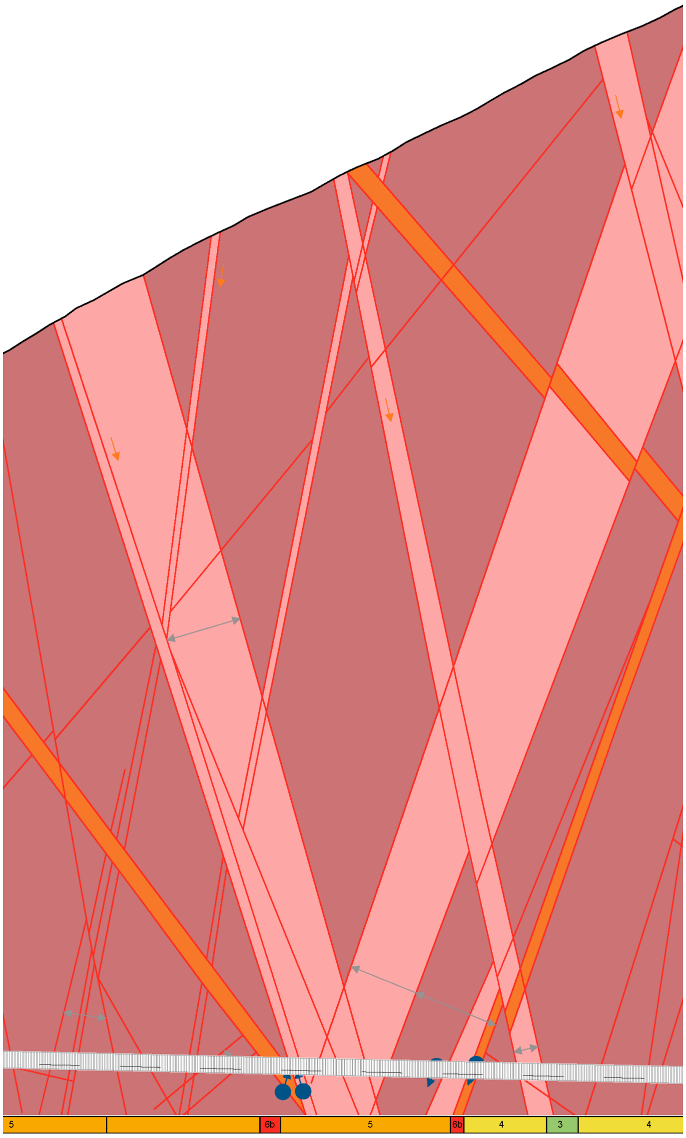

Figure 3.11: Section of the geological tunnel profile based on geological investigation prior to construction. At the bottom geological sections are shown with light green, yellow, orange and red being GA3, GA4, GA5 and GA6b respectively.

The geological profile in figure 3.11, shown above, is fairly precise, but somewhat shifted in reality, as the readings suggest. A geological section GA6b (shown in red at the bottom of the figure) is encountered during an expected GA5 section, hence including in the original readings, which is clearly visible in the sharp and sudden peaks that are highlighted. This can be concluded with some certainty, never however with 100% accuracy. Therefore, these measurements are then filtered out.

With other geotechnical sections this filtration is more imprecise, especially when analysing better geological zones such as GA1 and points belonging to GA2 or GA3. Filtration in these cases is more conservative, and possibly creates fairly large discrepancies between the results.

Another filtering method is that of the outliers. An example is shown on figure 3.12. As can be seen, an outlier was recorded at point 4 in the profile in one section of the tunnel. This is not a faulty measurement, but rather a purely local extreme deformation caused by a release of a block or a wedge, due to the lines of discontinuities, as explained in section 2.4.2. Wedge or block falls of this kind mostly occur in good geologies, where the rock mass is more than capable of supporting itself for extended periods of time, therefore they do not pose a threat to the structural stability of the tunnel. The rest of the tunnel walls and crown are intact and exhibit normal and expected behaviour, what is supported by the data in figure 3.12 as the other points do not exceed the norms. Consequently, this extreme measurement can be treated as an outlier, as it is a mere local anomaly which cannot be predicted very well, and was not designed for, while it would also make for an unfair comparison with the analytical and numerical solutions.

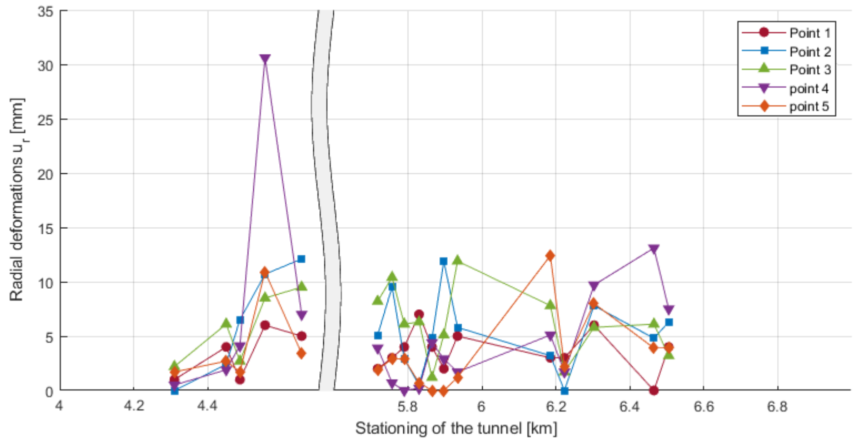

Figure 3.12: Measured deformations of all the 5 points for each measurement inside the geotechnical section GA1

Another factor affecting the measurements that cannot be altered, but has to be considered nonetheless when analysing results later on in the comparison, is the fact that the readings come from different parts of the tunnel. Although the parts belong to the same geotechnical section, they can be sometimes as far as 2-3km apart (hence the reason for splitting of figure 3.12 into two), and have somewhat different values for their defining parameters. This can account for the large variance and standard deviation of the measurements. Larger sample size reduces the margin of error to some extent, but deviation from the analytical and numerical calculations can and should be expected as with any site measurement.

Standard deviation before and after filtering was calculated, to check whether the measured data was more consistent and therefore reliable as a source of comparison in later chapters. The results from this comparison of pre- and post-filtering for geological section GA3, is presented in figure 3.13 below:

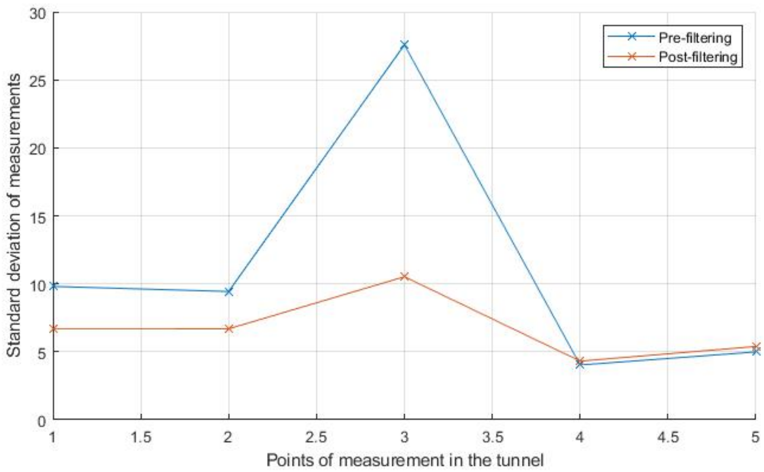

Figure 3.13: Standard deviation of measured deformations at the 5 points in the tunnel profile for geotechnical section GA 3

This analysis is carried out for all geological sections and their corresponding maximum and average deformations at each point are calculated. Vertical, horizontal and total deformations are used for comparison later on in the report, and such they are all presented in tables 3.8 and 3.9 below.

Point	**Geological section total deformation [mm]**				
	GA 1	**GA 2**	**GA 3**	**GA 4**	**GA 5**
1	7.0	8.6	11.7	19.5	28.1
2	12.1	8.7	14.6	18.3	28.3
3	11.9	13.0	17.3	14.3	38.3
4	13.1	10.4	14.3	12.0	23.1
5	12.4	6.8	13.1	14.0	23.1

Table 3.8: Maximum total deformations measured in geotechnical sections GA 1 to GA 5 from geotechnical monitoring of tunnel Višňové

Point	**Geological section total deformation [mm]**				
	GA 1	**GA 2**	**GA 3**	**GA 4**	**GA 5**
1	3.4	6.3	8.2	10.3	13.1
2	5.2	6.1	8.5	10.2	11.1
3	5.9	8.3	10.6	12.6	17.8
4	4.0	5.8	7.4	5.7	6.6
5	3.1	4.2	7.8	6.2	8.2

Table 3.9: Average total deformations measured in geotechnical sections GA1 to GA5 from geotechnical monitoring of tunnel Višňové

From the results in the tables 3.8 and 3.9 above, it can be seen that the deformations are not increasing linearly, what can be attributed to a small statistical sample and perhaps due to a not thorough enough filtration (which is caused by the lack of documentation during construction of the tunnel). Some randomness can be accepted when dealing with real measured deformations, however points 4 and 5 exhibit strange behaviour, not having larger deformations in higher geological sections. This is caused by the fact that the bench of the profile is excavated later than the crown, and the deformations, which are time dependent, do not have the necessary time to develop. It should be also noted, that while some of the measurements, namely those with lower stationing numbers (i.e. points on the left on the figure 3.12), are fairly newly excavated (roughly 4 months), therefore the deformations have not converged yet, hence showing lower values than expected. All of the deformations up to the 4^{th} of February have been considered. These reasons mean, that points 4 and 5 cannot be used for comparison in the later analysis, due to their inconsistency. In the upcoming chapters, only points 1,2 and 3 shall be used and discussed further.

4. Rock classification

This chapters aim is to briefly introduce the different rock mass classification theories developed throughout history, their assumptions, advantages and disadvantages, along with their uses and limitations. It should serve as a basis for the content of the upcoming chapters.

4.1 Introduction

During the early stages of a project, be it during feasibility or during preliminary design, rock mass classification is vital. As during these stages only limited information is available, these classifications help predict needed tunnel supports, expected deformations and other essential properties of the rock mass. These classification methods however, cannot be the sole instrument of a tunnel engineer, mainly in the later stages of the project, when more detailed geological and hydrogeological characteristics of the rock massif are obtained. Rather, they should be used together with other, more sophisticated design methods and procedures. The rock mass classification methods as well should not be used as stand-alone methods. In tunnel engineering it is heavily recommended to use multiple rock classifications (minimum 2 [E. Hoek, 2006]), as each one depends on a different variable. In this way it is possible to have a much clearer picture of the geological conditions on the site from the in-situ tests.

Another important aspect of using these methods is to „understand the limitations of rock mass classification schemes [Palmstrom and Broch, 2006]. Most classification schemes are based on existing engineering cases with certain geology. These empirically determined relationships have certain limits and too frequently the designer is unaware of these boundaries [Feng, 2016].

Also, only the basic concepts of the different rock mass classification are dealt with in this report, as numerous changes, updates and commentaries were made throughout the use of each of these methods.

4.2 Case history rock mass classification

First try at classification was made more than 125 years ago by Ritter (1879) attempted to formalise an empirical approach to tunnel design for the purpose of determining surface supports [Feng, 2016]. Later M.M. Protdjakov in 1908 tried to do so as well, but the method was rather unused. Since then numerous methods of classification were established and are used still today as a means of quick estimations and preliminary calculations.

4.2.1 Terzaghi

The first mention connection between rock mass classification and tunnel engineering was established in a paper by one of the founding fathers of soil mechanics, Karl Terzaghi, in 1946. It is based on the same assumption of the shape of the loosened part of the rock massif. However, it compliments the Protdjakov theory mentioned earlier, as Terzaghi method accounts for failure planes, which Protdjakov did not. Perhaps of the highest interest is the description of the 7 categories assumed, which consisted of clear descriptions and comments, the type of which are most useful to a civil engineer. Then may be the reason for it being used for full 30 years in USA [Pruška, 2000]. The categories with their respective descriptions made by Terzaghi can be seen in the table bellow, as they can help with understanding of later chapters:

Category	**Description**
Intact rock	Contains neither joints nor hair cracks. Hence, if it breaks, it breaks across sound rock. On account of the injury to the rock due to blasting, spalls may drop off the roof several hours or days after blasting. This is known as a spalling condition. Hard, intact rock may also be encountered in the popping condition involving the spontaneous and violent detachment of rock slabs from the sides or roof.
Stratified rock	Consists of individual strata with little or no resistance against separation along the boundaries between the strata. The strata may or may not be weakened by transverse joints. In such rock the spalling condition is quite common.
Moderately jointed rock	Contains joints and hair cracks, but the blocks between joints are locally grown together or so intimately interlocked that vertical walls do not require lateral support. In rocks of this type, both spalling and popping conditions may be encountered.
Blocky and seamy rock	Consists of chemically intact or almost intact rock fragments which are entirely separated from each other and imperfectly interlocked. In such rock, vertical walls may require lateral support.
Crushed but chemically intact rock	Has the character of crusher run. If most or all of the fragments are as small as fine sand grains and no recementation has taken place, crushed rock below the water table exhibits the properties of a water-bearing sand.
Squeezing rock	Slowly advances into the tunnel without perceptible volume increase. A prerequisite for squeeze is a high percentage of microscopic and sub-microscopic particles of micaceous minerals or clay minerals with a low swelling capacity.
Swelling rock	Advances into the tunnel chiefly on account of expansion. The capacity to swell seems to be limited to those rocks that contain clay minerals such as montmorillonite, with a high swelling capacity.

Table 4.1: Categories of rock in tunneling according to Terzaghi with their descriptions

Nonetheless, this theory has no use in modern tunnel engineering with shotcrete and rockbolt supports, as it is only useful for rock tunnels with steel supports.

4.2.2 Stand-up time

A classification based on a so-called stand-up time was derived by Lauffer in 1958. The proposed relationship was between the unsupported span and the rock mass quality. An unsupported span can be the tunnel span (shown on the left in figure 4.1) or the distance from the face of the tunnel to the closest support (shown on the right in figure 4.1). The calculations Lauffer proposed use the maximum value for the two. The main concept of this theory is that the span of the tunnel severely affect the stand-up time of the tunnel, where by stand-up time is understood the time available to install supports . For example a much smaller tunnel, like a pilot tunnel or a circular tunnel with a smaller radius, is able to stay unsupported /or with minimal support for much longer than a full sized tunnel.

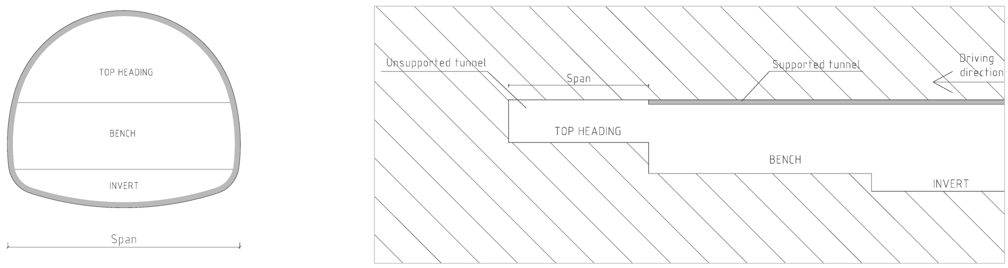

Figure 4.1: Span definition by Lauffer (1958) in stand-up time method

Hence the reason this theory is part of the NATM, as dividing the tunnel profile into smaller sections (benching) provides smaller spans and longer stand-up times. Another possibility as mentioned in Chapter 1, is the possibility to divide the profile into multiple drifts. However as mentioned earlier, these techniques in NATM can and should be used only in softer rock formations. This is due to the fact that softer rock (mudstone, shale, etc.) fails over time, as squeezing rock and swelling takes effect.

In hard rock the failure mechanisms are numerous and therefore cannot be simplified to this approach [Feng, 2016]. In hard rock the failure mode is assumed to occur immediately after excavation and is not time-dependent. An example with a rock wedge is that if the rock supporting it is removed, the wedge can fall at any given time, be it during blasting or during clearing works. This is not true for highly stressed rocks. These experience failure through spalling and slabbing (gradual failure) or through rock bursts (sudden failure). Supports for both scenarios of highly stressed rock, but also for hard rock, cannot be modelled and designed by the use of stand-up time method but preferably by accounting for stress-field changes.

It is also worth noting, that prior to the inclusion of the stand-up time method of classification to the NATM, some modifications were done, mostly by Pacher in a paper from 1974. Lauffers stand-up time method is however extremely conservative though, compared to modern tunneling methods.

4.2.3 RQD

Classification according to the RQD (Rock Quality Designation) index was derived by Deere in 1967. Quantitative assessment of the rock mass quality is made on the basis of drill core logs. The cores need a minimum diameter of 54,7 mm, and the RQD is defined as the percentage of intact pieces of the core longer than 100 mm over the total length of the core:

$$RQD = \frac{L_1 0}{L} \times 100 \tag{4.1}$$

An example of the procedure can be seen on figure 4.2 below:

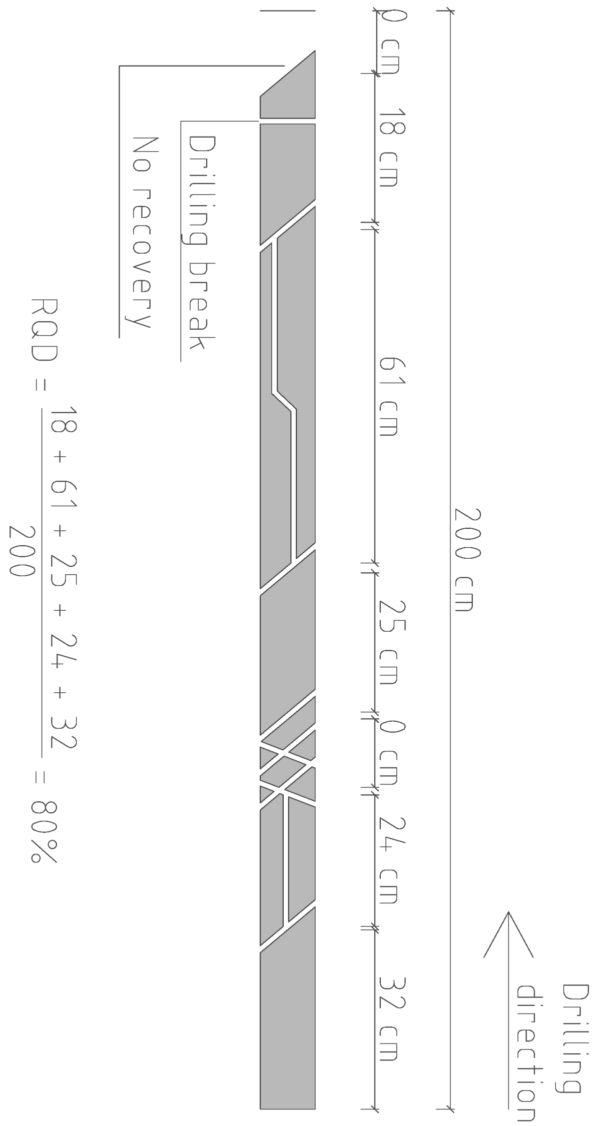

Figure 4.2: RQD calculation example from core drilling according to (1989)

The core drilling is recommended with a double tube cord core barrel [E. Hoek, 2006], and excluded from the calculations should be the core fractures caused by the drilling itself. A vital point within this theory is that the RQD index is very dependent on the inclination of the drilling, hence it represents the in-situ rock mass quality. Table 4.11 below shows the classification of the rock mass according to the RQD, with the added corresponding F_p and C_t values.

Rock Mass Quality	**RQD**	$\mathbf{C_T}$	$\mathbf{f_p}$
Very high	100 - 90	0 - 0.15	2.00 - 2.30
High	90 - 75	0.15 - 0.35	2.30 - 1.20
Moderate	75 - 50	0.35 - 0.70	1.20 - 0.70
Low	50 - 25	0.70 - 1.10	0.70 - 0.50
Very low	25 - 0	1.10 - 1.40	0.50 - 0.40

Table 4.2: Rock mass quality classification by the RQD method

One major modification to this theory was derived by Palmström (1982), to account for the situation when a drilled core is not available. In that case the RQD index is determined thanks to the known joint planes, exposed on the surface (i.e. face of the tunnel or pilot tunnel). In that case the relationship is as such:

$$RQD = 115 - 3.3\ Jv \tag{4.2}$$

Where:

J_v | volumetric joint count or the number of (sum of) joints counted per unit area

This Palmström modification can somewhat reduce the variance based on the direction/inclination. Similar to the fractures from drilling, blast fractures from face excavation should not be taken into account. Deere's RQD index was widely used particularly in North America. Attempts to relate RQD to Terzaghi's rock load factors and to rockbolt requirements in tunnels were also made [E. Hoek, 2006]. Nowadays the RQD index is mostly used as a component of the RMR and the Q-index methods.

4.2.4 RSR

Rock Structure Rating classification, or RMR for short, was developed by Wickham et al in 1972. The value is derived from the information from the geological investigations and the assumed support system of the tunnel (i.e. shotcrete, rock bolts with shotcrete, steel sets). This classification method is applicable only to relatively small tunnels with mostly steel support systems, and therefore it is scarcely used in modern tunnel design. The logic of this method and how the quasi-quantitative method was established is nonetheless interesting to see, as this paper showing RSR classification played a major role in the development of other classification schemes used today [E. Hoek, 2006]. The RSR index is a summation of the points of 3 parameters evaluated for the rock mass.

$$RSR = A + B + C \tag{4.3}$$

Where:

A	represents the geological conditions
B	represents the joint orientation and density
C	is based on the groundwater inflow and rock mass joints

While the parameters are determined by:

A	Type of rock (igneous, metamorphic, sedimentary) Hardness of the rock (hard, medium, soft, decomposed) Geologic structure (massive, slightly-, moderately- or intensely faulted/folded)

B	Distance between joints Joint orientation (strike and dip) Direction of tunnel drive (shown in figure 4.3)

C	Sum of parameters A and B Joint condition Expected groundwater inflow

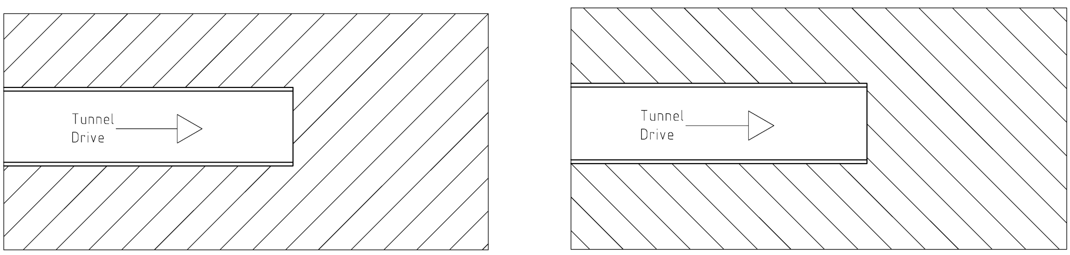

Figure 4.3: Drive direction against dip (left) and with dip (right)

Tables 4.3, 4.4 and 4.5 based on these parameters, where each of the possible combinations is assigned a value, and the maximum RSR value is 100 (meaning best quality rock), are pictured below:

	Basic Rock Type				Geological Structure			
	Hard	Medium	Soft	Decomposed				
Igneous	1	2	3	4		Slightly	Moderately	Intensively
Metamorphic	1	2	3	4		Folded or	Folded or	Folded or
Sedimentary	2	3	4	4	Massive	Faulted	Faulted	Faulted
Type 1					30	22	15	9
Type 2					27	20	13	8
Type 3					24	18	12	7
Type 4					19	15	10	6

Table 4.3: Table to find parameter A for the RMR system [E. Hoek, 2006]

	Strike ⊥ to Axis					Strike || to Axis		
	Direction of Drive					Direction of Drive		
	Both	With Dip		Against Dip		Either direction		
	Dip of Prominent Joints [a]					Dip of Prominent Joints		
Average joint spacing	Flat	Dipping	Vertical	Dipping	Vertical	Flat	Dipping	Vertical
1. Very closely jointed, < 2 in	9	11	13	10	12	9	9	7
2. Closely jointed, 2-6 in	13	16	19	15	17	14	14	11
3. Moderately jointed, 6-12 in	23	24	28	19	22	23	23	19
4. Moderate to blocky, 1-2 ft	30	32	36	25	28	30	28	24
5. Blocky to massive, 2-4 ft	36	38	40	33	35	36	24	28
6. Massive, > 4 ft	40	43	45	37	40	40	38	34

Table 4.4: Table to find parameter B for the RMR system [E. Hoek, 2006]

	Sum of Parameters $A + B$					
	13 - 44			45 - 75		
Anticipated water inflow	Joint Condition [b]					
gpm/1000 ft of tunnel	Good	Fair	Poor	Good	Fair	Poor
None	22	18	12	25	22	18
Slight, < 200 gpm	19	15	9	23	19	14
Moderate, 200-1000 gpm	15	22	7	21	16	12
Heavy, > 1000 gp	10	8	6	18	14	10

Table 4.5: Table to find parameter C for the RMR system [E. Hoek, 2006]

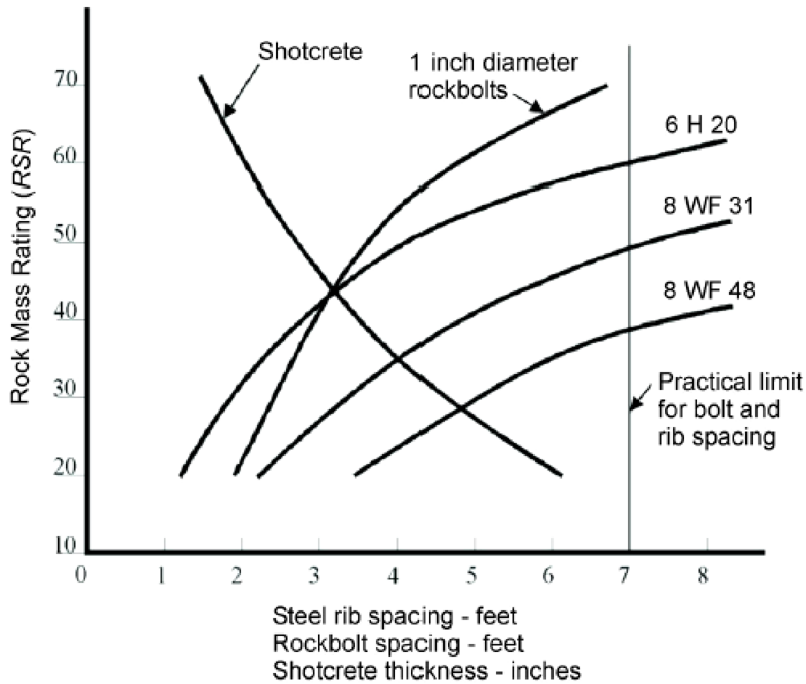

Figure 4.4: Graph showing the relationship between the RSR index and the needed support [E. Hoek, 2006]

Values in the tables vary according to the revision or the year of publishing, but the differences are rather small. The final RMR value can be then compared to the classification table 4.6 below:

Rock mass class	Excavation	Rock bolts (20 mm diameter, fully grouted)	Shotcrete	Steel sets
I - Very good rock *RMR*: 81-100	Full face, 3 m advance.	Generally no support required except spot bolting.		
II - Good rock *RMR*: 61-80	Full face , 1-1.5 m advance. Complete support 20 m from face.	Locally, bolts in crown 3 m long, spaced 2.5 m with occasional wire mesh.	50 mm in crown where required.	None.
III - Fair rock *RMR*: 41-60	Top heading and bench 1.5-3 m advance in top heading. Commence support after each blast. Complete support 10 m from face.	Systematic bolts 4 m long, spaced 1.5 - 2 m in crown and walls with wire mesh in crown.	50-100 mm in crown and 30 mm in sides.	None.
IV - Poor rock *RMR*: 21-40	Top heading and bench 1.0-1.5 m advance in top heading. Install support concurrently with excavation, 10 m from face.	Systematic bolts 4-5 m long, spaced 1-1.5 m in crown and walls with wire mesh.	100-150 mm in crown and 100 mm in sides.	Light to medium ribs spaced 1.5 m where required.
V – Very poor rock *RMR*: < 20	Multiple drifts 0.5-1.5 m advance in top heading. Install support concurrently with excavation. Shotcrete as soon as possible after blasting.	Systematic bolts 5-6 m long, spaced 1-1.5 m in crown and walls with wire mesh. Bolt invert.	150-200 mm in crown, 150 mm in sides, and 50 mm on face.	Medium to heavy ribs spaced 0.75 m with steel lagging and forepoling if required. Close invert.

Table 4.6: Classification table according to the scoring of RSR system [E. Hoek, 2006]

4.2.5 QTS

A local classification method used to help classify rock masses in Prague for metro construction [Pruška, 2000]. More information on this method is found Appendix A.

4.3 Geomechanics based classification (RMR)

RMR classification, or Rock Mass Rating was derived in 1976 by Bienawski and later updated in 1989, using data from hundreds of tunnels around the world. Unlike the RSR procedure, it uses 6 parameters rather than 3. These are as follows:

A	Uniaxial compressive strength of rock material
B	Rock Quality Designation (RQD)
C	Spacing of discontinuities
D	Characteristics of discontinuities
E	Groundwater conditions
F	Orientation of discontinuities

The final value representing the quality of the rock mass is determined through addition (or subtraction) of the individual category ratings, as specified in the following equation:

$$RMR = \sum(A + B + C + D + E - F) \tag{4.4}$$

The individual ratings are summarised in table 4.7 below:

A. CLASSIFICATION PARAMETERS AND THEIR RATINGS									
	Parameter		Range of values						
1	Strength of intact rock material	Point-load strength index	>10 MPa	4 - 10 MPa	2 - 4 MPa	1 - 2 MPa	For this low range - uniaxial compressive test is preferred		
		Uniaxial comp. strength	>250 MPa	100 - 250 MPa	50 - 100 MPa	25 - 50 MPa	5 - 25 MPa	1 - 5 MPa	< 1 MPa
	Rating		15	12	7	4	2	1	0
2	Drill core Quality *RQD*		90% - 100%	75% - 90%	50% - 75%	25% - 50%	<25%		
	Rating		20	17	13	8	3		
3	Spacing of		> 2 m	0.6 - 2 . m	200 - 600 mm	60 - 200 mm	< 60 mm		
	Rating		20	15	10	8	5		
4	Condition of discontinuities (See E)		Very rough surfaces Not continuous No separation Unweathered wall rock	Slightly rough surfaces Separation < 1 mm Slightly weathered walls	Slightly rough surfaces Separation < 1 mm Highly weathered walls	Slickensided surfaces or Gouge < 5 mm thick or Separation 1-5 mm Continuous	Soft gouge >5 mm thick or Separation > 5 mm Continuous		
	Rating		30	25	20	10	0		
5	Groundwater	Inflow per 10 m tunnel length (l/m)	None	< 10	10 - 25	25 - 125	> 125		
		(Joint water press)/ (Major principal σ)	0	< 0.1	0.1, - 0.2	0.2 - 0.5	> 0.5		
		General conditions	Completely dry	Damp	Wet	Dripping	Flowing		
	Rating		15	10	7	4	0		

B. RATING ADJUSTMENT FOR DISCONTINUITY ORIENTATIONS (See F)						
Strike and dip orientations		Very favourable	Favourable	Fair	Unfavourable	Very Unfavourable
Ratings	Tunnels & mines	0	-2	-5	-10	-12
	Foundations	0	-2	-7	-15	-25
	Slopes	0	-5	-25	-50	

C. ROCK MASS CLASSES DETERMINED FROM TOTAL RATINGS					
Rating	100 ← 81	80 ← 61	60 ← 41	40 ← 21	< 21
Class number	I	II	III	IV	V
Description	Very good rock	Good rock	Fair rock	Poor rock	Very poor rock

D. MEANING OF ROCK CLASSES					
Class number	I	II	III	IV	V
Average stand-up time	20 yrs for 15 m span	1 year for 10 m span	1 week for 5 m span	10 hrs for 2.5 m span	30 min for 1 m span
Cohesion of rock mass (kPa)	> 400	300 - 400	200 - 300	100 - 200	< 100
Friction angle of rock mass (deg)	> 45	35 - 45	25 - 35	15 - 25	< 15

E. GUIDELINES FOR CLASSIFICATION OF DISCONTINUITY conditions					
Discontinuity length (persistence) Rating	< 1 m 6	1 - 3 m 4	3 - 10 m 2	10 - 20 m 1	> 20 m 0
Separation (aperture) Rating	None 6	< 0.1 mm 5	0.1 - 1.0 mm 4	1 - 5 mm 1	> 5 mm 0
Roughness Rating	Very rough 6	Rough 5	Slightly rough 3	Smooth 1	Slickensided 0
Infilling (gouge) Rating	None 6	Hard filling < 5 mm 4	Hard filling > 5 mm 2	Soft filling < 5 mm 2	Soft filling > 5 mm 0
Weathering Ratings	Unweathered 6	Slightly weathered 5	Moderately weathered 3	Highly weathered 1	Decomposed 0

F. EFFECT OF DISCONTINUITY STRIKE AND DIP ORIENTATION IN TUNNELLING**			
Strike perpendicular to tunnel axis		Strike parallel to tunnel axis	
Drive with dip - Dip 45 - 90°	Drive with dip - Dip 20 - 45°	Dip 45 - 90°	Dip 20 - 45°
Very favourable	Favourable	Very unfavourable	Fair
Drive against dip - Dip 45-90°	Drive against dip - Dip 20-45°	Dip 0-20 - Irrespective of strike°	
Fair	Unfavourable	Fair	

Table 4.7: Table of values for the Rock Mass Rating System [E. Hoek, 2006]

According to the score, the rock mass is classified into one of the categories, which determine the tunneling method, stand-up time and the type of support needed. The ratings go from 10 to a 100, with the higher numbers meaning higher quality rock. When this classification method is used, the rock massif is divided into sections (quasi-homogeneous) which are rated separately. These section are usually delimited by faults, discontinuities or changes in rock or soil. In some cases this leads to dissection of the rock massif into very small sections.

Based on experience Bieniawski derived a relationship between RMR- and the Q-index. It was established as:

$$RMR = 9 \ \ln Q + 44 \tag{4.5}$$

and the RMR relationship towards E_{def}, the deformation modulus:

$$E_{def} = 2\ RMR - 100 \tag{4.6}$$

4.4 Q index

Classification of rock mass according to the Quality index was developed by BLLL (Barton,Liem,Lunde,Loset) in the Norwegian Geotechnical Institute in 1974. It is much like the previous methods, an empirical system with 5 parameters and the RQD index, which helps characterise the rock mass and determine the tunnel support required. The Q value varies on a log-scale from 0.001 to 1000. The equation to calculate the Q-index is as follows:

$$Q = \frac{RQD}{J_n} \times \frac{J_r}{J_a} \times \frac{J_w}{SRF} \tag{4.7}$$

Where:

RQD	Rock Quality Designation
J_n	Number of joint systems
J_r	Roughness of joints
J_a	Joint alteration
J_w	Water pressure
SRF	Stress reduction factor

As can be seen equation 4.8 is composed of 3 parts or larger parameters so to say. These are:

RQD/J_n	Degree of jointing or Block size
J_r/J_a	Joint frictions or Inter-block shear strength
J_w/SRF	Active stress

An engineer must have remember that the majority of the case histories are derived from mainly hard, jointed rocks including weakness zones. From soft rocks with few or no joints there are only few examples, and by evaluation of support in such types of rocks, other methods should be considered to be used in addition to the Q-system for support design. It is important to combine application of the Q-system with deformation measurements and numerical simulations in squeezing rock or very weak rock [NGI, 2015].

The Q-index method of classification can include other factors, such as joint orientation, which is used in other classification systems, most notably RMR and RSR, both explained in previous sections. However, with this addition the Q-index method would become less general, although more accurate, and its simplicity would vanish.

DESCRIPTION	VALUE	NOTES	
1. ROCK QUALITY DESIGNATION	*RQD*		
A. Very poor	0 - 25	1. Where *RQD* is reported or measured as ≤ 10 (including 0),	
B. Poor	25 - 50	a nominal value of 10 is used to evaluate *Q*.	
C. Fair	50 - 75		
D. Good	75 - 90	2. *RQD* intervals of 5, i.e. 100, 95, 90 etc. are sufficiently	
E. Excellent	90 - 100	accurate.	
2. JOINT SET NUMBER	J_n		
A. Massive, no or few joints	0.5 - 1.0		
B. One joint set	2		
C. One joint set plus random	3		
D. Two joint sets	4		
E. Two joint sets plus random	6		
F. Three joint sets	9	1. For intersections use ($3.0 \times J_n$)	
G. Three joint sets plus random	12		
H. Four or more joint sets, random, heavily jointed, 'sugar cube', etc.	15	2. For portals use ($2.0 \times J_n$)	
J. Crushed rock, earthlike	20		
3. JOINT ROUGHNESS NUMBER	J_r		
a. Rock wall contact			
b. Rock wall contact before 10 cm shear			
A. Discontinuous joints	4		
B. Rough and irregular, undulating	3		
C. Smooth undulating	2		
D. Slickensided undulating	1.5	1. Add 1.0 if the mean spacing of the relevant joint set is	
E. Rough or irregular, planar	1.5	greater than 3 m.	
F. Smooth, planar	1.0		
G. Slickensided, planar	0.5	2. J_r = 0.5 can be used for planar, slickensided joints having	
c. No rock wall contact when sheared		lineations, provided that the lineations are oriented for	
H. Zones containing clay minerals thick enough to prevent rock wall contact	1.0 (nominal)	minimum strength.	
J. Sandy, gravely or crushed zone thick enough to prevent rock wall contact	1.0 (nominal)		
4. JOINT ALTERATION NUMBER	J_a	ϕ_r degrees (approx.)	
a. Rock wall contact			
A. Tightly healed, hard, non-softening, impermeable filling	0.75		1. Values of ϕ_r, the residual friction angle,
B. Unaltered joint walls, surface staining only	1.0	25 - 35	are intended as an approximate guide to the mineralogical properties of the
C. Slightly altered joint walls, non-softening mineral coatings, sandy particles, clay-free disintegrated rock, etc.	2.0	25 - 30	alteration products, if present.
D. Silty-, or sandy-clay coatings, small clay-fraction (non-softening)	3.0	20 - 25	
E. Softening or low-friction clay mineral coatings, i.e. kaolinite, mica. Also chlorite, talc, gypsum and graphite etc., and small quantities of swelling clays. (Discontinuous coatings, 1 - 2 mm or less)	4.0	8 - 16	

Table 4.8: Table of parameters values for the Q-index system [E. Hoek, 2006]

4. JOINT ALTERATION NUMBER	J_a	ϕ_r degrees (approx.)	
b. Rock wall contact before 10 cm shear			
F. Sandy particles, clay-free, disintegrating rock etc.	4.0	25 - 30	
G. Strongly over-consolidated, non-softening clay mineral fillings (continuous < 5 mm thick)	6.0	16 - 24	
H. Medium or low over-consolidation, softening clay mineral fillings (continuous < 5 mm thick)	8.0	12 - 16	
J. Swelling clay fillings, i.e. montmorillonite, (continuous < 5 mm thick). Values of J_a depend on percent of swelling clay-size particles, and access to water.	8.0 - 12.0	6 - 12	
c. No rock wall contact when sheared			
K. Zones or bands of disintegrated or crushed	6.0		
L. rock and clay (see G, H and J for clay	8.0		
M. conditions)	8.0 - 12.0	6 - 24	
N. Zones or bands of silty- or sandy-clay, small clay fraction, non-softening	5.0		
O. Thick continuous zones or bands of clay	10.0 - 13.0		
P. & R. (see G.H and J for clay conditions)	6.0 - 24.0		
5. JOINT WATER REDUCTION	J_w	approx. water pressure (kgf/cm^2)	
A. Dry excavation or minor inflow i.e. < 5 l/m locally	1.0	< 1.0	
B. Medium inflow or pressure, occasional outwash of joint fillings	0.66	1.0 - 2.5	
C. Large inflow or high pressure in competent rock with unfilled joints	0.5	2.5 - 10.0	1. Factors C to F are crude estimates; increase J_w if drainage installed.
D. Large inflow or high pressure	0.33	2.5 - 10.0	
E. Exceptionally high inflow or pressure at blasting, decaying with time	0.2 - 0.1	> 10	2. Special problems caused by ice formation are not considered.
F. Exceptionally high inflow or pressure	0.1 - 0.05	> 10	
6. STRESS REDUCTION FACTOR		*SRF*	
a. Weakness zones intersecting excavation, which may cause loosening of rock mass when tunnel is excavated			
A. Multiple occurrences of weakness zones containing clay or chemically disintegrated rock, very loose surrounding rock any depth)		10.0	1. Reduce these values of *SRF* by 25 - 50% but only if the relevant shear zones influence do not intersect the excavation
B. Single weakness zones containing clay, or chemically dis-tegrated rock (excavation depth < 50 m)		5.0	
C. Single weakness zones containing clay, or chemically dis-tegrated rock (excavation depth > 50 m)		2.5	
D. Multiple shear zones in competent rock (clay free), loose surrounding rock (any depth)		7.5	
E. Single shear zone in competent rock (clay free). (depth of excavation < 50 m)		5.0	
F. Single shear zone in competent rock (clay free). (depth of excavation > 50 m)		2.5	
G. Loose open joints, heavily jointed or 'sugar cube', (any depth)		5.0	

Table 4.9: Table of parameters values for the Q-index system [E. Hoek, 2006]

DESCRIPTION	VALUE			NOTES
6. STRESS REDUCTION FACTOR			*SRF*	
b. Competent rock, rock stress problems				
	σ_c/σ_1	σ_t/σ_1		2. For strongly anisotropic virgin stress field (if measured): when $5 \leq \sigma_1/\sigma_3 \leq 10$, reduce σ_c to $0.8\sigma_c$ and σ_t to $0.8\sigma_t$. When $\sigma_1/\sigma_3 > 10$, reduce σ_c and σ_t to $0.6\sigma_c$ and $0.6\sigma_t$, where σ_c = unconfined compressive strength, and σ_t = tensile strength (point load) and σ_1 and σ_3 are the major and minor principal stresses.
H. Low stress, near surface	> 200	> 13	2.5	
J. Medium stress	200 - 10	13 - 0.66	1.0	
K. High stress, very tight structure (usually favourable to stability, may be unfavourable to wall stability)	10 - 5	0.66 - 0.33	0.5 - 2	
L. Mild rockburst (massive rock)	5 - 2.5	0.33 - 0.16	5 - 10	
M. Heavy rockburst (massive rock)	< 2.5	< 0.16	10 - 20	3. Few case records available where depth of crown below surface is less than span width. Suggest *SRF* increase from 2.5 to 5 for such cases (see H).
c. Squeezing rock, plastic flow of incompetent rock under influence of high rock pressure				
N. Mild squeezing rock pressure			5 - 10	
O. Heavy squeezing rock pressure			10 - 20	
d. Swelling rock, chemical swelling activity depending on presence of water				
P. Mild swelling rock pressure			5 - 10	
R. Heavy swelling rock pressure			10 - 15	

ADDITIONAL NOTES ON THE USE OF THESE TABLES

When making estimates of the rock mass Quality (*Q*), the following guidelines should be followed in addition to the notes listed in the tables:

1. When borehole core is unavailable, *RQD* can be estimated from the number of joints per unit volume, in which the number of joints per metre for each joint set are added. A simple relationship can be used to convert this number to *RQD* for the case of clay free rock masses: $RQD = 115 - 3.3\,J_v$ (approx.), where J_v = total number of joints per m^3 ($0 < RQD < 100$ for $35 > J_v > 4.5$).
2. The parameter J_n representing the number of joint sets will often be affected by foliation, schistosity, slaty cleavage or bedding etc. If strongly developed, these parallel 'joints' should obviously be counted as a complete joint set. However, if there are few 'joints' visible, or if only occasional breaks in the core are due to these features, then it will be more appropriate to count them as 'random' joints when evaluating J_n.
3. The parameters J_r and J_a (representing shear strength) should be relevant to the weakest significant joint set or clay filled discontinuity in the given zone. However, if the joint set or discontinuity with the minimum value of J_r/J_a is favourably oriented for stability, then a second, less favourably oriented joint set or discontinuity may sometimes be more significant, and its higher value of J_r/J_a should be used when evaluating *Q*. The value of J_r/J_a should in fact relate to the surface most likely to allow failure to initiate.
4. When a rock mass contains clay, the factor *SRF* appropriate to loosening loads should be evaluated. In such cases the strength of the intact rock is of little interest. However, when jointing is minimal and clay is completely absent, the strength of the intact rock may become the weakest link, and the stability will then depend on the ratio rock-stress/rock-strength. A strongly anisotropic stress field is unfavourable for stability and is roughly accounted for as in note 2 in the table for stress reduction factor evaluation.
5. The compressive and tensile strengths (σ_c and σ_t) of the intact rock should be evaluated in the saturated condition if this is appropriate to the present and future in situ conditions. A very conservative estimate of the strength should be made for those rocks that deteriorate when exposed to moist or saturated conditions.

Table 4.10: Table of parameters values for the Q-index system [E. Hoek, 2006]

In order to determine the needed support using the Q-index, the Equivalent Dimension *De* of the excavation is needed. This value is based on two more parameters, and the relationship is presented as:

$$D_e = \frac{Span\ or\ Height\ [m]}{ESR} \tag{4.8}$$

Where:

ESR	Excavation Support Ratio

The *ESR* represents the safety needed in the tunnel. For example a road tunnel needs a higher safety than a water tunnel, hence the ESR is lower for the former and higher for the latter. The full table of ESR values is listed in table 4.11 below:

Excavation category	ESR
Category A - Temporary mine opening	3-5
Category B - Permanent mine opening, water tunnels	1.6
Category C - Storage rooms, Water treatment plants, etc.	1.3
Category D - Power stations, major road and railway tunnels, etc.	1.0
Category E - Underground nuclear power stations, railway stations, etc.	0.8

Table 4.11: Rock mass quality classification by the RQD method

The calculated equivalent dimension D_e using equation 4.8 is subsequently plotted against the Q-index, and using a predefined chart, the support category can be established. The table has been modified since originally published to account for the use of FRC in modern tunneling. The updated chart is pictured on figure 4.5 below:

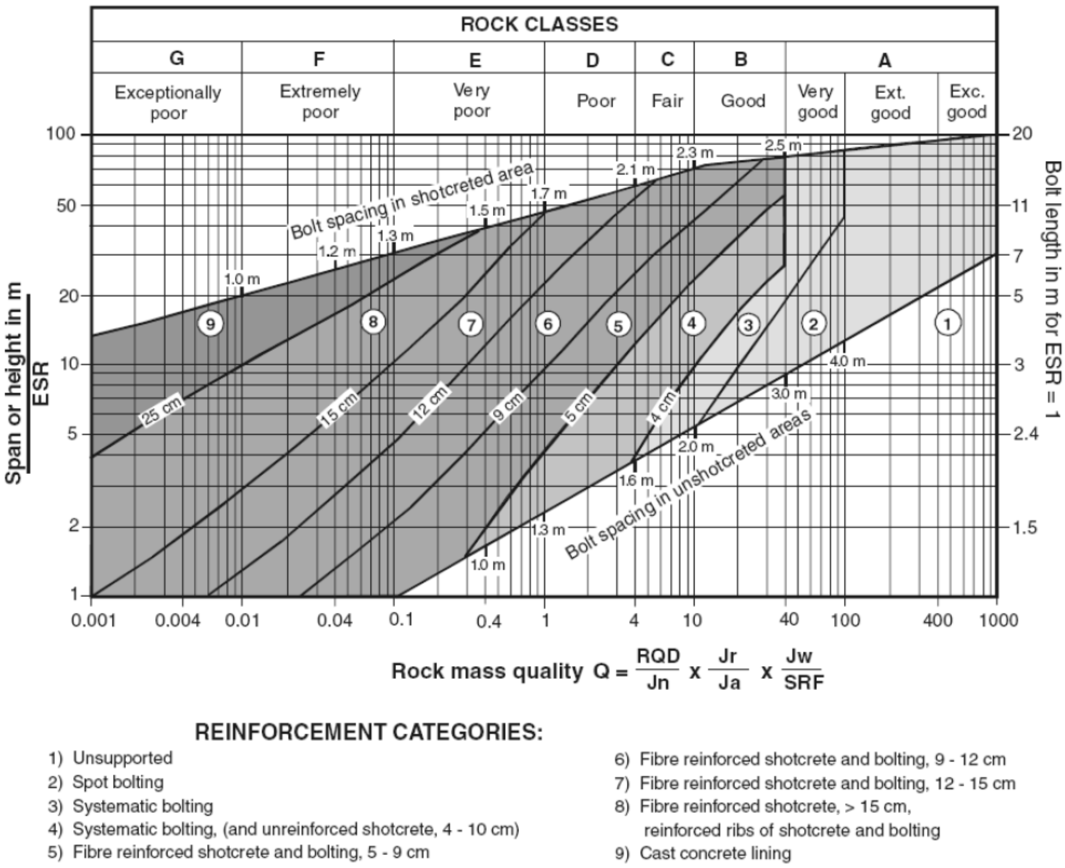

Figure 4.5: Chart of rock mass classification according to the Quality index method [E. Hoek, 2006]

Additional information was added to the method by Barton in 1980, when relationships for rock bolt length, maximum span length and roof support pressures. These are respectively stated as:

$$L = 2 + \frac{0.15\,B}{ESR} \tag{4.9}$$

$$Span_{max} = 2\ ESR\ Q^4 \tag{4.10}$$

$$P_{roof} = \frac{2\ \sqrt{J_n}\ Q^{\frac{1}{3}}}{3\ J_r} \tag{4.11}$$

These additions to the original system make the Q-index method very versatile and fairly obvious why it has become so popular and useful in tunnel engineering.

4.5 Uses

In tunnel engineering two methods of rock mass classification dominate. These are the RMR developed by Bienawski and the Q-system derived by Barton. The two methods have a lot of similarities, such as including the geology, geometry, but also design parameters and arriving at a quantitative value of rock mass quality [E. Hoek, 2006]. There are however some minor differences which separate the two, and give the engineer a different look at the rock mass. The different weights of the evaluated parameters, RMR using direct compressive strength, while the Q-system uses it only in reference to the in-situ stresses and the Q-system not considering geometry of the joints in the same way as RSR are some of the distinctions. The biggest distinction however, is the fact that RSR does not use a stress parameter, which is used in the Q-system as the SRF from equation 4.8.

When using the rock mass classification methods, it is suggested to first characterise the rock mass generally, and only then to assign the parameter ratings. The benefit of of this system is the complete and complex characterisation of the rock mass, along with the possibility to verify the classification work done. Another recommendation is to not specify only the mean values for the parameters, but rather use a range of observations/results. This way it is possible to not only know the dominating conditions, but also to be prepared for the conditions that may arise during the tunneling works. Histograms of the quasi-homogeneous zones are suggested for use.

It must also be noted as in previous sections, that at least two methods should be used to classify the rock mass. This side by side comparison give the engineer a better picture of the geological and hydro-geological conditions present on site.

5. Analytical methods

The purpose of this chapter is to introduce the concept of primary and secondary stress states in rock masses, and to briefly explain the concept of Passive earth pressure. Analytical solutions of deformations of the rock mass and the stresses exerted on the tunnel by the rock mass are also presented along with the solutions based on the Fenner-Pacher curves. All results are presented at the end of the chapter.

There are many analytical methods and theories that were developed in order to provide a safe and quick design of forces and the expected deformations in the lining of the tunnel. They are essential to understanding the behaviour of the rock mass or soil around the tunnel structure along with the structure itself. In recent times, these analytical solutions were displaced as the main calculation procedure by FEM models. However, these simple and somewhat reliable techniques are still used to verify the numerical models, and for teaching purposes for understanding of the tunnel behaviour. Nonetheless, before one can venture into the analytical solutions, understanding of stress states in rock mass is necessary.

5.1 Primary Stress State

Primary stress, produced by the massive acting as an elastic continuum is commonly described as the initial stress state of the undisturbed rock massive. These stresses can also be caused by swelling of the rock mass or thermal expansion/contraction. The primary stresses state can be divided into gravitational and tectonic, which is further subdivided into recent (rock mass forces), residual (overconsolidation) and swelling. Assuming the rock mass or soil is a continuum only loaded by its self-weight and obeys Hooke's law (elastic material) the vertical and horizontal gravitational stresses as calculated as such:

$$\begin{aligned} \sigma_z &= \gamma h \\ \sigma_x &= K_0 \sigma_z \end{aligned} \tag{5.1}$$

Where:

γ	Soil unit weight
h	Overburden height
K_0	Lateral earth coefficient
σ_z	Vertical stress

When dealing with a rock mass, the lateral earth coefficient is calculated in the following manner:

$$K_0 = \frac{\nu}{1-\nu} \tag{5.2}$$

Where:

ν	Poisson's ratio

However, if the structure is founded in soils, rather than intact rock, the calculation of the Lateral earth coefficient changes.

$$K_0 = 1 - \sin\phi \tag{5.3}$$

Where:

ϕ	Friction angle [°]

If in the overburden in the massive, more than one layer is found, the vertical stresses are found as:

$$\sigma_z = \sum_i^h \gamma_i h_i \tag{5.4}$$

A massive is non-homogeneous mixture of rock masses and soils, with different weathering and discontinuities. Therefore it is necessary to take this and the caused anisotropy into account. For this reason it is hard to determine the primary stress state through analytical solutions, and rather complex numerical models, with discontinuities and varying inclination of the layers, are used.

5.2 Secondary stress State

By disturbing the primary stress state which was in equilibrium, due to the tunnel excavation, deformations around the tunnel edge occur and force the stresses into a different state - secondary stress state. This change is visible in the forms of isolines near the tunnel face. A solution to this problem of a changed stress state, is possible through the use of an analytical solution with the assumptions of homogeneous isotropic and elastic material, where the excavated tunnel is circular.

5.2.1 Unilateral stress

For the calculation of plane stress in the surrounding of the tunnel a compatibility function, also nown as the Airy stress function, F is stated in polar coordinates as such:

$$F_z = \frac{\sigma_z}{4}\left(r^2 - 2r_0^2 \ln r + \frac{(r^2 - r_0^2)^2}{r^2}\cos 2\theta\right) \tag{5.5}$$

Where:

σ_z	principal vertical stress
r,ω	polar coordinates of point of interest
r_0	tunnel radius

$$\Delta F = \frac{\partial^2 F}{\partial r^2} + \frac{1}{r^2}\frac{\partial F}{\partial r^2} + \frac{1}{r}\frac{\partial^2 F}{\partial r} \tag{5.6}$$

Through the derivation of the equation 5.5 according to 5.6, the stresses around the excavated profile can be calculated.

$$\begin{aligned}
\sigma_\theta &= \frac{1}{2}\sigma_z\left(1+\frac{r_0^2}{r^2}-\left(1+3\frac{r_0^4}{r^4}\right)\cos 2\theta\right) \\
\sigma_r &= \frac{1}{2}\sigma_z\left(1+\frac{r_0^2}{r^2}-\left(1-4\frac{r_0^2}{r^2}+3\frac{r_0^4}{r^4}\right)\cos 2\theta\right) \\
\tau &= \frac{1}{2}\sigma_z\left(1+2\frac{r_0^2}{r^2}-3\frac{r_0^4}{r^4}\cos 2\theta\right)
\end{aligned} \tag{5.7}$$

Where the unknowns is the equations are given in figure 5.1 below:

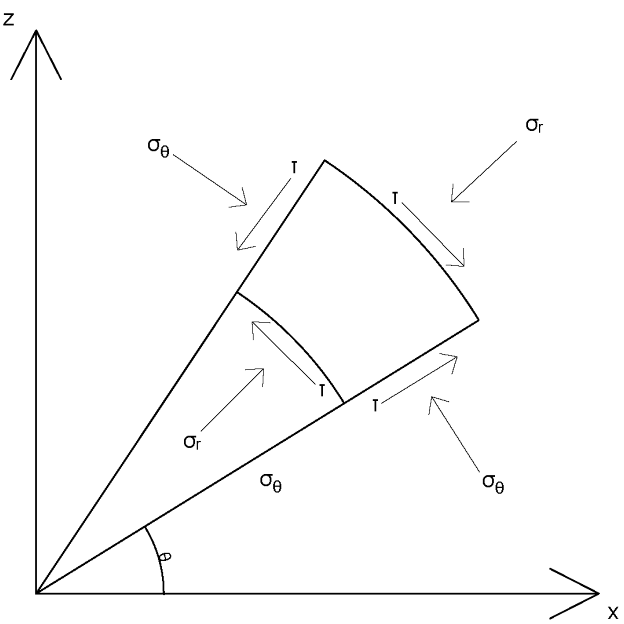

Figure 5.1: Airy's stresses shown in polar coordinates

5.2.2 Bilateral stress

The magnitude and the stress development around the tunnel, exposed to principal stresses (stress field of σ_z and σ_x) is given by the superposition, where two unilateral solutions are combined to give the complete solution.

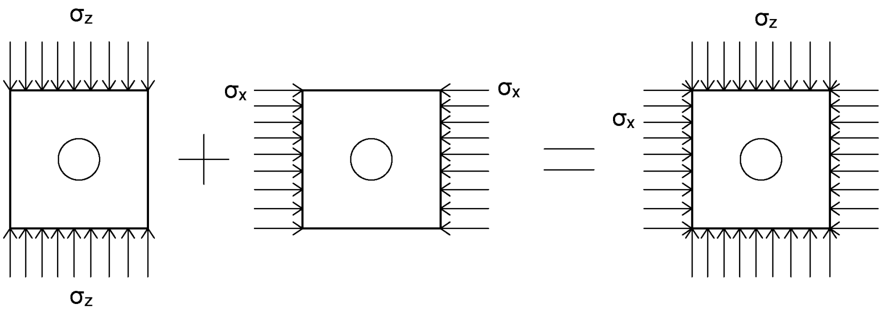

Figure 5.2: Superposition used to solve complex problems using basic solutions

This means the solution to the stresses at a given location are:

$$\begin{aligned}
&\sigma_\theta = \sigma_\theta^z + \sigma_\theta^x = \left(1+\frac{r_0^2}{r^2}\right)\frac{\sigma_z+\sigma_x}{2} + \frac{\sigma_z-\sigma_x}{2}\left(1+3\frac{r_0^4}{r^4}\right)\cos 2\theta \\
&\sigma_r = \sigma_r^z + \sigma_r^x = \left(1-\frac{r_0^2}{r^2}\right)\frac{\sigma_z+\sigma_x}{2} - \frac{\sigma_z-\sigma_x}{2}\left(1-4\frac{r_0^2}{r^2}+3\frac{r_0^4}{r^4}\right)\cos 2\theta \\
&\tau = \frac{\sigma_z+\sigma_x}{2}\left(1+2\frac{r_0^2}{r^2}-3\frac{r_0^4}{r^4}\right)\sin 2\theta
\end{aligned} \tag{5.8}$$

Where:

σ_z, σ_x	principal stresses
r, ω	polar coordinates of point of interest
r_0	tunnel radius

5.2.3 Changing load stress

If however, like in tunneling, the principal stresses change with the depth of the overburden, the above mentioned superposition does not apply. Superposition is once again used, but this time, the initial stress state and the disturbed (secondary) stress states are combined, and a close to exact solution is achieved.

The original primary stress state in Cartesian coordinate system is expressed as:

$$\begin{aligned}
&\sigma_{x0} = K_0\sigma_z\left(1-\frac{z}{H}\right) \\
&\sigma_{z0} = \sigma_z\left(1-\frac{z}{H}\right) \\
&\tau_{xz0} = 0
\end{aligned} \tag{5.9}$$

Once the stresses are transformed from Cartesian coordinate system to Polar coordinates, an expression for the stresses considering the changing principal stresses due to the overburden is achieved.

$$\sigma_r = \frac{\gamma(H - r_0\cos\theta)}{2}\Bigg(\Big(1-\frac{r_0^2}{r^2}\Big)(1+K_0) + \Big(1 - 4\frac{r_0^2}{r^2} + 3\frac{r_0^4}{r^4}\Big)(1-K_0)\cos 2\theta - \tag{5.10}$$
$$\frac{2(r\cos\theta - r_0\cos\theta)}{H - r_0\cos\theta}(K_0\sin^2\theta + \cos^2\theta)\Bigg)$$
$$\sigma_\theta = \frac{\gamma(H - r_0\cos\theta)}{2}\Bigg(\Big(1-\frac{r_0^2}{r^2}\Big)(1+K_0) + \Big(1 + 3\frac{r_0^4}{r^4}\Big)(1-K_0)\cos 2\theta -$$
$$\frac{2(r\cos\theta - r_0\cos\theta)}{H - r_0\cos\theta}(K_0\cos^2\theta + \sin^2\theta)\Bigg)$$
$$\tau = \frac{\gamma(H - r_0\cos\theta)}{2}\Bigg(\Big(1 + 2\frac{r_0^2}{r^2} - 3\frac{r_0^4}{r^4}\Big)(1-K_0)\cos 2\theta - \frac{2(r\cos\theta - r_0\cos\theta)}{H - r_0\cos\theta}(K_0\sin^2\theta + \cos^2\theta)\Bigg)$$

Where:

σ_z,σ_x	principal stresses
H	overburden - from centre of tunnel to surface
K_0	horizontal earth coefficient
r,θ	polar coordinates of point of interest
r_0	tunnel radius

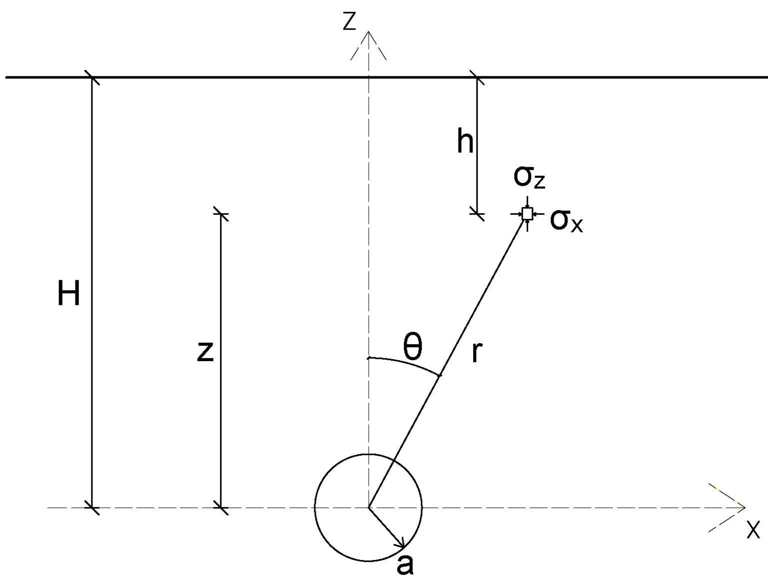

Figure 5.3: Solution for stresses with changing principal stresses

5.2.4 Plasticity

Understandably, in tunneling and geotechnics, plasticity is encountered on a regular basis. From this follows, that plastic calculation using analytical solutions were developed, although always with simplifications and assumptions. In this case, it is still a circular excavated profile of radius

r_0, with a hydrostatic stress state, due to which a circular plastic zone of radius R develops. This theory considers the maximum shear stress criterion otherwise know as the Tresca criterion:

$$\frac{\sigma_{\theta p} - \sigma_{rp}}{2} = \frac{\sigma_c}{2} \tag{5.11}$$

Where:

$\sigma_{\theta p}$	tangential stress in the plastic zone
σ_{rp}	radial stress in the plastic zone
σ_c	compressive strength of the rock mass

The equilibrium equation considering the given condition above can be rewritten as:

$$\frac{\partial \sigma_{rp}}{\partial r} + \frac{\sigma_{rp} - \sigma_{\theta p}}{r} = 0 \tag{5.12}$$

Where:

r	length of vector in polar coordinates

From the Tresca criterion the tangential stress $\sigma_{\theta p}$ in the plastic zone is derived, and inserted into the equilibrium equation 5.12. Once the integration constants have been found, the relationships for stresses in the plastic zone ($r_0 \leq r \leq R$) can be written as:

$$\begin{aligned} \sigma_{rp} &= \sigma_c \ln \frac{r}{r_0} \\ \sigma_{\theta p} &= \sigma_c (1 + \ln \frac{r}{r_0}) \end{aligned} \tag{5.13}$$

The radius of the plastic zone and the stresses in the elastic zone are then determined by:

$$\begin{aligned} R &= r_0 e^{\frac{2\sigma - \sigma_c}{2\sigma_c}} \\ \sigma_{rp} &= \left(1 + \frac{R^2}{r^2}\right)\sigma + \left(\sigma_c \ln \frac{R}{r_0}\right)\frac{R^2}{r^2} \\ \sigma_\theta &= \left(1 - \frac{R^2}{r^2}\right)\sigma - \left(\sigma_c \ln \frac{R}{r_0}\right)\frac{R^2}{r^2} \end{aligned} \tag{5.14}$$

Where:

σ_z	primary vertical stress in the middle of the excavation face

5.3 Deformations of rock mass

Force application and deformations of the rock mass can be described by a function of a number of changing parameters, which describe the action of the loading, conditions of mechanical changes and the effect of rock mass characteristics. This function can be generally written as:

$$F\left(\sigma,\varepsilon,\frac{\partial\varepsilon}{\partial t},\frac{\partial^2\varepsilon}{\partial t\partial r},\frac{\partial^2\varepsilon}{\partial r^2},\frac{\partial\sigma}{\partial r},\frac{\partial^2\sigma}{\partial r^2}\zeta,t,T,\phi,P_0\right)=0 \tag{5.15}$$

Where:

σ	stress
ε	strain
$\frac{\partial\varepsilon}{\partial t}$	deformation speed
$\frac{\partial^2\varepsilon}{\partial t^2}$	deformation acceleration (change of speed)
$\frac{\partial^2\varepsilon}{\partial t\partial r}$	local acceleration of deformation
$\frac{\partial\sigma}{\partial r}$	stress gradient
$\frac{\partial^2\sigma}{\partial r^2}$	change of stress gradient
ζ	type of loading
t	time
T	temperature
ϕ	mechanical modulus of rock mass (friction angle)
P_0	initial state of deformation

It is clear that equation 5.15 is very complex, and contains too many physical-mechanical processes, which are defined by a lot of parameters, therefore, in practice a simplified function of the deformations is used:

$$F\left(\sigma,\varepsilon,\frac{\partial\varepsilon}{\partial t},\zeta,t,\phi,P_0\right)=0 \tag{5.16}$$

According the the magnitude of stress, deformations are classified in general into 3 categories, which are similar to the ones described in figure3.8. First type of deformations are observed when the stresses in the rock mass are smaller than the long term strength of the rock mass σ_∞ (regarded as 60% of the instantaneous strength). These absolute deformations reach maximum values of ca. 50-60 mm. Second type of deformations happen when the stresses in the rock mass reach a level between the long term and instantaneous rock mass strength. Absolute displacements of up to 200 mm can be registered. The third type of deformations are deformations in the critical state, when the instantaneous strength of the rock mass is exceeded, and displacements larger than 200 mm can be observed on the tunnel walls or crown.

There are numerous theories regarding elastic deformations of circular profiles. Nonetheless, solutions according to Kastner and Obert-Duvall are presented below.

5.3.1 Kastner's Solution

Kastner based his solution in 1962 on Hooke's law and knowledge of stresses around the face of a tunnel, and derived the equations for the deformations of the crown and the walls of a circular tunnel section. The deformations of the tunnel crown are calculated

$$w = \int_a^\infty \Delta dr = \frac{1}{E}\int_a^\infty \left((\sigma_z - \sigma_{r0}) - \frac{1}{m}(\sigma_x - \sigma_{t0})dr\right) \tag{5.17}$$

Where:

σ_{r0}, σ_{t0}	normal stress at $\phi = 90°$
σ_{r1}, σ_{t1}	normal stress at $\phi = 0°$
σ_z	vertical stress
σ_x	horizontal stress
E	modulus of elasticity
m	Poisson's constant $\frac{1}{\nu}$
r_0	radius of tunnel

$$w = \frac{\sigma_z r_0}{E}\frac{2m^2 - 3m + 1}{m(m-1)} \tag{5.18}$$

The deformations of the walls of the tunnel are similarly derived and have the form of equation 5.19. It is however recommended to be used for profiles with larger radii.

$$u = \int_{r_0}^\infty \Delta dr = \frac{1}{E}\int_{r_0}^\infty \left((\sigma_x - \sigma_{r1}) - \frac{1}{m}(\sigma_z - \sigma_{t1})dr\right) \tag{5.19}$$

Once simplified, the equation looks as:

$$u = \frac{\sigma_z r_0}{E}\frac{m^2 - 4m + 1}{m(m-1)} \tag{5.20}$$

5.3.2 Obert and Duvall's Solution

Obert and Duvall derived their analytical solution in 1967. The radial and tangential deformations of the excavated tunnel are assumed to follow a linear behaviour, and the problem has to be simplified to a 2D problem. The solution is achieved through integration of equations for stresses and deformations in polar coordinates [Obert and Duvall, 1967].

$$\begin{aligned}
\frac{\partial u}{\partial r} &= \frac{1}{E}\sigma_\theta(1-\nu^2)\sigma - \nu(1+\nu) \\
\frac{u}{r} + \frac{1}{r}\frac{\partial v}{\partial \theta} &= \frac{1}{E}(1-\nu^2)\sigma_\theta - \nu(1+\nu)\sigma_r
\end{aligned} \tag{5.21}$$

Where:

u	radial displacement
v	tangential displacement
σ_r, σ_θ	normal stresses
r, θ	polar coordinates
ν	Poisson's constant

Substituting the equations for the stresses in polar coordinated into equation 5.21, and its later integration yields the following relationships:

$$\begin{aligned} u = {} & \frac{1-\nu^2}{E}\left(\left(\frac{\sigma_x+\sigma_y}{2}\right)\left(r+\frac{r_0^2}{r}\right)+\left(\left(\frac{\sigma_x-\sigma_y}{2}\right)\left(r-\frac{r_0^4}{r^3}+\frac{4r_0^2}{r}\right)\cos 2\theta\right)- \right. \\ & \frac{\nu(1-\nu)}{E}\left(\left(\frac{\sigma_x+\sigma_y}{2}\right)\left(r+\frac{r_0^2}{r}\right)-\left(\left(\frac{\sigma_x-\sigma_y}{2}\right)\left(r+\frac{r_0^4}{r^3}\right)2\cos 2\theta\right) \\ v = {} & \frac{1-\nu^2}{E}\left(-\left(\frac{\sigma_x-\sigma_y}{2}\right)\left(r+\frac{2r_0^2}{r}+\frac{r_0^4}{r^3}\right)\sin 2\theta\right)-\frac{\nu(1-\nu)}{E}\left(-\left(\frac{\sigma_x-\sigma_y}{2}\right)\left(r-\frac{2r_0^2}{r}+\frac{r_0^4}{r^3}\right)\sin 2\theta\right) \end{aligned} \tag{5.22}$$

Where:

r_0	radius of the tunnel

Perhaps the most interesting position of the deformations are in the tunnel crown and walls directly, and not in the rock mass behind them. This means that $a = r$, and equation 5.22 can be simplified into:

$$v = \frac{1-\nu^2}{E}\left(2r_0(\sigma_x-\sigma_y)\sin 2\theta\right) \tag{5.23}$$

From the equation 5.23 above, it is seen that the deformations depend on the same parameters as in the solution derived by Kastner, namely E, σ_x ,σ_y, ν and a. The difference of the Obert-Duvall solution to Kastner's, is the possibility to calculate the displacements at any position in the rock mass. This solution however, is based on the Hooke's law and the principle of elastic deformations of a plate with a hole, which uses the elastic modulus, E. In reality though, the interest lies purely in the deformations caused by the lowering of stresses at the face of the excavation. Once the values of displacements of the intact rock mass (which develop some distance ahead of the face) and considering the deformations due to the stress dissipation at the face, an equation giving more realistic deformations is obtained. Hence the deformations at the tunnel wall and crown are calculated using:

$$u_r = \frac{r_0\sigma_z}{4G}\left((1+K_0)\frac{r_0^2}{r^2}+(1-K_0)\cos 2\theta\left(\frac{4r_0^2}{r^2}-\frac{3r_0^4}{r^4}-\frac{4\nu r_0^2}{r^2}\right)\right) \tag{5.24}$$

Where:

G	shear modulus
K_0	coefficient of horizontal earth
θ	angle of point of interest running clockwise from the vertical from middle to crown

5.4 Rock pressure theories

Theories of rock mass stresses on tunnel constructions began developing during the start of the tunneling boom in Switzerland, in the second half of the 19$^{\text{th}}$ century. The first theories began developing in the 70s and 80s, with the major role played by Prof. W. Ritter. During and after the construction of the second Simplon tunnel connecting Switzerland and Italy, theories considering active and passive earth pressure were developed. It was observed that unlike in fluids or shallow soils, the earth pressure does not develop the same way in slid rock [Pruška, 2000]. In tunnels with overburdens of 500 m and more, it is most evident as these structures would not be able to withstand these enormous pressures.

Changes in pressure in the rock massive due to the excavation of a tunnel, were described through a process of zonal disintegration phenomenon. This is caused by the pressures exceeding the strength of the rock mass, causing an imbalance, forcing the rock mass at the excavation to deform or loosen. The stresses in this plastic zone however, never reach the surrounding pressures, meaning a zone with lower pressures is created around the tunnel, a so called Trompeter's zone (see figure 5.4), named after W. H. Trompeter, due to his theory from 1899. Around this zone a zone with increased pressures can be found. End of that zone is the boundary of influence of the tunnel construction on the rock massive.

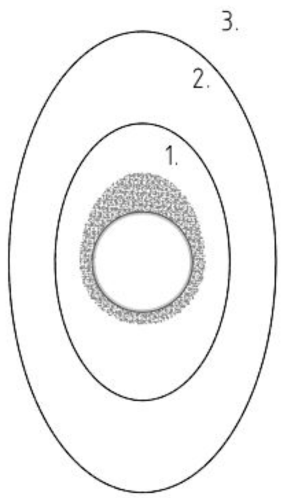

Figure 5.4: Ellipse showing the ground loosening zone according to W. H. Trompeter (1899) also known as the Trompeter zone

This ellipsoidal and zonal concept was used in many other theories derived after 1899. These became known as classical arch theories.

5.4.1 Classical arch theories

These empirical or semi-empirical methods all rely on the so-called loosening zone described above. Each theory however, assumes a different shape and size of the zone, depending on the assumptions made at the start. Classical arch theories though, can be further subdivided into two categories. Into theories which consider the overburden height and the ones which do not.

Kommerell's theory

Kommerell's theory is categorised as a classical arch theory that does not take into account the overburden height. This means there is no relationship between the overburden and the force or the pressure on the excavated tunnel. This simplification means that only the weight of the volume in the zone above the tunnel acts upon it.

The oldest and most widely known of these theories is that developed by Kommerell, who determined the height of the loading body from the deformations of the supporting structure in the opening [Szechy, 1973].

$$
\begin{aligned}
e &= \frac{h\delta}{100} \\
h &= \frac{100e}{\delta}
\end{aligned}
\tag{5.25}
$$

Where:

h	height of the ellipse
e	deformation height by loosening
δ	loosening coefficient (see table 5.1)

The loosening coefficient, δ, for the different soils or rock masses, are given empirically as:

Type of rock or soil	δ[%]
Loose granular soil (sand)	1-3
Moderately cohesive soil (dry clay)	3-5
Cohesive soil (marl, gravely clay)	5-8
Soft rocks (sandstone, limestone)	8-12
Solid, hard rocks	10-15

Table 5.1: Loosening coefficients by soil/rock type according to Kommerell

$$
\frac{x^2}{(b/2)^2} + \frac{y^2}{h^2} = 1 \tag{5.26}
$$

So it follows if equation 5.25 is substituted into expression 5.26 above, the following relationship is derived:

$$\frac{4x^2}{b^2} + \frac{y^2\delta^2}{10000^2} = 1 \tag{5.27}$$

Once the are of the loosening zone is known, the total load on the tunnel, once simplified, can be calculated as:

$$P = \gamma\,(Area\ of\ half\ ellipse) = \frac{25\gamma\pi be}{\delta} \tag{5.28}$$

Nonetheless, Kommerell's theory can and should only be used as a rough approximation due to a couple reasons. The first being that loosening is possible in granular soils or crushed rocks, whereas loosening is impossible in bulk solid rocks. The respective deflections of the bulk rock are much smaller than those of granular or crushed rock, which causes inaccuracies in the results. Secondly, linear relationship is assumed to exist between the deflection of the roof (e) and the height (h) of the loading mass. This relationship is purely empirical and cannot be verified by other models of experiments, hence it can deviate from reality.

Another disadvantage of the theory is the application to only flat roof tunnels mostly present in mines rather than road tunnels such as Višňové.

Fenner's theory

Fenner's theory from 1938, assumes an elliptical pressure zone, much like other theories belonging to the classical arch theories, with the boundary described by the following expressions:

$$\frac{4x^2}{(m-2)^2b^2} + \frac{y^2}{b^2} = 1 \qquad or \qquad \frac{x^2}{\left(\frac{m-2}{2}\right)^2 b^2} + \frac{y^2}{b^2} = 1 \tag{5.29}$$

Where:

m	Poisson's constant $(1/\nu)$
b	tunnel width

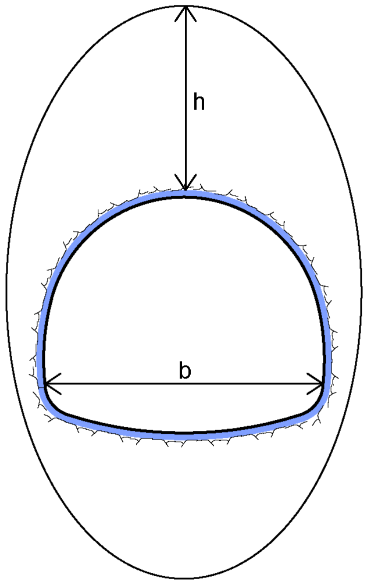

Figure 5.5: Ellipse showing the boundary of plastic deformations or ground loosening according to R. Fenner (1938)

The theory is based on loosening ground, and the same foundations used in this theory are applied to the Fenner-Pacher curves described in section 5.5. The stress in the upper and lower ends of the ellipse completely disappear, on the other hand the stresses in the sides of the ellipse (see figure 5.5) are maximal and are given by:

$$\sigma_{\tau max} = \frac{m^2}{(m-2)(m-1)} p \tag{5.30}$$

Where p is the pressure at the boundary of the plastic zone described by the ellipse and is given by the following relationship:

$$p = \frac{ha\gamma}{2r} - \frac{a\gamma}{2} + a\gamma \ln \frac{r}{a} \tag{5.31}$$

Where:

h	overburden height
a	tunnel radius
r	radius of plastic zone given by $0.5h(\frac{2}{1-\sin\phi} - 2)$
γ	tunnel width

The maximum pressure in the rock arch are found by the expression:

$$p_{max} = \frac{m^2}{(m-2)(m-1)} p \tag{5.32}$$

Where:

p | original overburden pressure ($p = \sigma z$)

Bierbäumer's theory

Bierbäumer's theory was developed during the construction of the great Alpine tunnels [Szechy, 1973], according to which the load on the tunnel is caused by the so-called loosening zone bounded by a parabola, whose height can be determined by:

$$h = \alpha H \tag{5.33}$$

Where:

α | reduction coefficient

And the shape of the loosening zone or the "pressure bulb" in figure 5.33 below.

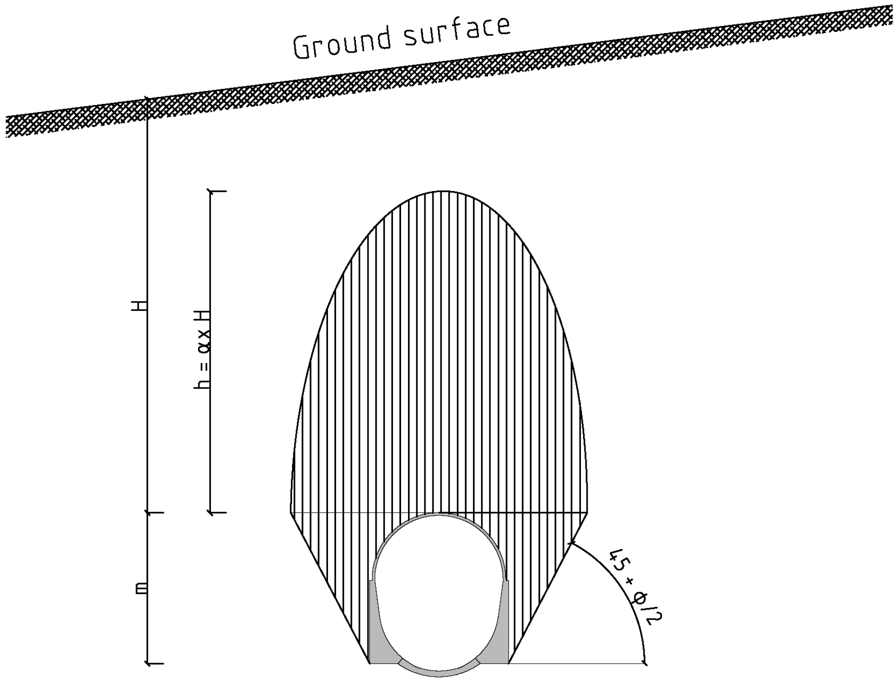

Figure 5.6: The loosening zone according to Bierbäumer

The approach to estimate the "reduction coefficient", α, is based on the assumption that the once the tunnel is excavated, the loosening material slides down along rupture planes. These can be seen in figure 5.7, where the weight of the soil in the loosening zone was countered by the friction force, at vertical sliding planes. This friction force can be calculated as:

$$S = fE = \tan\phi\left(\tan^2\left(45^\circ - \frac{\phi}{2}\right)\right)\frac{H^2\gamma}{2} = H^2\gamma\tan\phi\left(\tan^2\left(45^\circ - \frac{\phi}{2}\right)\right) \tag{5.34}$$

Where:

f	coefficient of friction = $\tan\phi$
ϕ	friction angle of rock mass
E	normal force acting on vertical sliding planes (areas of triangles DFB' and ECA' in figure 5.7
K_a	Rankine's active ratio = $\tan(45-\phi/2)$
γ	specific weight of soil
H	tunnel overburden (GS to crown)

$$W = \gamma\, Area\ of\ A'B'DC = HB\gamma = \left(b + 2m\tan\left(45^\circ - \frac{\phi}{2}\right)\right) \tag{5.35}$$

Where:

m	height of the tunnel opening
b	width of the tunnel opening
B	distance between the two sliding planes at the crown

As $P = W - 2S$, it follows that by substituting equations 5.34 and 5.34, we get:

$$P = H\gamma\left(b + 2m\tan\left(45^\circ - \frac{\phi}{2}\right)\right) - H^2\gamma\tan\phi\left(\tan^2\left(45^\circ - \frac{\phi}{2}\right)\right) \tag{5.36}$$

Once the load is calculated, the pressure on the crown of the tunnel is derived easily by dividing the load by the length B. Since all equations are in unit length, pressure in MPa is calculated as:

$$p = \frac{P}{B} = H\gamma\alpha = H\gamma\left(1 - \frac{H\tan\phi\tan^2(45^\circ - \phi/2)}{b + 2m\tan(45^\circ - \phi/2)}\right) \tag{5.37}$$

However Bierbäumer specified, if the overburden is larger than a couple hundred meters, more precisely if H > 5B, then the reduction factor, α, is not dependent on the overburden height, and is calculated as such:

$$\alpha = \tan^4\left(45^\circ - \frac{\phi}{2}\right) \tag{5.38}$$

Hence it can be seen that the whole height of the overburden, H, does not act on the tunnel, but only a reduced height, h, as is described in 5.33. The reason is the friction from the two "wedges" on figure 5.7, which is the so-called "arching effect" described in most of the tunneling literature.

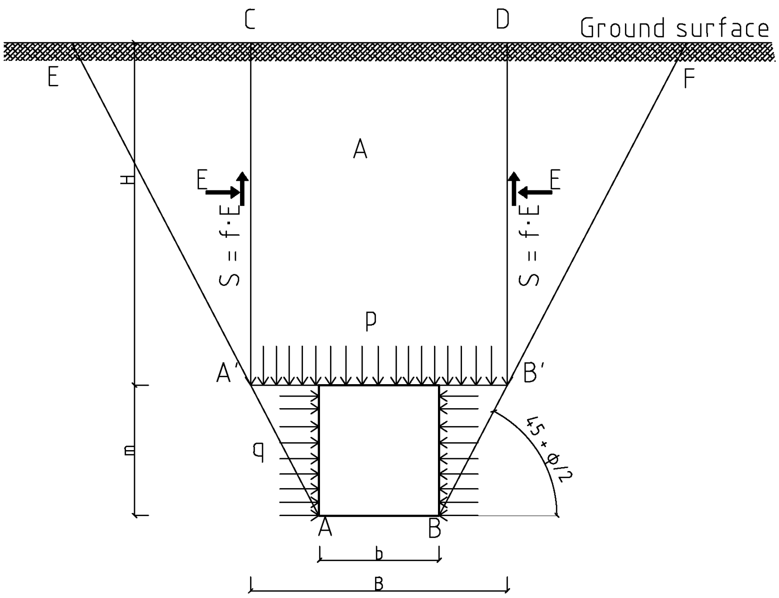

Figure 5.7: Assumption model of Bierbäumer's theory for the Maximum load

Other than the theory above, which Bierbäumer described as the maximum load on the tunnel crown. He also derived a simple minimum load applied onto the tunnel, it is of lower importance however. It should also be noted that Bierbäumer's theory could not be verified in practice, and that the best results with this theory are achieved in solid rock, or other materials with high shear strength.

Apart from the mentioned and described theories, in some instances, the stress on the invert of the tunnel has to be considered and calculated. These cases are usually found in soils, rather than rock masses. Some examples of these are swelling soils (usually clay) or soft soils which are pushed up due to the forces of the tunnel walls. These theories however, are not considered to be vital for the analysed geology of Tunnel Višňové, and therefore are not analysed in this report.

5.5 Fenner-Pacher Curve Theories (CCM)

One of the many different calculation methods of designing underground structures is the Fenner-Pacher curve, also known as convergence confinement method (or CCM). It was developed in 1964 by Pacher who investigated ground behaviour in an experimental tunnel. Feder and Arwanitakis in 1976 improved the convergence confinement method by implementing a linear elastic–ideal plastic material behaviour into the ground characteristic curve [Gschwandtner, G. G. Gschwandtner, and Galler, 2012]. A large majority of the convergence confinement methods are based off of the Mohr-Coulomb failure criterion (described in Appendix B), however in 1992 Carranza-Torres and Fairhurst have used the Hoek-Brown failure criterion within an elastic-perfectly plastic material.

Instead of a 3D problem, the convergence confinement method addresses a 2D plane strain problem of the ground and tunnel support interaction [M. e. a. Panet, 2001]. The basic principle is that during the excavation of the tunnel, the support system (shotcrete, rock bolts, etc.) is simultaneously erected, a principle used also as the basis of the NATM described in earlier chapters. The ground and the support have a theoretically perfect connection with no cavitation, providing good ground for their interaction. This interaction can be expressed by the means of 3 curves: The ground characteristic curve (GCC), the support characteristic curve (SCC) and the longitudinal deformation profiles (LDP), which only helps add the 3rd dimension to the problem.

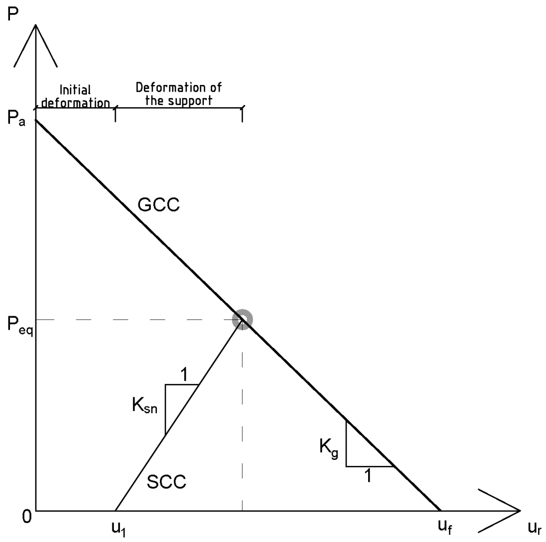

Figure 5.8: Fenner-Pacher curve for a elastic behaviour of the ground and the support, according to Deere (1969)

The GCC expresses the effective internal support pressure and radial deformation relationship at the surface of the tunnel. The curve is a representation of the reduction of pressure from primary stress level to 0. The ground tends to behave elastically until the pressure is reduced to a critical value, p_{crit}. Once the stresses fall below the critical value, plastic radial deformations or softening is encountered [Gschwandtner, G. G. Gschwandtner, and Galler, 2012].

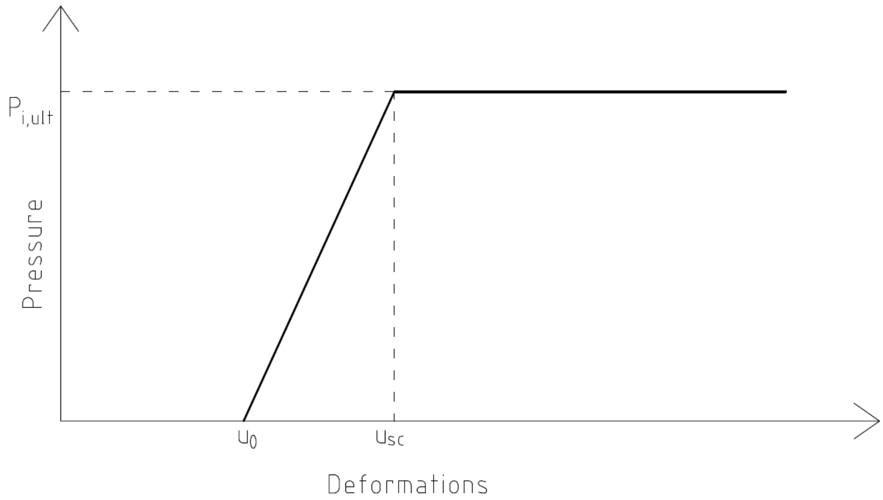

Figure 5.9: Example of a support characteristic curve (SCC)

The SCC shows the support measures taken to stabilise the tunnel deformations and their bearing capacity. The curve can be specified by the stiffness (K_{SN}), maximum sustainable stress ($p_{i,ult}$) and strain parameters ($u_{r,ult,pl}$). All of these parameters can be seen depicted on figure 5.9.

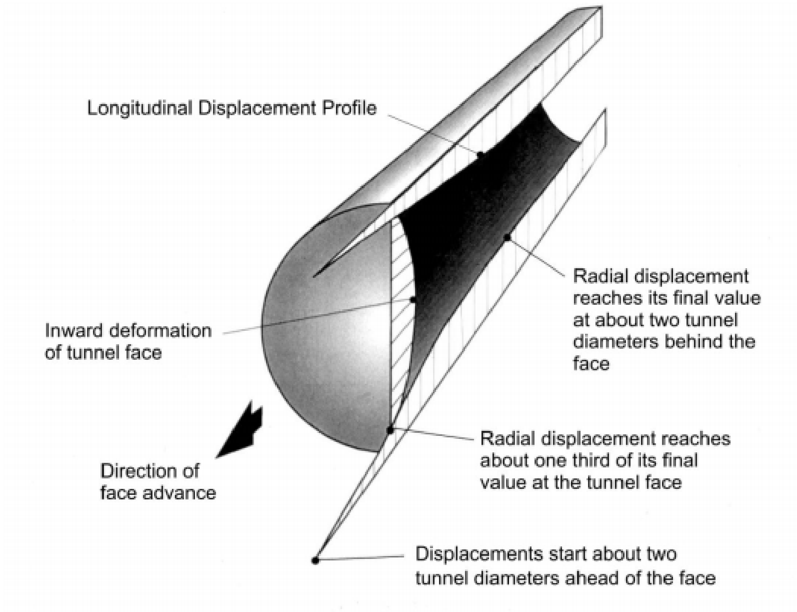

Figure 5.10: Development of the radial displacement relative to the face of the tunnel, visualised in 3D [E. Hoek, 2006]

The longitudinal deformation profile (LDP) determines the radial displacements of the tunnel in in regards to the distance from the excavation tunnel face [Gschwandtner, G. G. Gschwandtner, and

Galler, 2012]. A relationship can be established by taking into consideration the advance rate and the distance from the face of the tunnel.

$$x(t)[d] = \frac{x[m]}{v[m/d]} \tag{5.39}$$

In numerical models this so-called "pre-deformations" are considered by the pre-relaxation factor. The shape of the LDP depends on the theory used, as the results vary widely from theory to theory, including the support system and construction process. The LDP is not considered in some of the simplified 2D CCMs, however they are used in practice, as they provide valuable information with which numerical tunnel models can be checked.There exist numerous theories of establishing the GCCs, SCCs and LDPs, some of which will be presented below.

As a visual aid Deere's solution is useful. It is the simplest convergence confinement solution there is, as it assumes only linear elastic behaviour for both, the ground and the supports. Using a small number of parameters, the stiffness, or the characteristic curve gradients, of the two can be calculated easily and the ground-support interaction with its equilibrium point can be determined. The relationships for the characteristic curves are:

$$\begin{aligned} K_g &= \frac{tE_t}{a - \frac{t_c}{2}} \\ K_{sn} &= \frac{2E}{(1+K_0)(1+\nu)} \end{aligned} \tag{5.40}$$

Where:

t_c	concrete/shotcrete thickness
a	tunnel radius
ν	Poisson's number
K_0	coefficient of horizontal earth
E_t	modulus of elasticity of concrete/shotcrete
E	modulus of elasticity of the ground

The characteristic curves calculated in equations 5.40, can be seen plotted on figure 5.8. This solution is however used only as a teaching aid, due to the lack of realism, as the linear elastic behaviour is not usual for the ground nor the supports.

5.5.1 Ground Characteristic Curves

There are many ground characteristic curves derived throughout history of convergence confinement method. They are usually defined as the relationship between the support pressure, p_i, and the tunnel deformations, u_i, when plotted on a graph. Therefore it is necessary to examine the development of both. Nonetheless, each one is based on a different material failure criteria, be it Mohr-Coulomb or Hoek-Brown. In this section only Mohr-Coulomb models will be analysed.

Hoek

The theory is based on an assumption that the plastic failure of the material is defined by the Mohr-Coulomb failure criterion.

$$\sigma_1' = \sigma_{cm} + K_0 \sigma_3' \tag{5.41}$$

The uniaxial strength of the rock mass and the slope, k, of the axial stress against confinement stress plot, are given by:

$$\begin{aligned} \sigma_{cm}' &= \frac{2c' \cos\phi'}{(1-\sin\phi')} \\ K_0 &= \frac{1+\sin\phi'}{(1-\sin\phi')} \end{aligned} \tag{5.42}$$

Where:

σ_1'	axial stress causing failure
σ_3'	confining pressure
c'	cohesion of the rock mass
ϕ'	friction / shear angle of the rock mass

Another assumption on which the Hoek CCM is based on is that the tunnel is circular with radius r_0, is acted upon by a hydrostatic pressure, p_0, and has an internal support pressure p_i. Figure 5.11 depicts this setup. Plastic failure of the rock mass following the Mohr-Coulomb criterion, occurs when the support pressure, p_i, of the tunnel, drops below a critical value called the critical pressure p_{cr}.

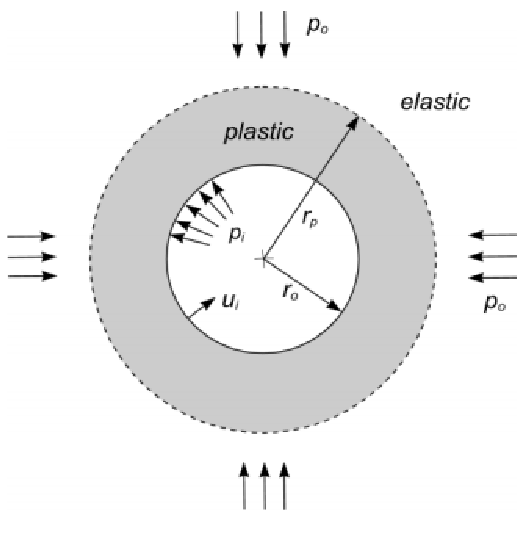

Figure 5.11: Plastic zone around the tunnel excavation [E. Hoek, 2006]

The critical pressure is expressed by:

$$p_{cr} = \frac{2p_0 - \sigma_{cm}}{1 + K_0} \tag{5.43}$$

Before failure however, when the internal pressure or the support pressure is still above the critical pressure, only elastic deformations a=occur at the tunnel walls and in its proximity. These are proposed to be calculated as:

$$u_{ie} = \frac{r_0(1+\nu)}{E_m}(p_0 - p_i) \tag{5.44}$$

When the support pressure inside of the tunnel decreases, as it does during relaxation after the excavations, plastic deformations arise around the tunnel walls. These plastic deformations have assumed radial symmetry, whose radius grows with the further lowering of the support pressures. This plastic radius is calculated using equation 5.45 below.

$$r_p = r_0\Big(\frac{2(p_0(K_0 - 1) + \sigma_{cm})}{(1+K_0)(K_0-1)p_i + \sigma_{cm}}\Big)^{\frac{1}{K_0-1}} \tag{5.45}$$

The subsequent plastic deformations occurring at the wall of the tunnel are expressed by:

$$u_{ip} = \frac{r_0(1-\nu)}{E}\Big(2(1-\nu)(p_0 - p_{cr})(\frac{r_p}{r_0}) - (1-2\nu))(p_0 - p_{cr})\Big) \tag{5.46}$$

Salencon

Another GCC which is assumed to behave according to the Mohr-Coulomb criterion was developed by Salencon in 1969. The rock mass is also assumed to be homogeneous and isotropic. The expressions derived by Salencon relate the dilation angle, radius of border between elastic and plastic zones, and the internal support pressure. The plastic radius is calculated as:

$$r_p = r_0\Big(\frac{2}{(k+1)}\frac{p_0 + \frac{\sigma_{cm}}{k-1}}{p_i + \frac{\sigma_{cm}}{(k-1)}}\Big)^{(\frac{1}{k-1})} \tag{5.47}$$

and the radial displacements as:

$$u_r = \frac{r}{2G}\chi \tag{5.48}$$

While the variables χ, k and k_ψ are:

$$
\begin{aligned}
\chi = (2\nu - 1)\left(p_0 + \frac{\sigma_{cm}}{k-1}\right) + \left(\frac{(1-\nu)(k^2-1)}{k+k_\psi}\right)\left(p_i + \frac{\sigma_{cm}}{k-1}\right)\left(\frac{r_p}{r_0}\right)^{(k-1)}\left(\frac{r_p}{r}\right)^{(k_\psi+1)} + \\
\left((1-\nu)\frac{(kk_\psi+1)}{k+k_\psi} - \nu\right)\left(p_i + \frac{\sigma_{cm}}{k-1}\right)\left(\frac{r}{r_0}\right)^{(k-1)} \qquad (5.49)
\end{aligned}
$$

$$k_\psi = \frac{1+\sin(\psi)}{1-\sin(\psi)}$$

$$k = \tan^2\left(45^\circ + \frac{\phi}{2}\right)$$

Where:

σ_{cm}	uniaxial compressive strength of the rock mass
ψ	dilation angle
ϕ	friction angle
r_0	radius of the tunnel
r_p	plastic radius
r	radius of the coordinate of interest
p_0	in-situ pressure
p_i	internal support pressure

This elasto-plastic model of the ground reaction, being one of the first to coin the term "loosening" plastic zone, described by the k_ψ, is used to this day by engineers, due to the fact it takes into account not just the friction angle, but also the dilatancy of the medium, which is an important rock mass and soil parameter.

Sulem - Panet

The Sulem and Panet based their ground characteristic curve on a 2D plane-strain simulation of the radial stress in the unexcavated medium, decreasing to 0, simulating no internal support. A parameter λ was used to describe this simulation of the stress path development, with $\lambda = 0$ in front of the tunnel face. Behind the tunnel face λ is increasing until 1, when the internal support pressure reaches 0 [Sulem, M. Panet, and Guenot, 1987].

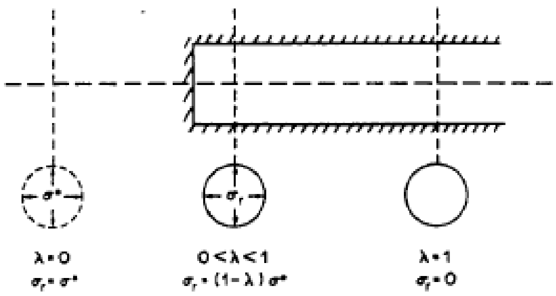

Figure 5.12: Development of the pressures and the confinement loss parameter λ in a tunnel [Sulem, M. Panet, and Guenot, 1987]

The plastic radius is calculated the same way as suggested by Salencon in 1969 in equation 5.47:

$$r_p = r_0\Big(\frac{2}{(K_0+1)}\frac{p_0+\frac{\sigma_{cm}}{K_0-1}}{p_i+\frac{\sigma_{cm}}{(K_0-1)}}\Big)^{(\frac{1}{K_0-1})} \tag{5.50}$$

The deformations in the radial direction are defined by the expression:

$$u_r = \lambda r_0 \frac{p_0}{2G}(\frac{r_p}{r_0})^2 \tag{5.51}$$

Where λ is the coefficient simulating excavation, also known as "confinement loss", described by Panet [M. e. a. Panet, 2001] as:

$$\lambda = \frac{1}{(K_0+1)}\Big(K_0 - 1 + \frac{\sigma_{cm}}{p_0}\Big) \tag{5.52}$$

Where:

σ_{cm}	uniaxial compressive strength of the rock mass
K_0	coefficient of lateral earth
r_0	radius of the tunnel
r_p	plastic radius
p_0	in-situ pressure
p_i	internal support pressure

5.5.2 Longitudinal Displacement Profiles

Similar to the other characteristic curves, a lot of work has been done to model the behaviour at, ahead and behind the tunnel face. Each theory is based on different assumptions which have to be considered when applying the LDP in a project. Some of the most used profiles are presented in the upcoming section.

Vlachopoulos-Dietrichs

Longitudinal displacement profiles help add the 3rd dimension to the simplified 2D problem using CCM, as described earlier. Hoek suggests using the LDPs developed by Vlachopoulos & Diederichs in 2009.

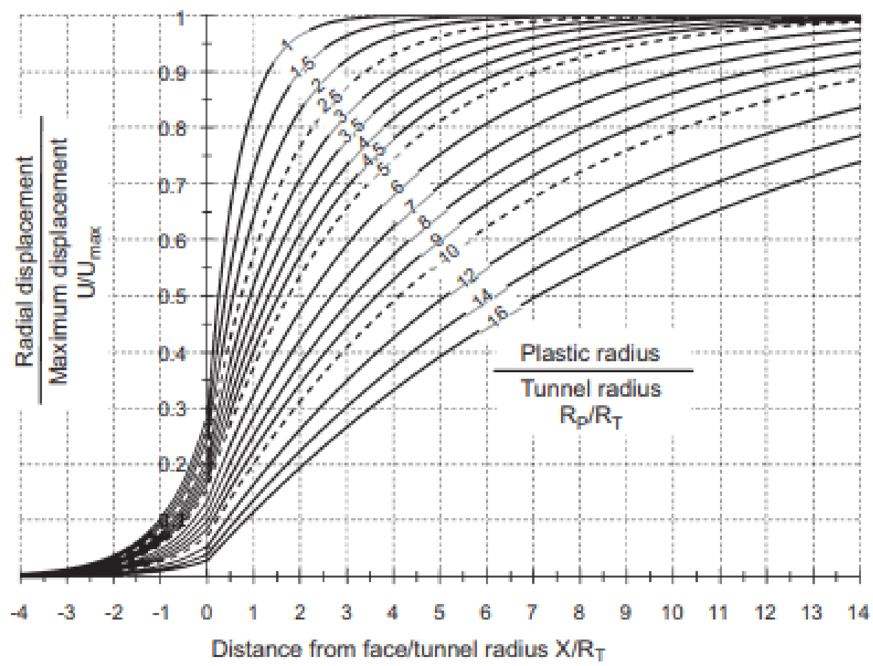

Figure 5.13: Examples of calculated LDPs by Vlachopoulos & Diederichs for different plastic radius to tunnel radius ratios which can be used as substitutes of the equations below [Vlachopoulos and Diederichs, 2009]

The displacement at the face can be calculated by the following equation:

$$u_{if} = \left(\frac{u_{pl,max}}{3}\right) e^{-0.15(r_p/r_0)} \tag{5.53}$$

Where:

$u_{pl,max}$	maximum displacements occurring at r_p

The maximum displacement noted above is calculated through equation 5.46 by substituting 0 for the internal support pressure p_i.The tunnel wall displacement ahead of the face ($x < 0$) are calculated as:

$$u_i = \frac{u_{if}}{u_{pl,max}} e^{x/r_0} \tag{5.54}$$

While the displacements behind the face ($x > 0$)are:

$$u_i = 1 - \left(1 - \frac{u_{if}}{u_{pl,max}}\right) e^{-(3x/r_0)(2r_p/r_0)} \tag{5.55}$$

When the LDP is plotted together with the GCC the deformations behind the face, where the supports are installed can be derived.

Chern et al.

This LDP curve comes from the RocSupport software, which used it as default in the beginning, but has since moved on to use the above mentioned Vlachopoulos & Diederichs' LDPs. This LDP does not come from a theory, rather it is a best fit to data gathered and published by Chern et al in 1998. The data was correlated to various parameters like in-situ stresses and cohesion to increase the reliability of this fit. It is an empirical solution considering plastic behaviour, unlike the LDP proposed by Vlachopoulos & Diederichs [M. Hoek E. D., 2018]. The data and the fit can be seen on figure 5.14 below:

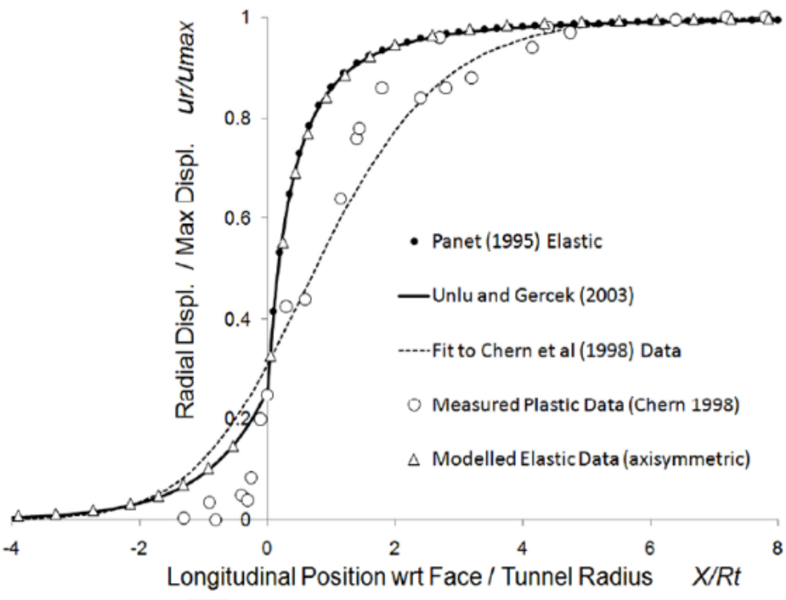

Figure 5.14: The measured plastic data by Chern from 1998 with the line of best fit [M. Hoek E. D., 2018]

The line of best fit to the data by Chern et al is expressed by:

$$u_i = u_{pl,max}\lambda = u_{pl,max}\frac{1}{(1+e^{\Lambda})^{1.7}} \tag{5.56}$$

Where Λ is expressed as a relationship between the distance to the tunnel face, x, and the tunnel radius r_0.

$$\Lambda = -\frac{x}{\frac{2r_0}{0.55}} \tag{5.57}$$

Unlu-Gercek

Just like many other theories for the LDP, the relationship developed by Unlu and Gercek, is based on numerical models. Most of these relationships only depend on the normalised distance to the face of the tunnel (x/r_0). Unlu and Gercek suggested adding another variable, the Poisson's ratio for the rock mass, as it affects the normalised elastic radial deformations ahead of the tunnel. The theory was developed on models with Poisson's values $0.05 < \nu < 0.45$, and hence, covers most of the rock masses available [Unlu and Gercek, 2003]. The LDP is divided into two parts as the data did not fit the sigmoid curve as well.

The displacement at the face of the tunnel hence has to be calculated separately using expression:

$$u_{if} = u_{pl,max}(0.22\nu + 0.19) \tag{5.58}$$

Expressions 5.59 for the deformations for the two parts, ahead and behind the face of the tunnel respectively, are presented below.

$$u_i = u_{if} - A_a u_{pl,max}\left(1 - e^{\left(B_a \frac{x}{r_0}\right)}\right) \qquad u_i = u_{if} - A_b u_{pl,max}\left(1 - \left(\frac{B_b}{A_b + \frac{x}{r_0}}\right)^2\right) \tag{5.59}$$

Where the constants *Aa*, *Ab*, *Ba* and *Bb* are:

$$\begin{aligned} A_a &= -0.22\nu - 0.19 \\ A_b &= -0.22\nu + 0.81 \\ B_a &= 0.73\nu + 0.81 \\ B_b &= 0.39\nu + 0.65 \end{aligned} \tag{5.60}$$

Effect of the support curve

LDP curves represent the deformation ahead, at and behind the face of the tunnel, neglecting any supports (i.e. unsupported tunnel). In modern tunneling however, supports are used. To bridge this gap, the LDP must change to account for the effect of the support in the tunnel. This means that the LDP ahead of the face remains unchanged, and only from the point of installation of the support does the curve change. The maximum displacement reached by the new LDP will be equal to that of the displacement at equilibrium of the SCC and GCC, rather than the maximum plastic deformation from the GCC alone. An example illustrating this can be seen in figure 5.15 below.

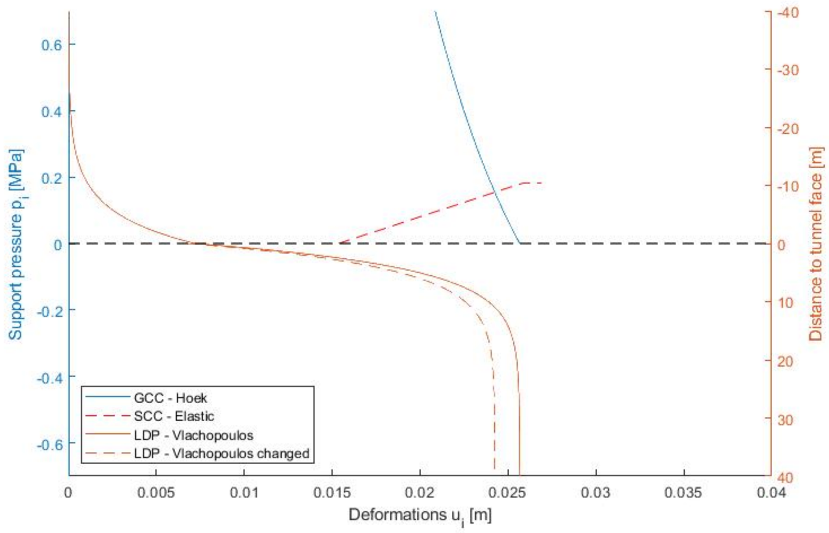

Figure 5.15: An example of a LDP curve by Vlachopoulos & Diederichs with and without considering the elastic support curve

There are no confirmed correct solution to this but there are a number of approaches, on how to produce this LDP curve considering supports. Some account for the time variable, meaning it considers the development of strength of the supports, while some do not. The method used in figure 5.15 is considering time dependency and was subdivided into 10 intervals.

5.5.3 Support Characteristic Curve

The characteristic curves for the supports whether it is steel arches (lattice girders or steel beams with I or H profiles) are estimated by Hoek and Brown to be linear elastic-perfectly plastic as shown in figure 5.9. This means only two values need to be calculated to determine the curve. The methods to calculate the point of maximum stress and the stiffness (slope) of the support are described below.

Shotcrete

The maximum stress, p_{scmax}, and the stiffness, K_{sc}, of a shotcrete lining of a circular tunnel are given as:

$$\begin{aligned} p_{scmax} &= \frac{\sigma_{sc}}{2}\left(1-\frac{(r_0-t_c)^2}{r_0^2}\right) \\ K_{sc} &= \frac{E_c(r_0^2-(r_0-t_c)^2}{2(1+\nu^2)(r_0-t_c)r_0^2} \end{aligned} \tag{5.61}$$

Where:

σ_{cc}	uniaxial compressive strength of the concrete
E_c	Elastic modulus of concrete
ν_c	Poisson's ratio of the concrete
t_c	concrete lining thickness
r_0	tunnel radius

This method does not consider the light reinforcement of the shotcrete through wire meshes. These meshes have an important role in preventing micro-cracks and creeping of the concrete, however, they do not contribute to the overall strength of the concrete in a significant manner, therefore they can be neglected.

Rock bolts

Rock bolts and cables applied to the tunnel have a complicated behaviour which is problematic for modelling analytically. For example, fully grouted rock bolts act as reinforcement of the rock in much the same way as reinforcing steel acts in concrete. As a result they change the shape of the characteristic curve rather than provide internal support equivalent to that given by steel sets or shotcrete linings [E. Hoek, 2006]. Ungrouted rock bolts, anchored only at the end, behave differently, such that they as if produce an internal pressure in the excavated tunnel much like in figure 5.16. Therefore, a simplified model was derived by Hoek only for ungrouted bolts.

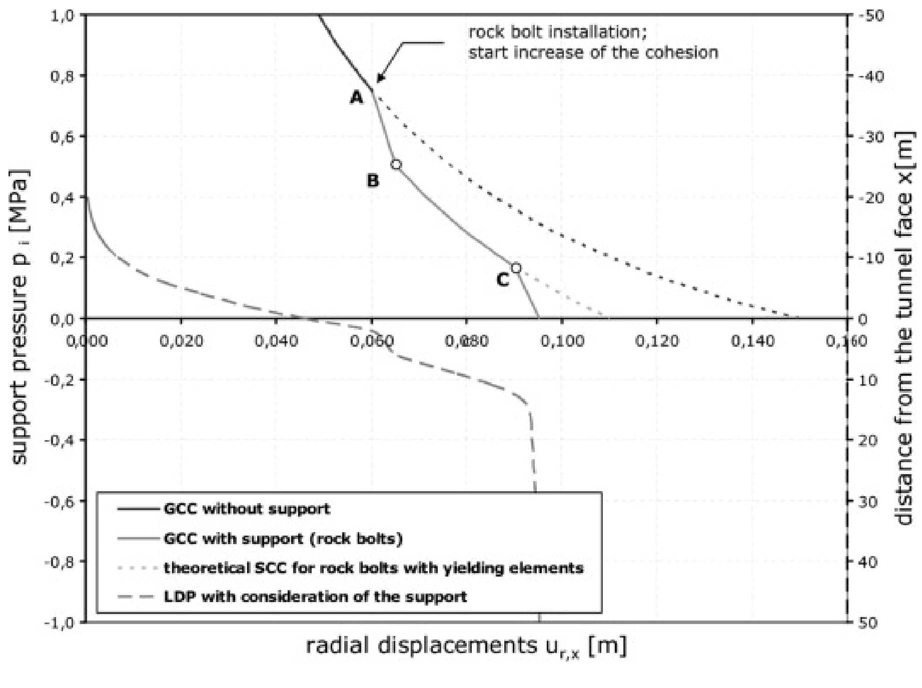

Figure 5.16: Improvement of cohesion due to Rock Bolt installation and its effect on the GCC [Gschwandtner, G. G. Gschwandtner, and Galler, 2012]

The maximum support pressure, p_{scmax}, and the stiffness, K_{sb}, are:

$$p_{scmax} = \frac{T_{bf}}{s_l s_c} \qquad K_{sb} = \frac{E_s \pi d_b^2}{4 l s_l s_c} \tag{5.62}$$

Where:

d_b	rock bolt / cable diameter
l	free length of rock bolt / cable
E_s	elastic modulus of rock bolt / cable
s_c	circumferential rock bolt / cable spacing
s_l	longitudinal rock bolt / cable spacing (in direction of tunnel)
T_{bf}	ultimate load for rock bolt / cable

Hoek recommends to use free length of the bolt, l, larger than the plastic zone, in a way to anchor itself in elastically behaving rock. Another recommended use of the rock bolts is a spacing (both longitudinal and circumferential) to be larger than half the bolt length.

Combined supports

if rock bolts are used in conjunction with a shotcrete lining, as often is the case, the stiffness of the support system is estimated by Hoek to be a simple sum of the individual stiffness's. Therefore:

$$K_{comb} = K_{sc} + K_{sb} \tag{5.63}$$

The maximum support pressure is given by the higher support pressure of the two supports, as one of the supports would have to bear more load, once the load bearing capacity of the weaker system is exceeded. The same theory is applied to the deformations.

Improvements to the support curve

In addition to the linear elastic-perfectly plastic support curve proposed by Hoek, there have been many improvements to the curve, however they are somewhat impractical and therefore, are often omitted from practice, as they defeat the purpose of a quick analytical solution opposed to a numerical one. Plastic deformations during strength development, time dependability and improvement of the rock mass cohesion rather than an actual support curve are just some of them. These however, are not considered in this report.

5.5.4 Discussion

The CCM is an interesting and logical approach to tunneling, describing the three basic components with graphs. the method however, does have its drawbacks, which limit its use in engineering practice. Some of these are:

Number of assumptions

Homogeneous and isotropic rock mass, circular tunnel profile with radial symmetry, small strain conditions and large overburden are just some of the assumptions of the CCM. Also worth noting is the disregard for dynamics, time-dependence and conditions of execution (methods of excavation) [Alejano, 2010].

Behaviour models

Elastic-perfectly plastic material behaviour model is not necessarily true for rock of higher quality (GSI > 30). This is due to the fact that rocks with higher quality exhibit larger strengths followed by strain-softening, and in cases of very good rock (GSI > 70), brittle behaviour is expected, rather than elastic-perfectly plastic. This means original CCM should be used only in low quality rock masses.

Model criteria for application

Each of the theories used to derive the curves used in CCM, are based on a set of extra limitations, and its authors recommend using their methods only in those circumstances. While Hoek in 1995 and Brady Brown in 2004 proposed methods for tunnels with high stresses and in highly jointed rock, Vlachopoulos & Diederichs based their analysis on typical weak rock (graphitic phyllite) in a wide range on in-situ stresses, making it applicable to a larger percentage of tunnels.

5.6 Results

The results from the theories presented above are given in the tables below. Discussion on their accuracy and comparison with the numerical analysis is presented later.

5.6.1 Deformations of rock mass

Deformations of the tunnel obtained using the rock mass deformation methods presented above, for all geotechnical sections are:

	Kastner		Obert - Duvall	
Geological section	u_{crown} [mm]	u_{wall} [mm]	u_{crown} [mm]	u_{wall} [mm]
GA1	30.37	9.28	14.29	6.80
GA2	28.63	7.69	13.40	7.54
GA3	49.01	11.26	22.86	14.89
GA4	47.17	8.88	21.99	16.29
GA5	56.65	8.18	26.48	21.99

Table 5.2: Calculated deformations of the tunnel crown and walls from selected analytical methods of the deflection of rock mass theories

As can be seen the results vary a fair amount between the theories, as expected, however the magnitude of the deformations obtained are within the expected range. However, when compared the measurements from the site in chapter 3, it can be seen that both the solutions show completely wrong ratios of tunnel crown to wall displacements. Kastner's solution overestimates the deformations by a very large percentage, which in different geotechnical section changes. This extreme variability of the results mean there is no applicability of the theory to this project. Obert-Duvall solution gives results that are closer to the maximum measured displacements from chapter 3, rather than the average, and even so they deviate to a large extent. The more correct maximum radial displacements in the crown, given the incorrect wall deformations mean this theory is not consistent and does not model the behaviour of the rock around the tunnel realistically. Therefore, the results should be regarded as untrustworthy.

5.6.2 Rock pressure theories

The rock pressure theory results in table 5.3 below, have been found to be severely deviating from one another, as can be seen. This only supports the arguments against such imprecise analytical solutions, which rock pressure theories are, in tunnel design. Comparison due to the lack of pressure gauges in the tunnel geotechnical monitoring is impossible, hence these theories will not be analysed further in the report.

	Rock pressure in the crown [kPa]		
Geological section	**Kommerell**	**Fenner**	**Bierbäumer**
GA1	9 348.1	1 364.1	5 532.2
GA2	9 737.6	1 384.1	5 570.0
GA3	10 623.0	1 322.2	7 407.3
GA4	11 047.1	1 335.8	8 261.9
GA5	11 598.8	1 435.0	10 000.0

Table 5.3: Calculated pressures on the tunnel structure in the top of the crown from analytical analysis of the different rock pressure theories

5.6.3 Convergence confinement method

Unlike the methods presented earlier for calculating deflections and pressures, CCM is part of the design of tunnel structures, mainly due to its simplicity matched with fair precision and small spread of the results based on the theory used for the individual curves. Another positive aspect of this theory is the visualisation, making it easier to understand and read. The following results have been obtained for the quasi-homogeneous section GA1 using the above mentioned GCC methods. The most interesting results from the ground reaction (GCC) are summarised in the tables 5.4, 5.5 and 5.6 below.

Calculated values	GCC - Hoek				
	u_{el} [mm]	u_{pl} [mm]	p_{cr} [kPa]	r_{pl} [m]	r_{pl}/r_0 [-]
GA1	18.35	25.66	2.55	6.41	1.17
GA2	17.8	25.31	2.24	6.51	1.19
GA3	31.33	49.59	2.08	6.96	1.27
GA4	31.01	51.84	1.96	7.25	1.32
GA5	38.29	76.00	2.26	7.98	1.45

Table 5.4: Output from analytical analysis of the ground characteristic curves using the Hoek theory for all geotechnical sections

Calculated values	GCC - Sulem-Panet				
	u_{el} [mm]	u_{pl} [mm]	p_{cr} [kPa]	r_{pl} [m]	r_{pl}/r_0 [-]
GA1	18.35	21.53	2.55	6.43	1.52
GA2	17.8	21.19	2.24	6.53	1.19
GA3	31.33	40.21	2.08	7.01	1.28
GA4	31.01	41.75	1.96	7.32	1.33
GA5	38.29	59.26	2.26	8.05	1.47

Table 5.5: Output from analytical analysis of the ground characteristic curves using the Sulem-Panet theory for all geotechnical sections

Calculated values	GCC - Salencon				
	u_{el} [mm]	u_{pl} [mm]	p_{cr} [kPa]	r_{pl} [m]	r_{pl}/r_0 [-]
GA1	18.35	23.92	2.55	6.43	1.17
GA2	17.8	23.58	2.24	6.53	1.19
GA3	31.33	46.11	2.08	7.01	1.28
GA4	31.01	48.46	1.96	7.32	1.33
GA5	38.29	71.51	2.26	8.05	1.47

Table 5.6: Output from analytical analysis of the ground characteristic curves using the Salencon theory for all geotechnical sections

Regrading the LDP using the different theories, the values for the deformations at the face and the deformations at instant of tunnel support installation, at a distance of a single excavation cycle (3, 2.2 and 1.7 meters for the different geotechnical sections) from the face. The calculated values and the shapes of the LDPs can be seen in table 5.7 and figure 5.17 below.

Geotechnical section	LDP Vlachopoulos-Diederichs		Unlu-Gercek		Chern et al.	
	u_{if} [mm]	u_0 [mm]	u_{if} [mm]	u_0 [mm]	u_{if} [mm]	u_0 [mm]
GA1	6.69	15.00	5.23	9.82	7.36	18.72
GA2	6.58	15.04	5.26	14.65	7.26	15.39
GA3	13.67	25.31	11.28	23.93	11.28	26.24
GA4	14.17	25.17	12.01	23.84	12.01	26.27
GA5	20.37	33.49	17.95	31.83	17.95	35.55

Table 5.7: Output from analytical analysis of the ground characteristic curves

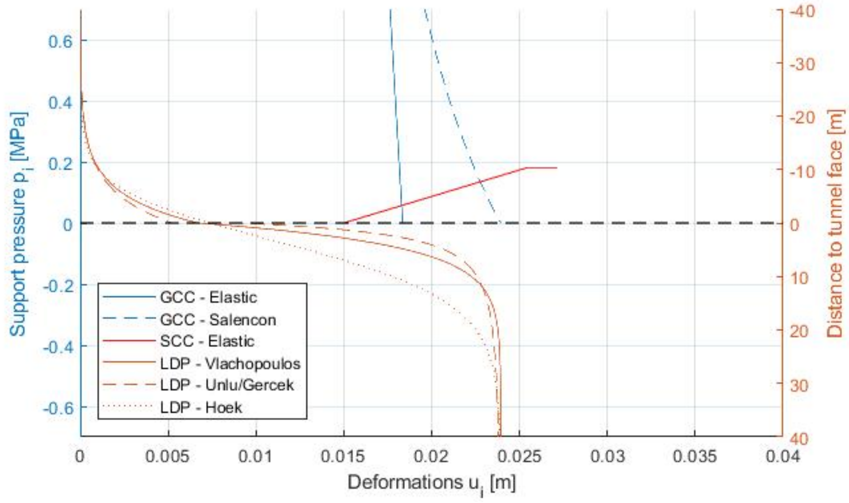

Figure 5.17: Different LDPs using Salencon's GCC maximum plastic deformation for GA1

The values coming from the interaction of the support curve with the ground curve, meaning their values at maximum support pressure and the equilibrium state are presented below alongside graphical representation. The influence of the rock bolts as mentioned previously is fairly small on the actual support curve, especially in this homogeneous section GA1-3, therefore its contribution has been neglected.

Geotechnical section	Hoek u_{sc} [mm]	$u_{sc,max}$ [mm]	u_{eq} [mm]	p_{eq} [kPa]	$r_{p,eq}$ [m]	$r_{p,eq}/r_0$ [-]
GA1	10.45	25.45	24.25	154.0	6.29	1.15
GA2	10.45	25.49	23.70	150.5	6.36	1.16
GA3	10.25	35.57	36.74	600.7	6.27	1.15
GA4	10.16	35.33	34.96	688.2	6.26	1.14
GA5	10.07	43.55	43.35	871.6	6.41	1.17

Table 5.8: Output from analytical analysis of the ground and support characteristic curves using Vlachopoulos & Diederichs LDP for all geotechnical sections

	Sulem-Panet					
Geotechnical section	u_{sc} [mm]	$u_{sc,max}$ [mm]	u_{eq} [mm]	p_{eq} [kPa]	$r_{p,eq}$ [m]	$r_{p,eq}/r_0$ [-]
GA1	10.45	25.45	21.00	97.31	6.35	1.15
GA2	10.45	25.49	20.56	95.9	6.43	1.17
GA3	10.25	35.57	33.86	447.3	6.43	1.16
GA4	10.16	35.33	32.75	534.2	6.48	1.18
GA5	10.07	43.55	41.08	670.7	6.70	1.22

Table 5.9: Output from analytical analysis of the ground and support characteristic curves using Vlachopoulos & Diederichs LDP for all geotechnical sections

	Salencon					
Geotechnical section	u_{sc} [mm]	$u_{sc,max}$ [mm]	u_{eq} [mm]	p_{eq} [kPa]	$r_{p,eq}$ [m]	$r_{p,eq}/r_0$ [-]
GA1	10.45	25.45	22.80	128.8	6.32	1.15
GA2	10.45	25.49	22.31	126.0	6.40	1.17
GA3	10.25	35.57	35.32	525.8	6.36	1.17
GA4	10.16	35.33	33.90	614.0	6.40	1.17
GA5	10.07	43.55	42.30	779.2	6.57	1.20

Table 5.10: Output from analytical analysis of the ground and support characteristic curves using Vlachopoulos & Diederichs LDP for all geotechnical sections

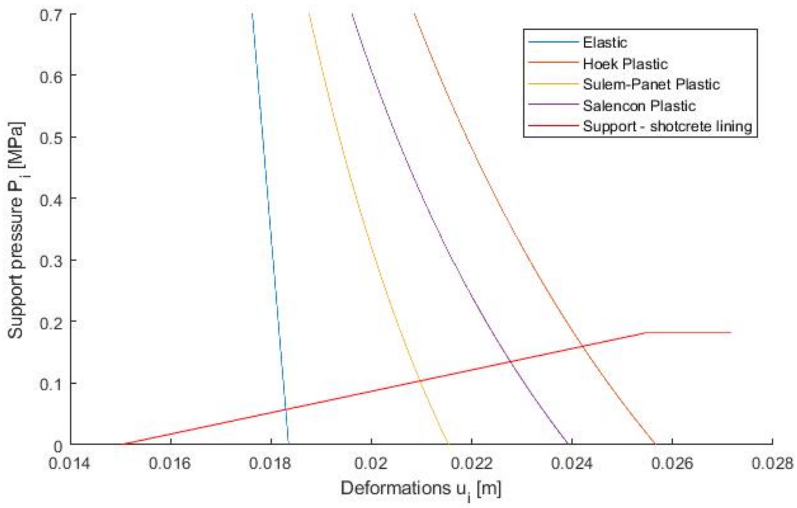

Figure 5.18: Different GCCs and their interaction with the elastic SCC for geotechnical section GA1

The radial deformations from the convergence confinement method are approaching the expected solution, unlike the Deformation theories above. It can be seen that the deformations at equilibrium state, when the secondary lining is installed, are fairly close to the measured values. Mainly, the radial displacements are predicted equal whether they occur at the crown or the walls, as is expected and shown from the geotechnical monitoring. However, even this theory does not provide satisfactory results that can be thoroughly and solely relied upon.

5.6.4 Conclusion

The analytic processes still have their significance today, as it is possible to achieve usable approximations for a given problem with relatively little work in a short amount of time. As soon as the solutions contain non-linear constitutive laws or complicated geometries, analytic processes reach their limits [B. Maidl, Maidl, and U. Maidl, 2014]. A further disadvantage of analytic processes is that they generally include no information about failure mechanisms. The determination of the failure load or the determination of the failure state is, however, one of the most important tasks in geomechanics, since the failure state is mostly used as a basis for the definition of safety margins [Schweiger, 1995]. These disadvantages, above all the cross-sections of tunnels that often deviate from circular, were the initial reasons for the development of numerical methods in tunnelling [B. Maidl, Maidl, and U. Maidl, 2014].

6. Numerical models

The geotechnical monitoring measurements inside the tunnel, shown in chapter 3, have to be compared to the numerical models, defined in a geotechnical finite element software Plaxis 2D and 3D. The models and its results along with a comparison to the monitoring results will be presented. Optimisation of the models will be performed.

6.1 The models

In this numerical analysis of the tunnel 2 different models were used. The complete model used for deformation and stress results was using Plaxis 2D. The other model was a 3D Plaxis model which was used only to obtain the deconfinement parameter to be used in the 2D model. This method of modelling allows the 2D model to account for deformations during the excavation phases, while also simplifying thew model from 3D to much simpler to calculate 2D model. This simplification means a more precise model with a higher number of elements.

As mentioned in previous sections, the model using given geotechnical properties deviates from the measured deformations to some extent, as can be seen in section 6.2. the aim of this report is to do a back-analysis and optimise these input parameters in such a way to reach results found during the geotechnical monitoring. The details of the optimisation are explained in section 6.1.5.

Both of the models used for comparison to the analytical method and for the back-analysis consist of numerous parts, each one vital to produce a correct result from the analysis. These parts are described in more detail in the following sections for each model.

6.1.1 Geology and soil material models

The soil parameters from section 3.1, were unaltered by any optimisation as can be the case when laboratory data is available. The soil was modelled according to a Mohr-Coulomb and Hoek-Brown material models. The reason for these models rather than the hardening soil and Cam-Clay models, is the fact that the tunnel is found in fairly strong rock, mainly geotechnical section GA1, whereas these models are more often than not used to represent granular material. Another major reason for these models is the lack of data. During the site investigation and the geological and hydro-geological investigation, focus was laid on the Mohr-Coulomb and the Hoek-Brown (derived from RockLab) parameters presented in appendix B. The parameters used in the model were the following:

Rock type property	GA1	GA2	GA3	GA4	GA5
Overburden [m]	655	520	360	300	300
GSI	65	58	48	38	30
E [MPa]	6 000	5 000	2 000	3 700	1 400
E_{rm} [KPa]	25 000	17 000	9 000	4 400	1 500
ν [-]	0.13	0.15	0.17	0.19	0.21
γ [kN/m^3]	27.1	27.1	27.1	26.9	26.8
ϕ [°]	55	53	47	44	42
ψ [°]	0.33	0.32	0.28	0.26	0.25
c [kPa]	1 150	1 000	800	700	550
σ_c [MPa]	125	100	80	70	50
m_i [MPa]	33	30	27	22	18
D [MPa]	0	0	0	0	0
K_0	0.18	0.15	0.27	0.29	0.30

Table 6.1: Geotechnical properties of all geotechnical sections used in Mohr-Coulomb and Hoek-Brown material models before optimisation

There is no layering of the rock mass, as it is assumed to be a homogeneous material. The reasoning for this is the changing positions of the joints along the tunnel length. To account for the discontinuities, loosening zone and block failure analyses are performed in other software, these however, are not considered in this report. In order to save calculation time and to reduce the model as much as possible, the overburden height was not completely modelled. Rather a 80 m overburden was created with a 1 m thick elastic layer on top with the exact weight of the overburden. This model is preferred over the surface loading which can create an unstable model. The modelling parameters and techniques are applied to both the 2D and 3D models.

6.1.2 Structure and meshing

The tunnel is modelled as a full tunnel, as using the vertical symmetry line of the tunnel profile was not possible. The tunnel is modelled as hollow, with the lining being represented by a plate with the thickness corresponding to the primary lining thickness and the material properties of shotcrete described in table 6.2. Plates are used in order to be able to check the bending moments, axial and shear forces in the lining. The difference between possible volume elements and plate elements as means of modelling the primary lining of the tunnel was not considered.

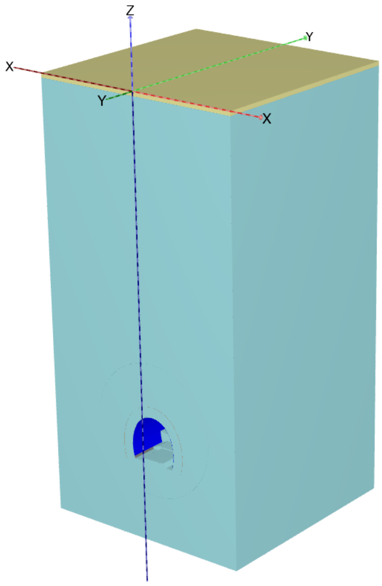

Figure 6.1: Model of the tunnel excavation in Plaxis 3D

The plate is modelled using an elastic material model, with the strength properties of normal concrete.

Material property	**Shotcrete C30 (FRC)**
σ_c (uniaxial) [MPa]	30
γ $[kN/m^3]$	25
E_c [MPa]	33 000
ν [-]	0.2

Table 6.2: Material properties of shotcrete (fibre reinforced concrete) used in the support class A2/1p

The mesh is generically generated, with element sizes chosen appropriately. One circular zone of refinement, with radius of 15 m, was established, in order to produce more accurate results, as can be seen on figure 6.2. The mesh for the 3D model consists of the default 10-node tetrahedron elements, whereas in the 2D a choice for 15-node elements was made.

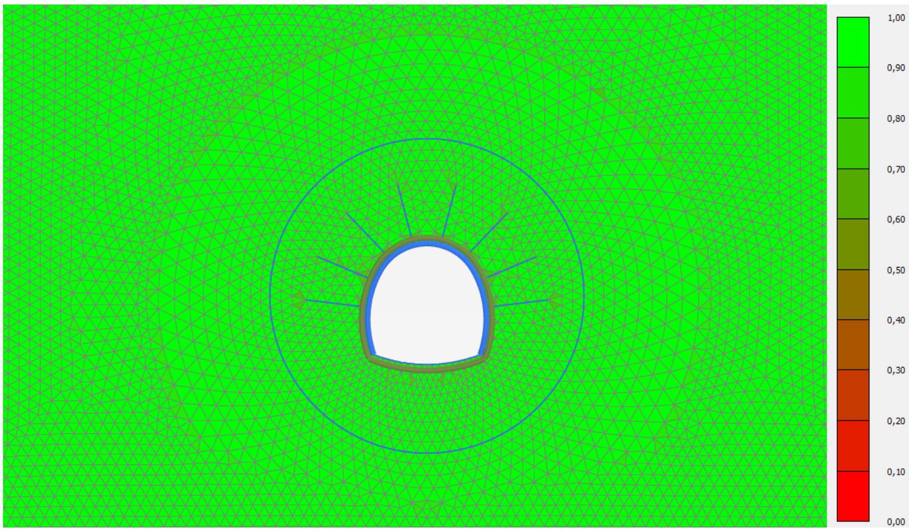

Figure 6.2: Quality plot of the mesh used in the 2D numerical models with 1 being the highest quality

Interfaces are another important consideration in Plaxis modelling, as they improve the model by creating a special connection between the geo-material and the structure, in this case the tunnel lining. Sharp corners which are present in tunneling at the end of the lining, can produce singularities which would not occur in real life, and are more than less a model problem. These interfaces extruded beyond the excavation, much like in figure 6.3 below, help with these singularities by reducing them eliminating them all together. Interfaces were applied only to the negative side of the tunnel lining, meaning only in the contact places with the rock mass, and not on the inside of the tunnel, where the rock volume is excavated.

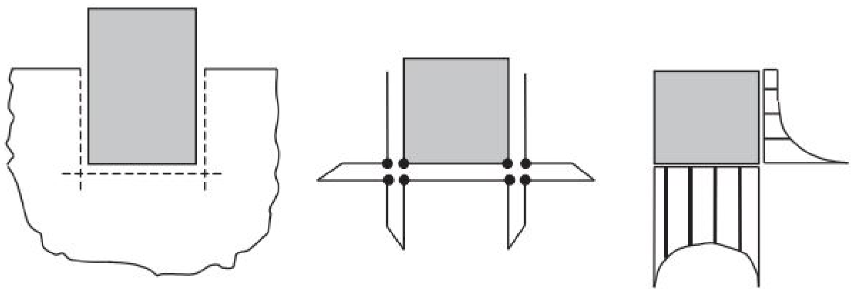

Figure 6.3: Effect of the interfaces on the stresses in the model in critical sports like sharp corners i.e. ends of tunnel linings

6.1.3 Phases

After the K_0 procedure (calculating the horizontal earth coefficient), which is the initial phase, the phases of excavation and primary lining installation are modelled in a sequence as it would happen on site. After each of the excavation phase, a so-called "nil-step" is used to regenerate equilibrium for the next calculation. This reduces the instability of the model. Due to the comparison of the analytical methods, no usual design phases are used, rather only plastic calculations are executed in order to calculate the unfactored deformations and pressures to allow a fair comparison.

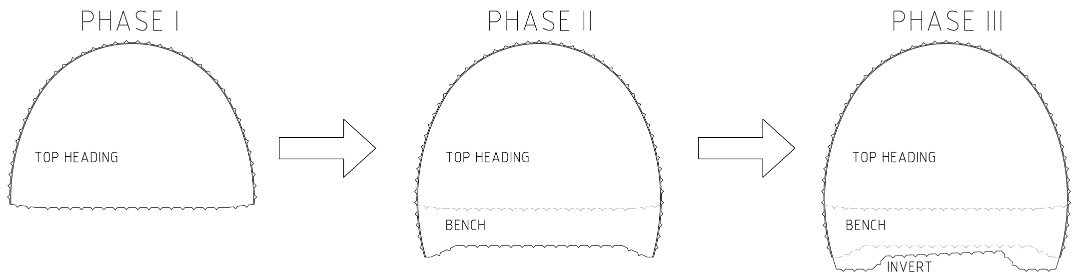

Figure 6.4: Phases of construction used for Plaxis 3D modelling

The phases in the 3D model were established much like a typical NATM excavation sequence would be as can be seen on figure 6.4, which shows the excavation phases. First the volume of rock is excavated while the lining itself has one phase delay. This is so for all the sections of the tunnel (top heading, bench and invert). These phases are repeated until the whole 50 m soil volume modelled is excavated. and the whole tunnel has the plate lining activated. Using this method, a deconfinement parameter can be found. The calculation method of this parameter and additional details are explained in subsection 6.1.4.

For a 2D model, the above mentioned phases are much in the same manner only repeated once. The final stage where plate lining is activated provides the final results for stress and deformations used in the lower section 6.2.

6.1.4 Deconfinement

Deconfinement is soil or rock mass relaxation during the phase between when the mass has been excavated and the lining installed. It is a 3D arching effect, also called the β-method [Tutorial, 2018]. Deconfinement is very well graphically illustrated in LDP curves from section 5.5.2. As the excavation nears the soil strata of interest, the rock or soil is experiencing loosening which allows some deformations to form and pressures to move closer to equilibrium. In a 3D model there is no need for deconfinement parameters as it is complex enough to deal with this problem within the model itself. In 2D models however, this parameter has to be inserted if real values of deformations are to be generated in the output.

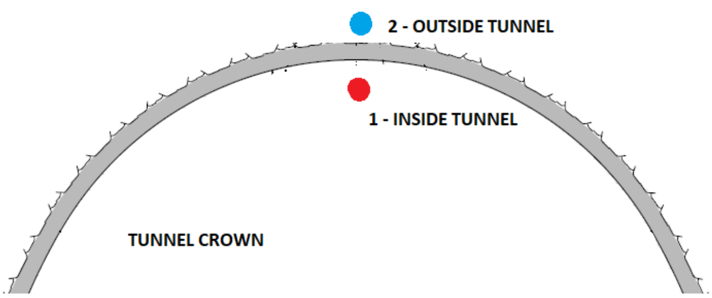

Figure 6.5: Location of stress points of interest for calculation of deconfinement parameter from a 3D model

The way this deconfinement parameter has to be calculated is using output from a 3D model, which is explained above. The entire tunnel is modelled, phase by phase, until the tunnel is running through the entire model volume. Two points at the end of the tunnel, and their stresses, are assessed, which are placed in the crown, with one point just inside the tunnel, and one just outside, as shown on figure 6.5 above. The stresses throughout the phases of these two points are then plotted together on one graph. The point located inside the tunnel has similar levels of vertical stress up to the point of excavation, at which the stress drops to 0, understandably, as there is no soil volume. The point located just outside the tunnel exhibits much the same behaviour, only the stress once the tunnel is fully excavated does not drop down to 0, rather only to some value. The ratio of this "left-over" stress to the nominal stress at start of excavation, is the deconfinement ratio or parameter. Typical values range anywhere between 30-80% with some even going up to 90%. A plot of these can be seen on figure 6.6 below:

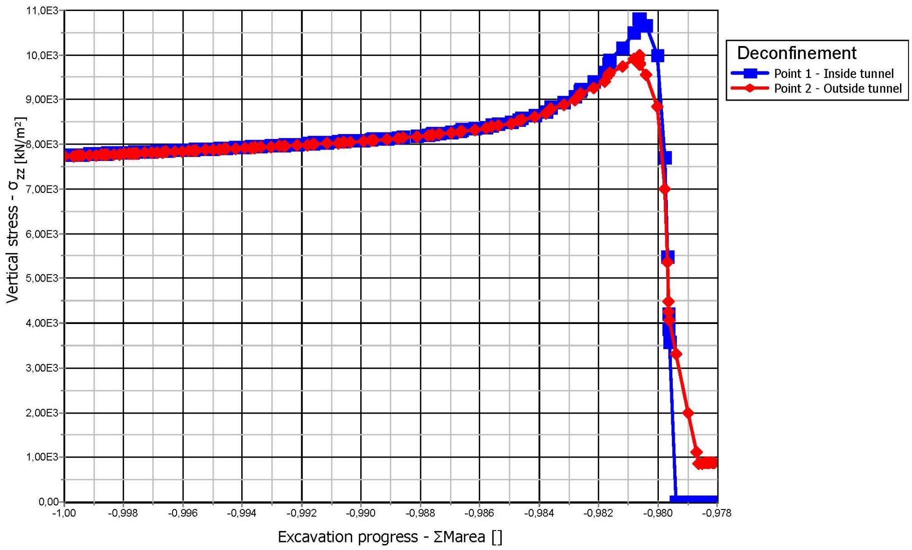

Figure 6.6: Vertical stresses plotted against excavation progress for the whole tunnel from a 3D model for geotechnical section GA5

This deconfinement analysis was performed for all geotechnical sections in the manner explained above. The results from this analysis are presented in table 6.3 below:

Geotechnical section	Deconfinement [%]
GA 1	5
GA 2	6
GA 3	8
GA 4	10
GA 5	12

Table 6.3: Deconfinement parameters for each geotechnical section

6.1.5 Optimisation

One of the aims of this report along comparison is a back-analysis of the material model parameters provided by the hydro-geological investigation prior to the start of construction. Since this investigation has its limits, the given parameters have a certain degree of accuracy. These inaccuracies create a difference between the theoretical numerical model established and the real-time measurements from the construction site. To optimise the excavation process, whether it is to save time by increasing excavation rates, or saving materials by decreasing lining thickness and rockbolt numbers, or both, optimised input parameters have to be found.

In perfect situations laboratory results with all the important data would be provided, so this optimisation can be done semi-automatically through the respective PLAXIS feature. In this project unfortunately, it was impossible to gather the necessary data from 3rd party geologists. Optimisation therefore, is performed completely manually. In each of the material models, Mohr-Coulomb and Hoek-Brown, dominating parameters were chosen, which were tweaked gradually. The aim of this increase of decrease was to create a model that would reflect the real measurements presented in chapter 3. The parameters for the Mohr-Coulomb material model were Young's modulus E and friction angle ϕ and cohesion c. For the Hoek-Brown it is the rock mass Young's modulus E_{rm}, intact rock parameter m_i and rock mass rating GSI. Of course by this method of optimisation many different combinations are possible, however all have the same effect of optimising the structure and saving construction costs. The results from this optimisation are presented in the upcoming section.

However, it was established that in order to model the displacements around the 5 points of interest would require another parameter to be changed, and that is the lateral earth coefficient, K_0. This parameter was changed for the Mohr-Coulomb material model and once optimisation of this model was completed, the same lateral earth coefficient was used in the Hoek-Brown model. This parameter was set to a high value in order to be able to model the large wall displacements. The final optimised K_0 values are found in the section below, namely table 6.8.

6.2 Results

The models used for the final results described above, had to be first verified, in order to confirm its reliability. This was done through a number of checks described in the sections below. Once the models were established as reliable, final results were extracted to be used for comparison to the real measured data and the analytical solutions, from which relevant conclusions were drawn.

6.2.1 Validation of the model

The numerical models, in order to be used, should be verified to the largest extent possible. In this report verification of the models is done through the analysis of the failure mechanism and the convergence analysis of the model.

Failure mechanism

The stresses and strains in each of the Cartesian directions have been thoroughly analysed, and a comparison to the expected behaviour was established and determined to be matching. As can be seen from the stress plot on figure 6.7 below, stresses develop around the tunnel much like in completely circular sections. The only major difference is the formation of singularities at the sharp corners of the excavated profile during any construction stage. These singularities are present even when interfaces are applied and the most refined mesh possible and thus unavoidable.

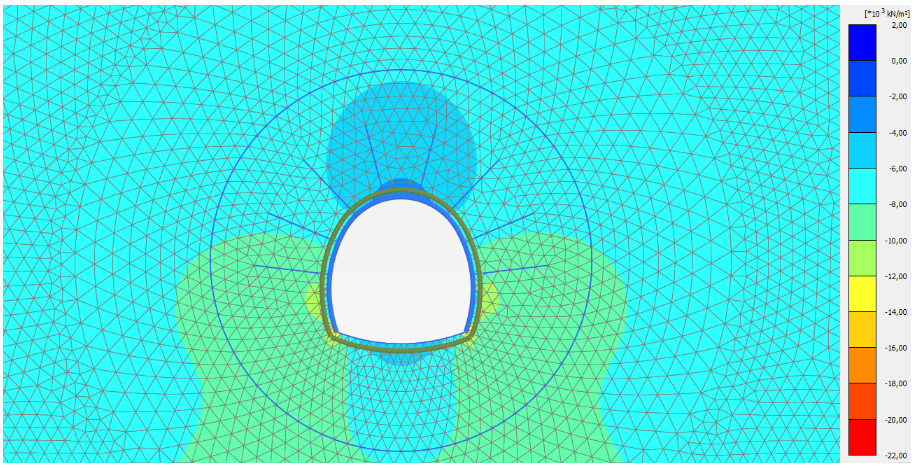

Figure 6.7: Vertical stress development around the fully excavated profile in GA5

The plastic points, from figure 6.8, around the tunnel excavation are also occurring similarly to the expectations. They correlate with reality by being present only in the areas of high compression, while tension cut-off points correlate with the areas of highest tensile stresses. Since plasticity is how singularities dissipate the excess stresses to the surrounding parts of the rock mass or soil, it is only natural we find these plastic points exactly in the sports where singularities occur. They also correspond to the plastic radius mentioned throughout the report.

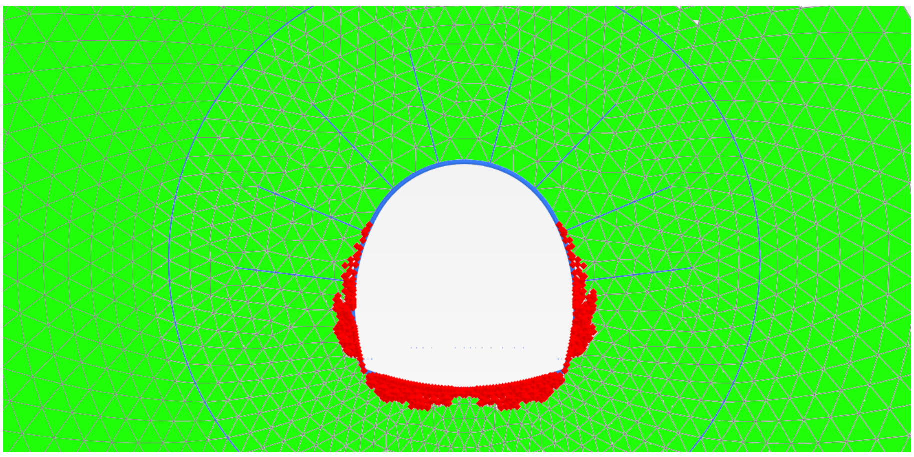

Figure 6.8: Plastic (in red) and tension cut-off points (in blue) around the fully excavated profile in GA5 using the Hoek-Brown material model

Due to this analysis it was concluded that the model predicts the behaviour of both the soil and the structure with a fair degree of accuracy. Hereby this model was verified and served as an additional comparison to the geotechnical monitoring.

Convergence

Convergence analysis is a necessity for any numerical model. In this case, convergence was performed by running a number of models with the same structure and geology, while increasing the degree of refinement of the mesh in the circular area around the tunnel, described earlier. Deformations at the 5 specified points were noted for every single model with the different meshes, and the results are summarised in figure 6.9 below.

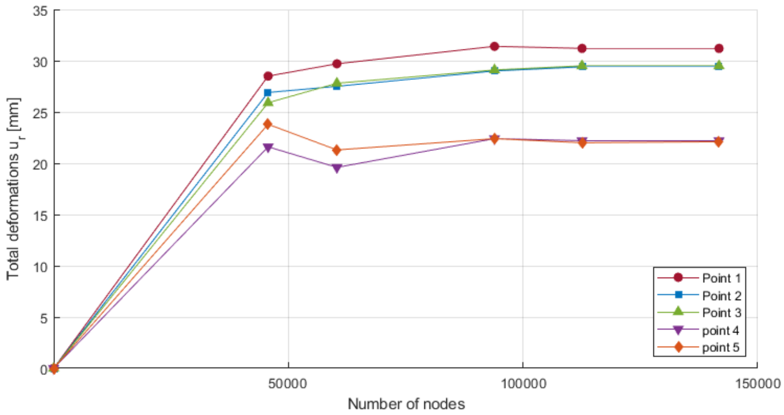

Figure 6.9: Convergence analysis of the deformations at 5 the different points in respect to the number of nodes in the GA 5 Hoek-Brown model

As can be seen, this particular model for GA-3 using the Mohr-Coulomb material model converged at a number of around 140 000 nodes. All models were ran through this convergence analysis with the number of nodes all falling within the similar range. Of course simplification to a 2D problem allowed for the use of the most detailed model, which was at the limit of the Plaxis mesh generator. The convergence of each model reached values of around 1% for points 1,2 and 3, while the remaining two reached values of around 2%.

6.2.2 Results from original models

From the results of the original numerical models summarised in tables 6.4 and 6.5 below, a number of conclusions and observations can be made. The Mohr-Coulomb material model seems to represent the real deformations measured on site fairly well, especially in the lower geotechnical sections (GA 1 and GA 2). Once the conditions get worse in the tunnel, the real and the modelled deformations diverge. This is mostly due to the difficulty of modelling weathered rock and Flysch behaviour using Mohr-Coulomb, which causes large under-predictions of the strength parameters and hence over-predictions of deformations. It is a conservative model giving rough results with larger relative errors, then the Hoek-Brown, especially in rocks such as granite [Cai, Gengshe, and Wang, 2014], what can be seen in this comparison as well.

Geo. Section	Point 1	Point 2	Point 3	Point 4	Point 5
GA 1	11.6	9.9	9.9	6.2	6.0
GA 2	21.0	16.4	16.4	9.3	9.3
GA 3	26.1	22.1	22.0	10.6	10.5
GA 4	51.8	25.5	24.6	8.8	8.2
GA 5	49.7	20.8	22.3	8.3	8.3

Table 6.4: Final values of total deformations at the measured points from a 2D numerical model from all geotechnical section GA 1-5 before optimisation, for the Mohr-Coulomb material model

Hoek-Brown on the other hand exhibits the opposite behaviour. The predicted deformations in good geology is severely smaller than that of the Mohr-Coulomb and more importantly even the real measured results. In bad geology though, the Hoek-Brown model excels and predicts the deformations with a relative error of less than 7%. The extreme under prediction of the lower geotechnical sections, namely GA1 is hard to defend with mechanical issues, and the only excuse for such deviations are wrong geological interpretation. Since it is not very common to use this material model in Slovakia and the fact that this model does not work on the principle of rock-mechanics but rather empirical data and tables, mistakes are possible, mainly due to the low quality of geological investigation in Central Europe.

Geo. Section	Point 1	Point 2	Point 3	Point 4	Point 5
GA 1	2.7	1.1	1.1	0.4	0.4
GA 2	7.5	6.4	6.4	4.0	3.9
GA 3	10.3	7.3	7.2	3.7	3.7
GA 4	16.0	5.9	6.0	4.5	4.5
GA 5	31.1	35.0	35.7	26.8	28.1

Table 6.5: Final values of total deformations at the measured points from a 2D numerical model from all geotechnical section GA 1-5 before optimisation, for the Hoek-Brown material model

If the results are to be compared to the analytical solutions using the same geotechnical parameters, a number of differences are to be seen depending on the theory. While the Obert-Duvall solution results from table 5.2, under-predicted the deformations that are to develop in the crown, in comparison to the Plaxis Mohr-Coulomb model, the wall deflections do not fit either of the measured points correctly. This, though, is caused by the measured points in the geotechnical monitoring and in the Plaxis model (which are identical) not being placed in the exact middle of the wall, but rather below and above. This middle point is the assumed point by Obert-Duvall which is based on a perfectly circular tunnel section. Further analysis however, revealed that the deformations from the 2D model are not represented by this theory for these given geotechnical sections and tunnel geometry.

Kastner's solution from table 5.2 on the other hand over-predicts the crown displacements in the better geotechnical conditions (GA 1-3), but comes closer to Plaxis results in geotechnical sections GA4 and GA5. The wall displacements generated by this theory nonetheless, are extremely close to the numerical results for points 4 and 5. From this comparison, one could argue the use of Kastner's solution, in worse geotechnical conditions, and in turn Obert-Duvall method, in better geotechnical conditions, as a sort of upper-bound solution that could be used as guidance and quick check for modelling outputs. Nevertheless, the arguments explained in subsection 5.6.1 make it clear that the model although simple, does not model the rock behaviour well enough to be used officially in calculations. This does not mean it should be disregarded completely, but other analytical methods should be explored rather than the two solutions mentioned above.

Convergence confinement method (CCM) may be such a method. The results are somewhat more consistent and show a gradual increase in deformations across the different geotechnical sections, something what is expected and to a certain extent seen in the geotechnical monitoring results from subsection 3.3.2. If we analyse the results for the deformations at equilibrium u_{eq} from tables 5.8, 5.9 and 5.10, the results seem to be over-predicted, when compared to both the Mohr-Coulomb and the Hoek-Brown in better geology and the opposite is true in the worse geological conditions. The results however are still closer to the numerical, than the above mentioned Kastner or Obert-Duvall solution. Another point is the fact that the CCM comes closer to the real measured values of deformations than the actual 2D numerical models, even if somewhat over-predicted. This suggests that the CCM method is fairly reliable and supports its use in numerous countries, like Slovakia and Czech Republic, as the choice of analytical method in tunnel design.

6.2.3 Results from optimised models

As explained above the real measured data do not always correspond to the output from the numerical models. This brings about the necessity to optimise the parameters which are presented in table 6.8. Since the coefficient of lateral earth was the same and the two material models function in different ways, it is virtually impossible and extremely time consuming to create the models with same results. Added to that is the large variation of actual results which differ to a large extent namely in the wall of the tunnel, where points 2,3 and 4,5 exhibit different results, as is shown in figure 6.10 below.

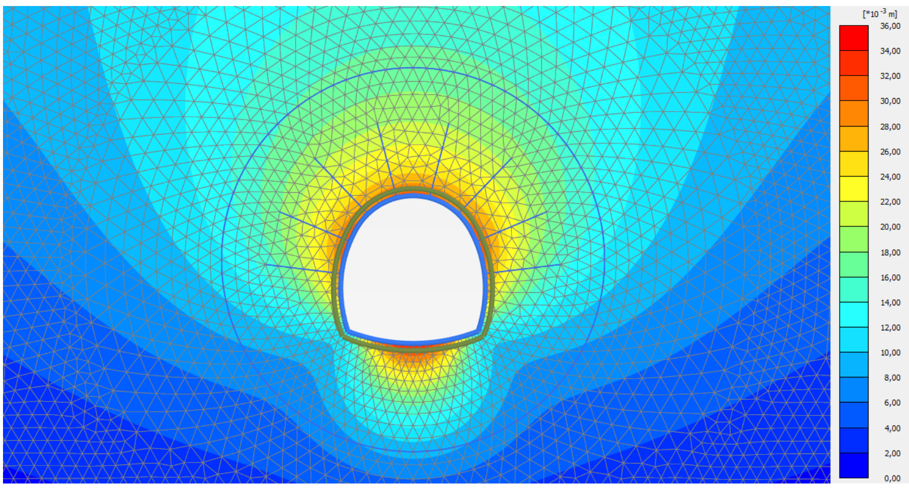

Figure 6.10: Total displacements around the tunnel in geotechnical section GA 5 using the Hoek-Brown material model

This optimisation did manage to reduce the relative error of the deformations of most of the points considered.

Geo. Section	Point 1	Point 2	Point 3	Point 4	Point 5
GA 1	11.6	9.9	9.9	6.2	6.0
GA 2	9.1	7.7	7.7	4.9	4.9
GA 3	15.3	13.6	13.5	6.9	6.9
GA 4	20.2	19.5	19.5	14.9	14.9
GA 5	31.1	35.0	35.7	26.8	28.1

Table 6.6: Final values of total deformations at the measured points from a 2D numerical model from all geotechnical sections GA 1-5 after optimisation, for the Mohr-Coulomb material model

As expected the Mohr-Coulomb parameters had to be increased so smaller deformations are achieved. Lower geotechnical sections less so, but worse geologies, like that of GA 5 was radically optimised with almost 50% increase in the Young's modulus and almost 30% to cohesion. This just proves the conservativeness of this theory and the possible saving mainly in unfavourable conditions as such. Understandably, using the original results pre-optimisation from table 6.5, it is clear that the strength parameters for the Hoek-Brown have to be decreased rather than increased, chiefly for GA 1-3. The changes to the parameters are not as drastic as to the former material model, with maximum changes of 10% to both the E_{rm} and m_i parameters.

Geo. Section	Point 1	Point 2	Point 3	Point 4	Point 5
GA 1	12.1	11.9	11.8	8.5	8.5
GA 2	9.1	7.8	7.8	4.9	4.7
GA 3	15.2	13.6	13.6	5.8	5.8
GA 4	19.0	18.7	18.7	13.7	13.8
GA 5	31.2	29.4	29.5	22.2	22.1

Table 6.7: Final values of total deformations at the measured points from a 2D numerical model from all geotechnical sections GA 1-5 after optimisation, for the Hoek-Brown material model

The final optimised values from table 6.8 compared to the ones from table 3.3, show that there is still a lot to be demanded from geological investigations as the data provided for the models, has a large relative error, particularly for the most widely used Mohr-Coulomb model.

Rock type property	GA1	GA2	GA3	GA4	GA5
Overburden [m]	655	520	360	300	300
GSI	65	58	40	38	32
E [MPa]	6 000	8 500	5 500	2 600	2 000
E_{rm} [KPa]	14 000	14 000	6 200	2 500	1 450
ν [-]	0.13	0.15	0.17	0.19	0.21
γ [kN/m^3]	27.1	27.1	27.1	26.9	26.8
ϕ [°]	58	58	56	45	42
ψ [°]	0.33	0.32	0.28	0.26	0.25
c [kPa]	2 000	1 700	1 200	1 000	700
σ_c [MPa]	125	100	80	70	50
m_i [MPa]	33	27	25	22	18
D [MPa]	0	0	0	0	0
K_0	0.90	0.90	0.90	0.90	0.90

Table 6.8: Optimised rock parameters for Mohr-Coulomb and Hoek-Brown material models according to real measured data

From this analysis it is clear that both of the material models give fair estimates of the deformations in the tunnel, although leaving much to be desired in their precision. Tunnelling is a complex field in which precise models cannot be used effectively due to the immense amount of cross sections with differing geologies. Therefore simplifications are needed and for this reason it is always suggested to use the more conservative model, which is the Mohr-Coulomb, even though Hoek-Brown models rock better behaviour more realistically, a fact reflected in the results of the deformations.

6.2.4 Discussion

The results presented above show the importance of back-analysis and the necessity to understand material models and modelling assumptions and uncertainties. Some of the uncertainties and model drawbacks have to be mentioned and included in the analysis for the sake of completeness. Firstly Plaxis 2D has a limitation on the mesh that is possible to generate. Even with the highest mesh settings and largest mesh refinement around the tunnel, producing about 250 thousand nodes, was not small enough. This meant that the actual points analysed differ by a couple millimetres from one another and therefore the exact values could be slightly different.

Another question remaining to be answered is what kind of material model resembles the rock behaviour of this given geology the best. As is clear from the results and the subsequent analysis, the model of the tunnel could be further improved. One of the methods to do so is to perhaps use the Jointed Rock material model available in Plaxis 2D. It allows for a rock formation resembling that of a simplified Flysch. This model could be a more realistic approach to modelling, but for such a material model more parameters are needed, than the ones provided. A solution to the problem without the need for new parameters is to incorporate a slip plane (or numerous), by the use of interfaces with reduced shear strength. This though, increases the complexity of the model, while operating again without concrete evidence of positioning of rock joints and their subsequent shear strength.

7. Comparison & Conclusion

In this chapter the entire report is summarised and an analysis and discussion of the results are presented.

In this report a fairly thorough analysis of the deflections and the stresses in the tunnel Višňové has been performed and presented. The main concepts of tunnel engineering in general are shown along side the typical procedures for the different methods. Rock mass classifications, a technique used for preliminary calculations are described, along with analytic solutions for deflections and stresses inside of tunnels, covering the whole spectrum of analytic solutions in tunnel engineering. Numerical models were established, in order to evaluate the analytical methods. For comparison of the results, namely the analytical and numerical calculations, geotechnical monitoring measurements gathered during the excavation of the tunnel were used. Lastly back-analysis of the numerical models was performed to check the accuracy of the models and geological investigation.

The results from the analytical methods are somewhat widespread. This is due to the different assumptions on which the independent theories are based on. While some theories assumed circular sections, others allowed for oval shapes, some even flat roofed mine-like tunnels. This variety created the large disparity of the results. When compared to the results from the numerical Plaxis 2D models, the most inaccurate theory observed was Obert-Duvall's theory due to the largely under predicted deformations in good geological conditions and over predicted in bad geology. Kastner's solution on the other hand estimates the deformations to be much larger than in reality or even the Mohr-Coulomb numerical model, making it by far the most conservative of the analytical methods. All of the different analysed curves in convergence confinement method were also found to be on the conservative side due to the lack of ability to differentiate between crown and wall displacements. This however was true only for comparison with numerical models as real measurements provided very similar deflections for the crown and the wall. Nonetheless, it is the most accurate method of the ones analysed, with great added visualisation, which comes close to the actual expected results with small relative errors with fractional calculation times and unmatched by all other analysed theories.

However, when the numerical model results are compared to the actual measurement from the site, the results are somewhat inaccurate. While the Mohr-Coulomb model predicts overly large deformations in all considered points and geotechnical sections, the Hoek-Brown model under predicted deformations in better geological conditions, but accurately determined displacements in bad geology. Also, while in both, the analytical and the numerical method, a larger displacement is expected in the crown of the tunnel and smaller displacements in the walls, the opposite is found on the site. The reasons for this unforeseen difference may be numerous, including weaker strength of the rock mass, or more and/or weaker discontinuities within the rock than found by the hydrogeological investigation. Some measurements were even found to be in the critical warning state, proving the hydrogeological investigation was not as accurate, as is the case in many projects. If these results are filtered out results from numerical models resemble those of the measurements. Slight deviations are still present though and require optimisation in order to save costs and construction time. This was achieved through tweaking of input parameters done to a larger extent in the Mohr-Coulomb model. Despite this, the Mohr-Coulomb remains the most reliable material model if insufficient data is given thanks to its highly safe conservative predictions, unlike the sometimes unexpected and dangerous empirical Hoek-Brown material model.

The analyses performed in this report show that somewhat precise results can be achieved through both numerical and analytical solutions, only knowledge of the theories and the range of application has to be known. Another observation from the results is, that in tunnel engineering not all events can be predicted and actual conditions in the tunnel may vastly differ from the expectations. This brings about the need for simplification and hence conservative results are needed. It is for these reasons that the Mohr-Coulomb material model and the Convergence Confinement Method dominate the tunnel design industry mainly in Eastern Europe.

Literature

AASHTO, 2010, *Technical manual for design and construction of road tunnels-civil elements*. English. Washington, D.C. ISBN: 9781560514572.

Afshani, Alireza and Hirokazu Akagi, 2015, "Artificial ground freezing application in shield tunneling". In: *Japanese Geotechnical Society Special Publication* 3, pp. 71–75. DOI: 10.3208/jgssp.v03.j01.

Alejano, Leandro, 2010, "Why the convergence confinement method is not much used in practice". English. In: *Conference: Rock Mechanics in Civil and Environmental Engineering - Proceedings of the European Rock Mechanics Symposium, EUROCK 2010*, pp. 347–350.

Anagnostou G. Serafeimidis, K., 2007, "The dimensioning of tunnel face reinforcement". In: p. 7.

B. Thanh Le, R N. Taylor, 2012, "Binh Thanh Le, R Neil Taylor". In:

Baumann, Th and M. Betzle, 1984, "Investigation of the performance of lattice girders in tunnelling". English. In: 17, pp. 67–81. ISSN: 0723-2632. DOI: 10.1007/BF01042710.

Broska, Igor and Pavel Uher, 1994, "Evolution of the western Carpathian granite magmatism: age, source rock, geotectonic setting and relation to the Variscan structure". English. In: URL: https://www.researchgate.net/publication/280020860_Evolution_of_the_western_Carpathian_granite_magmatism_age_source_rock_geotectonic_setting_and_relation_to_the_Variscan_structure.

Cai, Meifeng, Yang Gengshe, and Jin'an Wang, 2014, *Transit Development in Rock Mechanics*. English. ISBN: 978-1-138-02730-5.

Černá Vydrová, Linda, 2015, "COMPARISON OF TUNNELLING METHODS NATM AND ADECO-RS". In: *Stavební obzor - Civil Engineering Journal* 24. DOI: 10.14311/CEJ.2015.01.0003.

Chen, Dianmin, 1994, "Design of Rock Bolting Systems for Undergorung Excavations". PhD thesis. University of Wollongong.

Dao, Van-Hung and Dao, 2009, "Tunnel design considering stress release effect". English. In: 2, pp. 87–95. ISSN: 1674-2370. DOI: 10.3882/j.issn.1674-2370.2009.03.009.

Date, Kensuke, R J Mair, and K Soga, 2008, "Reinforcing effects of forepoling and facebolts in tunnelling". In:

Dr. Sauer and Partners, n.d. http://projects.dr-sauer.com/taxonomy/term/43. Accessed: 2018-12-04.

Feng, 2016, *Rock Mechanics and Engineering*. English. ISBN: 1-138-02763-4.

G. Thompson, A and Ernesto Villaescusa, 2014, "Case Studies of Rock Reinforcement Components and Systems Testing". In: *Rock Mechanics and Rock Engineering*. DOI: 10.1007/s00603-014-0583-z.

Gschwandtner, Gunter G. Gschwandtner, and Robert Galler, 2012, “Input to the application of the convergence confinement method with time-dependent material behaviour of the support”. English. In: 27, pp. 13–22. ISSN: 0886-7798. DOI: 10.1016/j.tust.2011.06.003.

Hoek, Evert, 2006, *Practical Rock Engineering*. English.

Hoek Evert Diederichs, Mark., 2018, *The 2008 Kersten Lecture Integration of geotechnical and structural design in tunneling*.

Kabai, Imre, 2005, *Geotechnika I.* ID: 91245. Műegyetemi Kiadó.

Karakus, Murat and R Fowell, 2004, “An insight into the New Austrian Tunnelling Method (NATM)”. In: Conference: The 7th Regional Rock Mechanics Symposium, Sivas.

Kim, H. J. et al., 2018, “Performance evaluation of lattice girder and significance of quality control”. English. In: 82, pp. 482–492. ISSN: 0886-7798. DOI: 10.1016/j.tust.2018.08.058.

Kim, Jungjoo et al., 2015, “Structural performance of final lining according to the rock load shape”. In: *KSCE Journal of Civil Engineering* 20. DOI: 10.1007/s12205-015-0308-1.

Kim, Seungjun et al., 2012, “Evaluation of the Structural Performance of Tetragonal Lattice Girders”. In: *International Journal of Steel Structures* 13. DOI: 10.1007/s13296-013-1004-y.

Kirsch, Ansgar, 2009, *On the Face Stability of Shallow Tunnels in Sand*. English. Logos Verlag Berlin GmbH, p. 212. ISBN: 9783832521493.

Komselis C., Blayney N. Hindle D., 2005, “The use of lattice girders in the construction of tunnels”. In:

Krishnan, R., 2000, *Tunnels and Underground Structures: Proceedings Tunnels Underground Structures*. English. Routledge, p. 700. ISBN: 9781351406666.

Maidl, Bernhard, Maidl, and Ulrich Maidl, 2014, *Handbook of Tunnel Engineering II*. English. ISBN: 3-433-03049-9.

Ministerstvo dopravy, výstavby a regionálneho rozvoja SR Sekcia cestnej dopravy a pozemných komunikácií, 2016, *Technicko-Kvalitatívne Podmienky - Geotechnický Monitoring pre Tunely a Prieskumné Štôlne*.

Mousivand, M. Mousivand and M. Maleki, 2018, “Constitutive Models and Determining Methods Effects on Application of Convergence–Confinement Method in Underground Excavation”. English. In: *Geotechnical and geological engineering* 36 no. 3, pp. 1707–1722. DOI: 10.1007/s10706-017-0426-2.

NGI, 2015, *Using the Q-system*. NGI.

Obert, Leonard and Wilbur I. Duvall, 1967, *Rock mechanics and the design of structures in rock*. English, p. 650. ISBN: 0-08-044606-X.

ÖGG, Austrian Society for Geomechanics, 2014, *Geotechnical Monitoring in Conventional Tunnelling*. English.

Oslo-Navet, KVU, 2015, *Tunnelboremaskiner (TBM)*.

Ottosen, Niels and Matti Ristinmaa, 2005, *Mechanics of Constitutive Modeling*. English, <xocs:firstpage xmlns:xocs=""/>. ISBN: 0-08-044606-X. DOI: 10.1016/B978-0-08-044606-6.X5000-0.

Pacher, Franz, 1964, "Deformationsmessungen in Versuchsstollen als Mittel zur Erforschung des Gebirgsverhaltens und zur Bemessung des Ausbaus". German. In: *Grundfragen auf dem Gebiete der Geomechanik / Principles in the Field of Geomechanics: XIV. Kolloquium der Österreichischen Regionalgruppe (i. Gr.) der Internationalen Gesellschaft für Felsmechanik / 14th Symposium of the Austrian Regional Group (i. f.) of the International Society for Rock Mechanics Salzburg, 27. und 28. September 1963*, pp. 149–161. DOI: 10.1007/978-3-662-25703-6_12.

Palmstrom and Broch, 2006, "Use and Misuse of rock mass classification System with particular reference to the Q-system]". In: *Tunnels and Underground Space Technology* 21.10, pp. 575–593.

Panet, M. et al., 2001, "Recommendations on the convergence-confinement method". English. In: *AFTES Report* Version 1.

Pastor, José L. et al., 2016, "Microstructure and durability of fly ash cement grouts for micropiles". English. In: 117, pp. 47–57. ISSN: 0950-0618. DOI: 10.1016/j.conbuildmat.2016.04.154.

Patel R. Patel R., B. Kashiyani and H. Patel, 2013, "A Review on Application of Shotcrete in Tunnel Construction for Better Performance". In: *IJSRD - International Journal for Scientific Research Development* 1.

PLAXIS, 2018, *PLAXIS 2D Material Models Manual 2018*.

Pruška, Jan, 2000, *Podzemní stavby 10*. Czech.

Schweiger, H.F., 1995, *Ein Beitrag zur Anwendung der Finiten-Element-Methode in der Geotechnik*. German.

Sulem, J., M. Panet, and A. Guenot, 1987, "An analytical solution for time-dependent displacements in a circular tunnel". English. In: 24, pp. 155–164. ISSN: 0148-9062. DOI: 10.1016/0148-9062(87)90523-7.

Szechy, K., 1973, *The Art of Tunneling*. English. 2nd Edition. Akadémiai Kiadó.

Tun, S. W. and S. K. Singal, 2016, "Management of Hydropower Tunnels to Prevent Collapse and Remedial Measures". In: *Hydro Nepal*.

Tunneling Online, n.d. https://tunnelingonline.com/graz-leoben-offer-masters-program-natm-engineering/natm/. Accessed: 2018-12-04.

Tunnelling, ITA WG Mechanized, 2000, *Recommendations and Guidelines for Tunnel Boring Machines (TBMs)*.

Tutorial, PLAXIS, 2018, *PLAXIS 2D Tutorial Manual 2018*.

Unlu, T. and H. Gercek, 2003, "Effect of Poisson's ratio on the normalized radial displacements occurring around the face of a circular tunnel". English. In: 18, pp. 547–553. ISSN: 0886-7798. DOI: 10.1016/S0886-7798(03)00086-5.

Vlachopoulos, N. and M. S. Diederichs, 2009, “Improved Longitudinal Displacement Profiles for Convergence Confinement Analysis of Deep Tunnels”. English. In: 42, pp. 131–146. ISSN: 0723-2632. DOI: 10.1007/s00603-009-0176-4.

Vojkan, Jovičić and Šušteršič Jakob, 2008, “Use of Fibrereinforced Shotcrete for Primary Lining in the Dekani Tunnel”. In: *Quark*.

Zhang, Dingli, Qian Fang, and Haicheng Lou, 2014, “Grouting techniques for the unfavorable geological conditions of Xiang’an subsea tunnel in China”. In: *Journal of Rock Mechanics and Geotechnical Engineering* 6. DOI: 10.1016/j.jrmge.2014.07.005.

II Appendix

A. QTS index

Classification of soils and rock masses according to the QTS index is a regional classification method, derived by Tesař in 1977, based on the experiences from the construction of the Prague metro. Hence why it is only a regional classification method. However, it is used throughout Czech republic and Slovakia during classification or rock masses.

The TS points are calculated accordingly, while the number of classification points is lowered based on different criteria.

$$TS = 10 \log \sigma_c + 26.2 \log d + 6.2H \tag{A.1}$$

Where:

σ_c	uni-axial compressive strength of the soil/rock
d	distance between the discontinuities
H	depth of the analysed soil/rock

The final QTS value is calculated from the TS value obtained above, and the reduction caused by the reduction parameters.

$$QTS = TS - \alpha - \beta - \gamma - \delta \tag{A.2}$$

The reduction parameters are:

Parameter	Explanation	Reduction points
α	Due to discontinuities oriented 30°-80° against the driving direction, or 30°-90° with the driving direction	0 - 11.5 TS
β	Due to unfavourable slanted, straight, or smooth joints with clay fill larger than half the tunnel profile	0 - 17.5 TS
γ	Due to groundwater flow without a hydrostatic pressure	0.5 - 4 TS
δ	Due to water ingress and flushing out of smaller particles	2 - 12 TS

Table A.2: Reduction parameters in QTS classification

Technological groups were created and are summarised in the table below, where the TS index runs between 30 and 100.

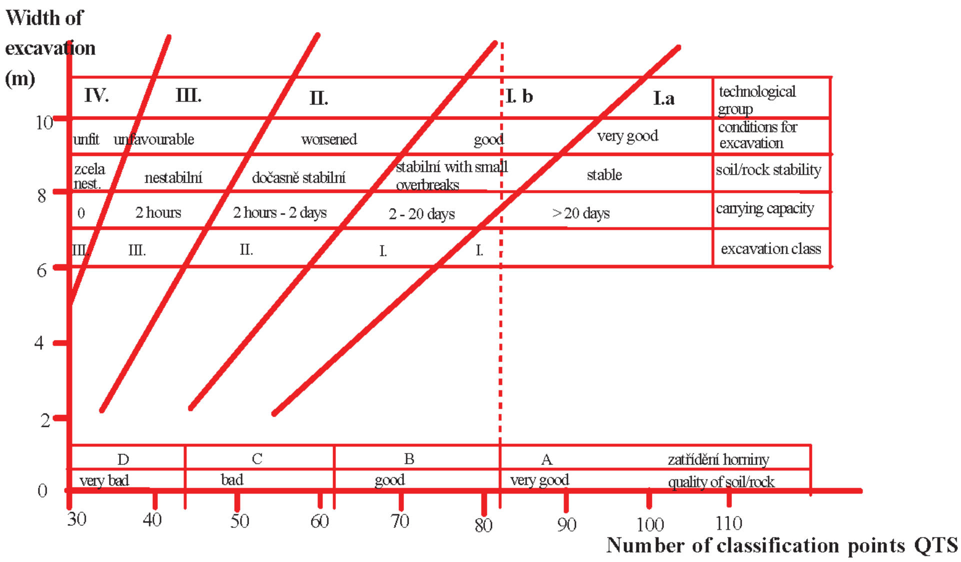

Figure A.1: The classification table for a QTS system

B. Modelling of soils in Plaxis

This appendix describes four material models that are included in the software PLAXIS 3D. In the final design the Hoek-Brown and the Hardening Soil model is used, of which the latter is based on the Mohr-Coulomb and the Modified Cam-Clay model, therefore those are also explained below. The basis is PLAXIS, 2018 and further information about this topic can be found in that document and in Ottosen and Ristinmaa, 2005. But before going into the detailed analysis of the theories mentioned, a general introduction into material modelling is necessary and can be found in the following section.

B.1 Basics of material modelling

Every material model describes a relationship between stresses and strains with the help of mathematical expressions. In the program PLAXIS 3D, all the material models are expressed with infinitesimal increments of stress, i.e. stress rates, $\dot{\sigma}$ and infinitesimal increments of strain, i.e. strain rates, $\dot{\varepsilon}$. Consequently, using the Cartesian coordinate-system (see figure B.1), the effective stress rate tensor is the following:

$$[\dot{\sigma}'] = \begin{bmatrix} \dot{\sigma_x}x' & \dot{\sigma_{xy}}' & \dot{\tau_{xz}}' \\ \dot{\sigma_{yx}}' & \dot{\sigma_y}y' & \dot{\sigma_{yz}}' \\ \dot{\sigma_{zx}}' & \dot{\sigma}'_{zy} & \dot{\sigma}zz' \end{bmatrix} \tag{B.1}$$

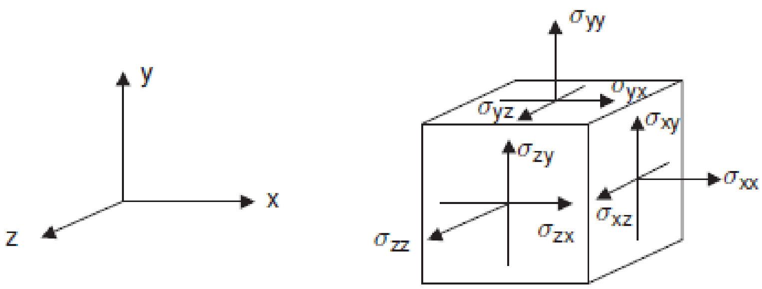

Figure B.1: Representation of the general 3D coordinate system and the sign convention for stress [**Plaxis**]. Note, that in PLAXIS 3D the z direction as the vertical axis.

As the yield criteria are implemented in the principal stress space, as depicted on figure B.2, it is necessary to determine the principal stresses. In this case all the shear components are zero and the principal stresses can be calculated as the eigenvalues of the stress tensor:

$$\det\left([\dot{\sigma}'] - [\dot{\sigma}'][I]\right) = 0 \tag{B.2}$$

Where the $[I]$ represents the identity matrix. The calculated principal stresses are then organised in the following manner:

$$\sigma_1' \leq \sigma_2' \leq \sigma_3' \tag{B.3}$$

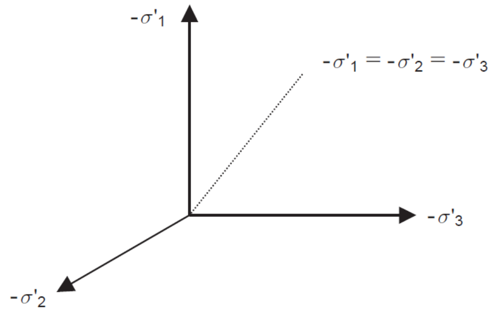

Figure B.2: Representation of the principal stress coordinate system [**Plaxis**]

It is very useful to also have stress invariants which are independent of the orientation of the used coordinate system. Two of the stress invariants is the isotropic or mean effective stress, p' and the equivalent shear stress, q:

$$p' = \frac{1}{3}\left(\sigma'_{xx} + \sigma'_{yy} + \sigma'_{zz}\right) \tag{B.4}$$

$$q = \sqrt{\frac{1}{2}\left(\left(\sigma'_{xx} - \sigma'_{yy}\right)^2 + \left(\sigma'_{yy} - \sigma'_{zz}\right)^2 + \left(\sigma'_{zz} - \sigma'_{xx}\right)^2 + 6\left(\sigma xy^2 + \sigma_{yz}^2 + \sigma_{zx}^2\right)\right)} \tag{B.5}$$

The last equation, i.e. q reduces to $|\sigma'_1 - \sigma'_3|$ for triaxial conditions, namely: $\sigma'_2 = \sigma'_3$. After this the principal stresses are also written based on the stress invariants:

$$\sigma'_1 = p' + \frac{2}{3}q\,\sin\left(\theta - \frac{2}{3}\pi\right) \tag{B.6}$$

$$\sigma'_2 = p' + \frac{2}{3}q\,\sin(\theta) \tag{B.7}$$

$$\sigma'_3 = p' + \frac{2}{3}q\,\sin\left(\theta + \frac{2}{3}\pi\right) \tag{B.8}$$

Where θ is called the Lode's angle and is actually the third stress invariant, and it can be calculated as follows:

$$\theta = \frac{1}{3}\arcsin\left(\frac{27}{2}\frac{J_3}{q^3}\right) \qquad \text{with } J_3 \text{ being:} \tag{B.9}$$

$$J_3 = \left(\sigma'_{xx} - p'\right)\left(\sigma'_{yy} - p'\right)\left(\sigma'_{zz} - p'\right) - \left(\sigma'_{xx} - p'\right)\sigma_{yz}^2 - \left(\sigma'_{yy} - p'\right)\sigma_{zx}^2 - \left(\sigma'_{zz} - p'\right)\sigma_{xy}^2 + 2\sigma_{xy}\sigma_{yz}\sigma_{zx} \tag{B.10}$$

Moving on to the definition of strains, the strain tensor has the same appearance as the stress tensor in equation B.1, however every $\dot{\sigma}'$ is substituted with the strain, ε or the strain rate, $\dot{\varepsilon}$. Since strains are the derivatives of the displacements, u, they are calculated this way:

$$\varepsilon_{ij} = \frac{1}{2}\left(\frac{\partial u_i}{\partial j} + \frac{\partial u_j}{\partial i}\right) \tag{B.11}$$

Where i and j can be x, y or z from the Cartesian coordinate system. The shear strain, γ, is defined as: $\varepsilon_{ij} + \varepsilon_{ji}$. In a similar manner as for the stresses, principal strains $(\varepsilon_1, \varepsilon_2, \varepsilon_3)$ and strain invariants can be determined. The invariants are the volumetric strain, ε_v and the deviatoric strain, ε_q.

$$\varepsilon_v = \varepsilon_{xx} + \varepsilon_{yy} + \varepsilon_{zz} = \varepsilon_1 + \varepsilon_2 + \varepsilon_3 \tag{B.12}$$

$$\varepsilon_q = \sqrt{\frac{2}{9}\left((\varepsilon_{xx} - \varepsilon_{yy})^2 + (\varepsilon_{yy} - \varepsilon_{zz})^2 + (\varepsilon_{zz} - \varepsilon_{xx})^2\right) + \frac{1}{3}\left(\gamma_{xy}^2 ! \gamma_{yz}^2 + \gamma_{zx}^2\right)} \tag{B.13}$$

ε_q can be reduced to $\frac{2}{3}|\varepsilon_1 - \varepsilon_3|$ for triaxial conditions. For elasto-plastic models, the strains have the following form, i.e. they are decomposed to elastic (e) and plastic (p) parts:

$$\{\varepsilon\} = \{\varepsilon^e\} + \{\varepsilon^p\} \tag{B.14}$$

The relationship between stresses and strains is expressed by the constitutive condition, which includes the material stiffness matrix, M.

$$\{\dot{\sigma}'\} = [M]\{\dot{\varepsilon}\} \tag{B.15}$$

The simplest model in PLAXIS is based on Hooke's law and is called Linear Elastic model. This provides the basis of the linear part of the Mohr-Coulomb model, which one is presented in the next section.

B.2 Mohr-Coulomb model

The Mohr-Coulomb model is a simple linear elastic, perfectly plastic model, which can be used in feasibility studies as a first approximation of soil behaviour. The basic idea of this model is depicted on figure B.3. As mentioned before, the linear elastic part of the model is based on Hooke's law, while the perfectly plastic part is based on the Mohr-Coulomb failure criterion. The full name of the model should be therefore linear elastic, perfectly plastic model with Mohr-Coulomb criterion, however, for the sake of simplicity it is referred to Mohr-Coulomb model. When plasticity is mentioned, one should think about irreversible strains developing. To find out whether it occurs or not in a given case, the failure function, f, is introduced, which is a function of stress and strain. When $f = 0$, plastic yielding occurs, and this condition can be drawn in the principal stress space, see figure B.2. This would result in a yield surface, and if stress states result in points that are inside this surface, then the behaviour is purely elastic, no plastic strains occur.

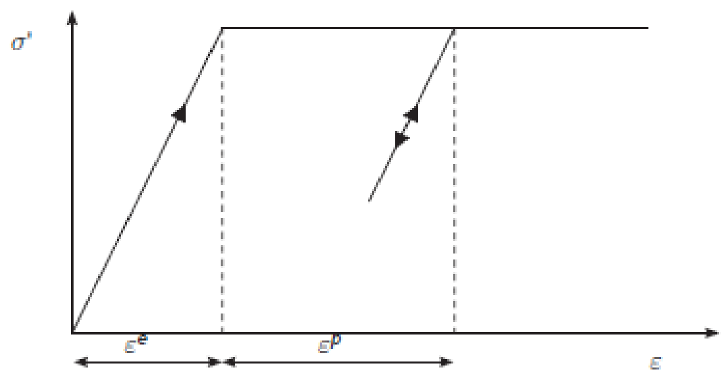

Figure B.3: Representation of an elastic, perfectly plastic material [**Plaxis**].

The basic principle of elasto-plasticity is stated in equation B.14, for what Hooke's law can be applied:

$$\{\dot{\sigma}'\} = [D^e]\{\dot{\varepsilon}^2\} = [D^e](\{\dot{\varepsilon}\} - \{\dot{\varepsilon}^p\} \tag{B.16}$$

Plastic strain rates, $\dot{\varepsilon}^p$, are proportional to the derivative of the yield function with respect to the stresses, i.e. associated plasticity. But for the Mohr-Coulomb yield criterion this would overestimate dilatancy, that is the reason why a plastic potential function, g, is introduced as well. When $f \neq g$ is called non-associated plasticity. With the help of g the plastic strain are written as:

$$\{\dot{\varepsilon}^p\} = \lambda \frac{\partial g}{\partial\{\sigma'\}} \tag{B.17}$$

Where λ is a plastic multiplier and is equal to 0 for purely plastic behaviour, but for plastic behaviour it is either 0 or greater than 0:

$$\lambda = 0 \qquad \text{for:} \qquad f < 0 \qquad \text{or:} \qquad \frac{\partial f^T}{\partial\{\sigma'\}}[D^e]\dot{\varepsilon} \leq 0 \qquad \text{Elasticity} \tag{B.18}$$

$$\lambda > 0 \qquad \text{for:} \qquad f = 0 \qquad \text{and:} \qquad \frac{\partial f^T}{\partial\{\sigma'\}}[D^e]\dot{\varepsilon} > 0 \qquad \text{Plasticity} \tag{B.19}$$

These two equations can be used afterwards to get the relationship between the effective stress rate, $\{\dot{\sigma}'\}$, and strain rates, $\{\dot{\varepsilon}\}$:

$$\{\dot{\sigma}'\} = \left([D^e] - \frac{\alpha}{d}[D^e]\frac{\partial g}{\partial\{\sigma'\}}\frac{\partial f^T}{\partial\{\sigma'\}}\right)\{\dot{\varepsilon}\} \quad \text{with:} \quad d \quad = \frac{\partial f^T}{\partial\{\sigma'\}}[D^e]\frac{\partial g}{\partial\{\sigma'\}} \tag{B.20}$$

The α parameter serves as a switch: it can have a value of 0 or 1, for elastic and plastic behaviour, respectively. In order to be able to apply equation B.17 to a yield criterion with multiple surfaces such as the Mohr-Coulomb model, it needs to be extended:

$$\dot{\varepsilon}^p = \lambda_1 \frac{\partial g_1}{\partial\{\sigma'\}} + \lambda_2 \frac{\partial g_2}{\partial\{\sigma'\}} + \ldots \tag{B.21}$$

To obtain the λ parameters the same number of yield functions, f, is used. The Mohr-Coulomb yield criterion contains of six quasi independent yield functions and it makes sure that Coulomb's friction law is obeyed in any plane within a material element:

$$f_{1,a} = \frac{1}{2}\left(\sigma_2' - \sigma_3'\right) + \frac{1}{2}\left(\sigma_2' + \sigma_3'\right)\sin\phi - c\,\cos\phi \leq 0 \tag{B.22}$$

$$f_{1,b} = \frac{1}{2}\left(\sigma_3' - \sigma_2'\right) + \frac{1}{2}\left(\sigma_3' + \sigma_2'\right)\sin\phi - c\,\cos\phi \leq 0 \tag{B.23}$$

$$f_{2,a} = \frac{1}{2}\left(\sigma_3' - \sigma_1'\right) + \frac{1}{2}\left(\sigma_3' + \sigma_1'\right)\sin\phi - c\,\cos\phi \leq 0 \tag{B.24}$$

$$f_{2,b} = \frac{1}{2}\left(\sigma_1' - \sigma_3'\right) + \frac{1}{2}\left(\sigma_1' + \sigma_3'\right)\sin\phi - c\,\cos\phi \leq 0 \tag{B.25}$$

$$f_{3,a} = \frac{1}{2}\left(\sigma_1' - \sigma_2'\right) + \frac{1}{2}\left(\sigma_1' + \sigma_2'\right)\sin\phi - c\,\cos\phi \leq 0 \tag{B.26}$$

$$f_{3,b} = \frac{1}{2}\left(\sigma_2' - \sigma_1'\right) + \frac{1}{2}\left(\sigma_2' + \sigma_1'\right)\sin\phi - c\,\cos\phi \leq 0 \tag{B.27}$$

In the yield functions the friction angle, ϕ, and the cohesion, c appear as plastic model parameters. All the 6 conditions applied as $f_i = 0$ represent a fixed hexagonal cone in the principal stress space, as shown in figure B.4 below.

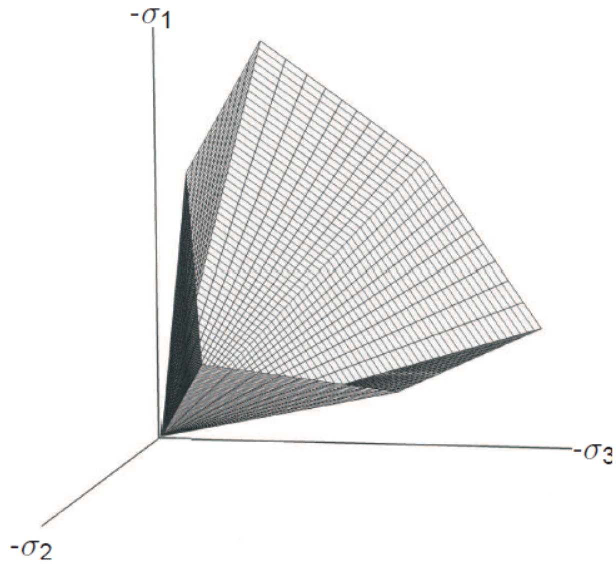

Figure B.4: Representation of the Mohr-Coulomb yield surface with c=0 [**Plaxis**].

There are six from the aforementioned plastic potential functions as well:

$$g_{1,a} = \frac{1}{2}\left(\sigma_2' - \sigma_3'\right) + \frac{1}{2}\left(\sigma_2' + \sigma_3'\right)\sin\psi \tag{B.28}$$

$$g_{1,b} = \frac{1}{2}\left(\sigma_3' - \sigma_2'\right) + \frac{1}{2}\left(\sigma_3' + \sigma_2'\right)\sin\psi \tag{B.29}$$

$$g_{2,a} = \frac{1}{2}\left(\sigma_3' - \sigma_1'\right) + \frac{1}{2}\left(\sigma_3' + \sigma_1'\right)\sin\psi \tag{B.30}$$

$$g_{2,b} = \frac{1}{2}\left(\sigma_1' - \sigma_3'\right) + \frac{1}{2}\left(\sigma_1' + \sigma_3'\right)\sin\psi \tag{B.31}$$

$$g_{3,a} = \frac{1}{2}\left(\sigma_1' - \sigma_2'\right) + \frac{1}{2}\left(\sigma_1' + \sigma_2'\right)\sin\psi \tag{B.32}$$

$$g_{3,b} = \frac{1}{2}\left(\sigma_2' - \sigma_1'\right) + \frac{1}{2}\left(\sigma_2' + \sigma_1'\right)\sin\psi \tag{B.33}$$

The third plasticity parameter is the dilatancy angle, ψ, which is necessary to model positive plastic volumetric strain increments, i.e. dilatancy, similar as observed in reality. For $c > 0$ tension occurs and tensile stresses, σ_t, increase with cohesion. However, in reality soils cannot sustain tensile stresses or only to a very small extent. This is modelled as tension cut-off, i.e. Mohr circles with positive principal stresses are not allowed. This tension cut-off justifies the introduction of another 3 yield function:

$$f_4 = \sigma_1' - \sigma_t \leq 0 \tag{B.34}$$

$$f_5 = \sigma_2' - \sigma_t \leq 0 \tag{B.35}$$

$$f_6 = \sigma_3' - \sigma_t \leq 0 \tag{B.36}$$

The default setting for the allowable tensile stress, σ_t, is 0.

B.2.1 Parameters of the Mohr-Coulomb model

Young's modulus, E

If a triaxial test is implemented, the result from figure B.5 is obtained, which shows 3 E moduli. The initial slope of the stress-strain curve is called E_0, which is a tangent modulus, while the secant modulus is indicated with E_{50} and corresponds to 50% of the strength. For loading of soils, generally the E_{50} is used, but for soils with large linear elastic range can be realistic to use E_0. Moreover, for cases with unloading, the unloading-reloading modulus, E_{ur}, is needed instead of the E_{50}.

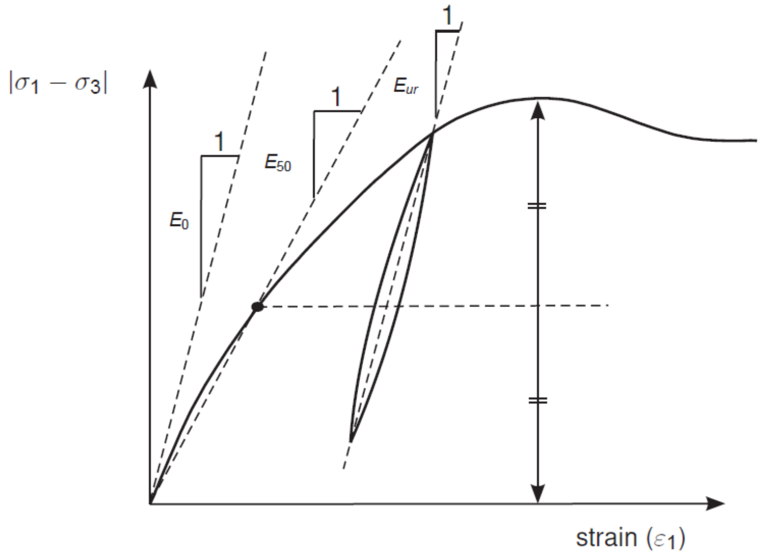

Figure B.5: Definition of the different stiffness moduli for drained triaxial test results. [**Plaxis**]

Instead of Young's modulus two alternative parameters can be specified: the shear modulus, G and the oedometer modulus, E_{oed}:

$$G = \frac{E}{2(1+\nu)} \tag{B.37}$$

$$E_{oed} = \frac{(1-\nu)E}{(1-2\nu)(1+\nu)} \tag{B.38}$$

Poisson's ratio, ν

Standard drained triaxial tests may result in low initial value for the Poisson's ratio, ν_0, which can be for some cases realistic, for example for unloading problems. However, in general higher ν values are recommended to use. For one-dimensional compression it is very simply to choose the Poisson's ratio to give a realistic value of K_0. This means that ν is evaluated by matching K_0:

$$K_0 = \frac{\sigma'_h}{\sigma'_v} \qquad \Longleftrightarrow \qquad \frac{\sigma'_h}{\sigma'_v} = \frac{\nu}{1-\nu} \tag{B.39}$$

Cohesion, c or undrained shear strength, s_u

The cohesion parameter can be used to model the effective cohesion, c' of the soil with the effective friction angle, ϕ'. The cohesion parameter may be used to model the undrained shear strength, s_u with the friction angle being 0, $\phi = \phi_u = 0$. In this case the Mohr-Coulomb criterion reduces to the Tresca criterion, as figure B.6 below shows.

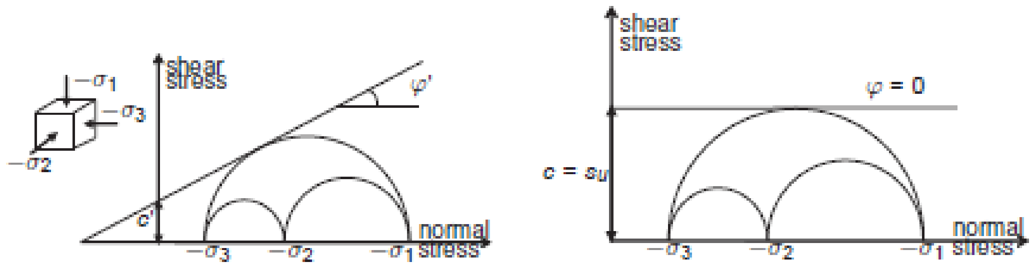

Figure B.6: Left side: Mohr-Coulomb criterion with effective strength parameters. Right side: Tresca criterion with undrained strength parameters. [**Plaxis**]

Cohesionless sands, when $c = 0$ can be modelled on PLAXIS, however, a value of $c > 0.2$ kPa is advised to use as a minimum.

Friction angle, ϕ

In relation to what is stated above, figure B.6 also shows the use of the friction angle of those cases. High friction angles should be avoided in the early state of a project, typical values for sand are in the order of 30-40 degrees, while for clay and silt it is between 20-30 degrees. The friction angle also determines the shear strength, and the Mohr-Coulomb criterion gives a better description of soil strength than the Drucker-Prager criterion.

Dilatancy angle, ψ

In general clay soils usually show little dilatancy, $\psi \approx 0$, apart from heavily overconsolidated layers. For sand, the dilatancy angle depends on both the density and the friction angle. For quartz sands the order of magnitude is $\psi \approx \phi - 30°$. For friction angles of less than 30° however, the ψ is 0 is most cases. No dilatancy cut-off option is available for this model.

Tensile strength, σ_t

By default this is 0, i.e. tension cut-off is used, but it can be changed by the user or allowable tensile strength may be entered.

It is a simple model, as only 6 parameters are required, two elastic and three plasticity parameters and the tensile strength for tension cut-off. However, it neglects important characteristics of the soil behaviour, therefore should only be applied for initial studies.

B.3 Modified Cam-Clay model

In this model a logarithmic relation is assumed between the void ratio, e, and the mean effective stress, p', when looking on the virgin curve on a consolidation curve, as equation B.40 shows. When this equation is plotted with axes e and $\ln p'$ a straight line is obtained. During unloading and reloading a different line can be achieved, which is described by equation B.41. In reality infinite number of lines exist in the $p'-e$ plane and each corresponds to a particular value of the preconsolidation stress, p_p.

$$e - e^0 = -\lambda \ln\left(\frac{p'}{p^0}\right) \qquad \text{(virgin isotropic compression)} \qquad \text{(B.40)}$$

$$e - e^0 = -\kappa \ln\left(\frac{p'}{p^0}\right) \qquad \text{(virgin unloading and reloading)} \qquad \text{(B.41)}$$

Where

λ	Cam-Clay isotropic compression index.
κ	Cam-Clay isotropic swelling index.

λ describes the compressibility of the material in primary loading, while κ does the same but during unloading and reloading. λ corresponds to C_c from the consolidation test and κ is the same as C_r, see the right side of figure B.7. In the Modified Cam-Clay model the yield surface is the following:

$$f = \frac{q^2}{M^2} + p'\left(p' - p_p\right) \qquad \text{(B.42)}$$

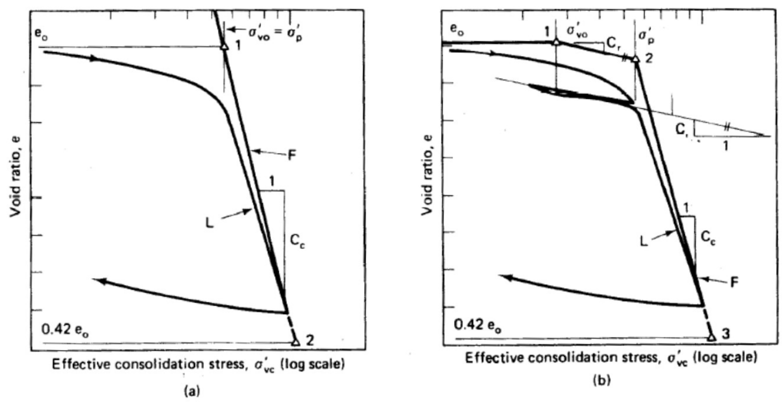

Figure B.7: Compression curves for soil types a) peat, b) sandy clay with 1) loading, 2) reloading [Kabai, 2005]

When the yield surface is considered, which has the formula of $f = 0$, then an ellipse appears in the $p'-q$ plane, as figure B.8 shows. As it is knows the stress surface is a boundary for the elastic stress states, i.e. stress paths inside this boundary result only in elastic strain increments, otherwise both elastic and plastic strain increments are produced.

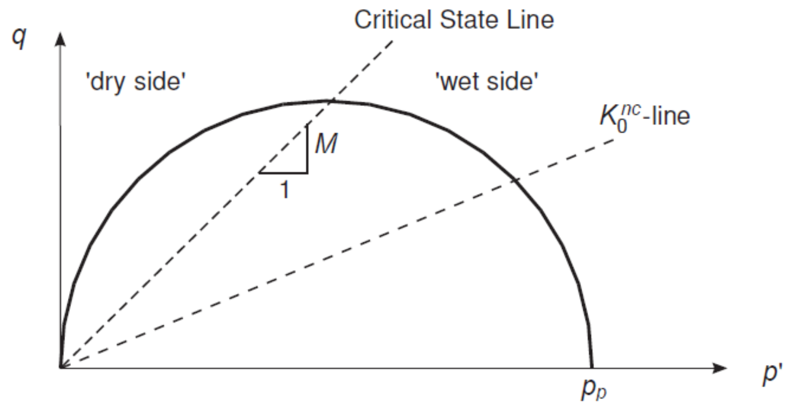

Figure B.8: Representation of a yield surface in the $p' - q$ plane. [**Plaxis**]

The top of the ellipse above intersects the following line in the $p' - q$ plane:

$$q = Mp' \qquad \text{(critical state line, CSL)} \tag{B.43}$$

The critical state line gives the relation between p' and q when failure happens, so this applies to the critical state. The constant M is the tangent of the critical state line, and gives a value for what extent is the q dependent on p'. Therefore M can be considered as a friction constant, moreover, it gives the height of the ellipse. While the preconsolidation stress, p_p specifies the size of the ellipse. As figure B.8 depicts the left side of the CSL is the 'dry side', while the left side is the 'wet side'. The 'dry side' can be thought of as a failure surface, since in this region the plastic yielding is associated with softening, i.e. failure, and the q values in that region can take unrealistic values.

B.3.1 Parameters of the Modified Cam-Clay model

Poisson's ratio, ν_{ur}

This is an elastic parameter, and would usually a value between 0.1 and 0.2.

Cam-Clay swelling index, κ, and Cam-Clay compression index, λ

When a one-dimensional compression test is implemented which includes isotropic unloading, then the logarithm of the mean stress should be plotted against the void ratio, e in order to obtain the two lines fitted to the respective parts of the curve. The slopes of two lines give λ and κ.

Tangent of the critical state line, M

The M should be based on the friction angle, ϕ to make sure to get the correct shear strength. The CSL can be compared to the Drucker-Prager failure line and represents a circular cone. So M can be the following:

$$M = \frac{6\ \sin\phi}{3-\sin\phi} \quad \text{for initial compression stress states} \quad \left(\sigma_1' \leq \sigma_2' = \sigma_3'\right) \tag{B.44}$$

$$M = \frac{6\ \sin\phi}{3+\sin\phi} \quad \text{for triaxial extension stress states} \quad \left(\sigma_1' = \sigma_2' \leq \sigma_3'\right) \tag{B.45}$$

$$M \approx \sqrt{3}\sin\phi \quad \text{for plain strain stress states} \tag{B.46}$$

M also affects the value of the coefficient of the lateral earth pressure, K_0^{nc}, in a state of normal consolidation. When M is chosen so that the correct shear strength is obtained, then the corresponding K_0^{nc} is too high. The exact equation for the relation between M and K_0^{nc} can be found in **Plaxis** in equation (2.44).

Initial void ratio, e_{init}

The void ratio at the initial state, before the test started.

This model allows too high shear stresses and may give softening behaviour for particular stress paths. Even though the model is simple, since only 5 input parameters are needed, the overall conclusion is that the use of this model is not recommended for practical applications.

B.4 Hardening Soil model

The Hardening Soil model is an advanced model, as it takes many characteristics of the soil into consideration:

- It includes both shear and compression hardening. Shear hardening is for modelling irreversible strains due to primary deviatoric loading, while compression hardening is for modelling irreversible plastic strains due to primary compression in oedometer loading. Note, that the yield surface of a hardening plasticity model is not fixed in the principal stress space, but it can expand.
- It can model the behaviour of both soft and stiff soils. The model introduces an m parameter which is meant for defining the stress dependent stiffness. For soft soils it is realistic to use $m = 1$, and for stiff soils $m = 0.5$.
- It is based on the Mohr-Coulomb failure criterion, therefore requires parameters ϕ, c, ψ, and basically combines it with the Modified Cam-Clay model. Therefore, the yield surface keeps its hexagonal shape, but receives a cap, as shown on figure B.9.

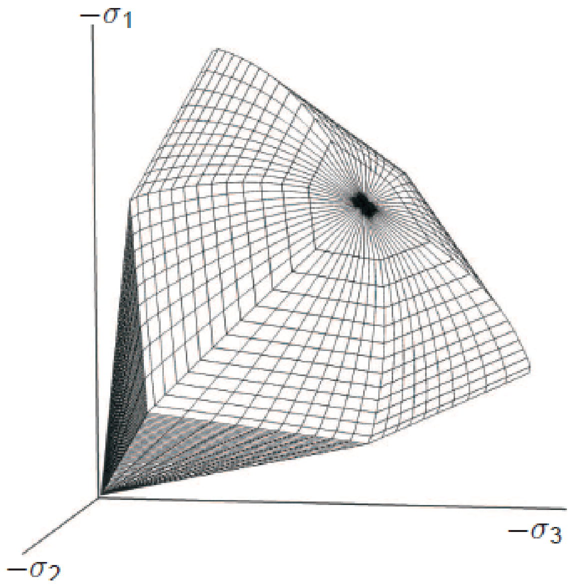

Figure B.9: Representation of the yield surface in the principal stress space. [**Plaxis**]

For the oedometer conditions the following relationship is suggested:

$$E_{oed} = E_{oed}^{ref} \frac{\sigma}{p^{ref}}^{m} \tag{B.47}$$

If soft soils are considered with $m = 1$, a simple relationship exists between the modified compression index, λ^*:

$$E_{oed}^{ref} = \frac{p^{ref}}{\lambda^*} \tag{B.48}$$

$$\lambda^* = \frac{\lambda}{(1+e_0)} \tag{B.49}$$

A tangent oedometer modulus is considered, where p^{ref} is the reference pressure used in the oedometer test. In the calculation of λ^* the Cam-Clay compression index, λ is included. The e_0 In a similar manner there is a relationship between the unloading-reloading modulus, E_{ur} and the modified swelling index, κ^*, which then relates to the Cam-Clay swelling index, κ:

$$E_{ur}^{ref} \approx \frac{2p^{ref}}{\kappa^*} \tag{B.50}$$

$$\kappa^* = \frac{\kappa}{(1+e_0)} \tag{B.51}$$

The basic idea of the Hardening Soil model is to assume a hyperbolic relationship between the vertical strain, ε_1 and the deviatoric stress, q in primary triaxial loading, as figure B.10 shows. For this case the equation of ε_1 is as follows with the included parameters as well:

$$-\varepsilon_1 = \frac{1}{E_i}\frac{q}{1-\dfrac{q}{q_a}} \qquad \text{for:} \quad q < q_f \tag{B.52}$$

$$E_i = \frac{2E_{50}}{2-R_f} \tag{B.53}$$

$$q_f = \left(c\cot\phi - \sigma_3'\right)\frac{2\sin\phi}{1-\sin\phi} \tag{B.54}$$

$$R_f = \frac{q_f}{q_a} \leq 1 \tag{B.55}$$

Where

E_i	Initial stress
q_a	Asymptotic value of the shear strength
q_f	Ultimate deviatoric stress
R_f	Failure ratio, $R_f = 0.9$ as default setting

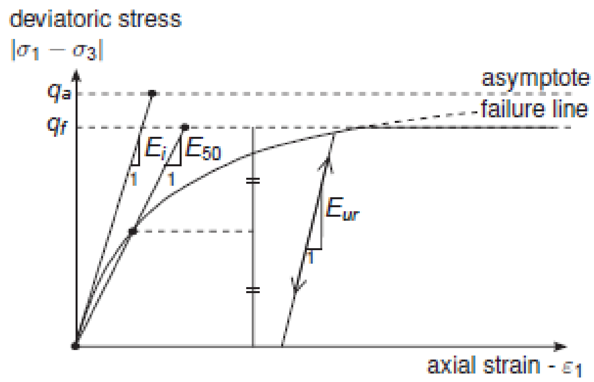

Figure B.10: Hyperbolic stress-strain relation in primary loading for a drained triaxial test. [**Plaxis**]

The yield function is given in the form:

$$f = \bar{f} - \gamma^p \tag{B.56}$$

With $\bar{f}$ being a function of stress and the strain-hardening parameter, γ^p is a function of plastic strains:

$$\bar{f} = \frac{2}{E_i}\frac{q}{1-\dfrac{q}{q_a}} - \frac{2q}{E_{ur}} \tag{B.57}$$

$$\gamma^p = -(\varepsilon_1^p - \varepsilon_v^p) \approx -2\varepsilon_1^p \tag{B.58}$$

Where everything is already defined before, and ε_v^p denotes the plastic volumetric strains. In fact, ε_v^p is relatively small for hard soils, therefore the approximation above. If for a given γ^p value the yield function is made equal to 0, and can be visualised in the $p' - q$ plane with a yield locus, as figure B.11 indicates. Therefore, γ^p is associated with mobilised friction. Because of the used equations (B.57), (B.58), (B.62) and (B.63), the shape of the loculi depends on the parameter, m. That is why for $m = 1$ a straight line is obtained, while for lower values slightly curved lines. Figure B.11 shows an example with m being equal to 0.5, and for increasing γ^p.

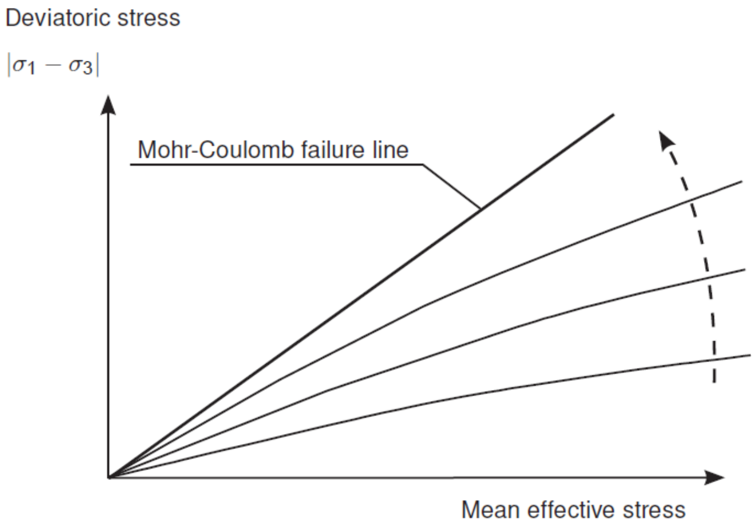

Figure B.11: Successive yield loci for various constant values of the hardening parameter, γ^p. [**Plaxis**]

As illustrated before on figure B.9 the yield surface includes a cap, which closes the elastic region for compressive stress paths, i.e. compression hardening. It has the equation of:

$$f_c = \frac{\tilde{q}^2}{M^2} + (p')^2 - p_p^2 \tag{B.59}$$

Where M is related to K_0^{nc}, p' is defined in equation (B.4) and for general states of stress $\tilde{q}$ can be used instead of q:

$$\tilde{q} = \sigma_1 + (\alpha - 1)\sigma_2 - \sigma_3 \tag{B.60}$$

$$\alpha = \frac{3 + \sin\phi}{3 - \sin\phi} \tag{B.61}$$

The magnitude of the yield cap is given by the preconsolidation stress, p_p. The failure function of the yield cap, $f_c = 0$ appears as an ellipse with its centre being the origin, as figure B.12 shows. So the ellipse has the length of p_p on one axis, and Mp_p on the other axis.

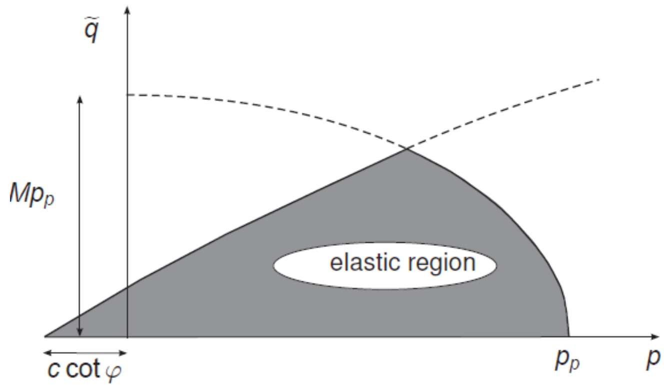

Figure B.12: Representation of the yield surface in the $p-\tilde{q}$ plane. [**Plaxis**]

B.4.1 Failure parameters of the Hardening Soil model

These are the same as for the Mohr-Coulomb model: cohesion, c, friction angle, ϕ, dilatancy angle, ψ and tensile strength, σ_t. These are described in section B.2.1.

B.4.2 Soil stiffness parameters of the Hardening Soil model

These are three different moduli: the secant stiffness from drained triaxial test, E_{50}^{ref}, tangent stiffness from primary oedometer loading, E_{oed}^{ref} and unloading-reloading modulus, E_{ur}^{ref}. Moreover, the m parameter for the stress-level dependency of stiffness. E_{50}^{ref} and E_{ur}^{ref} are depicted on figure B.13, but in Plaxis E_{ur}^{ref} is set as $3E_{50}^{ref}$ by default. The only difference from figure B.5 is that $\sigma_3' = -p^{ref}$.

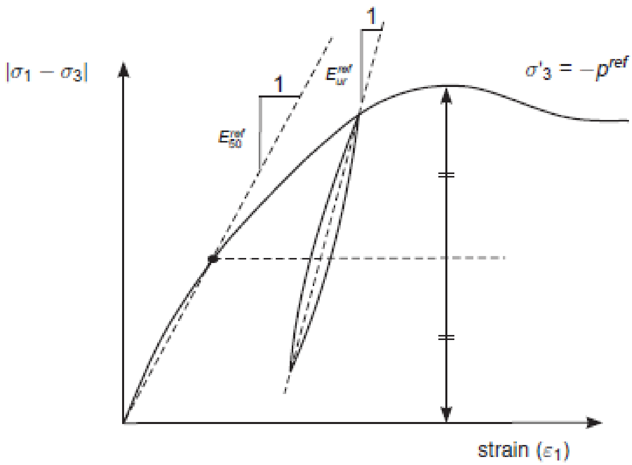

Figure B.13: Definition of the different stiffness moduli for drained triaxial test results. [**Plaxis**]

The stress-dependent stiffnesses are defined as:

$$E_{50} = E_{50}^{ref} \left(\frac{c\ \cos\phi - \sigma_3' \sin\phi}{c\ \cos\phi + p^{ref} \sin\phi} \right)^m \tag{B.62}$$

$$E_{ur} = E_{ur}^{ref} \left(\frac{c\ \cos\phi - \sigma_3' \sin\phi}{c\ \cos\phi + p^{ref} \sin\phi} \right)^m \tag{B.63}$$

$$E_{oed} = E_{oed}^{ref} \left(\frac{c\ \cos\phi - \dfrac{\sigma_3'}{K_0^{nc}} \sin\phi}{c\ \cos\phi + p^{ref} \sin\phi} \right)^m \tag{B.64}$$

B.4.3 Advanced parameters of the Hardening Soil model

Additionally, another 5 parameters can be determined by the user, however, it is advised to use the default settings. For example, p^{ref} is by default 100 kPa, and the K_0 for normal consolidation is $K_0^{nc} = 1 - \sin\phi$.

The Hardening Soil requires 13 parameters, therefore it can describe the soil behaviour under loading and reloading more realistically. It is better than the Mohr-Coulomb model, because in the latter the user has to choose a fixed value of Young's modulus, while in reality that is dependent on the stress level. The Hardening Soil model also includes the possibility of dilatancy cut-off, which considers the fact that after extensive shearing, dilating materials arrive in a state of critical density where dilatancy has to come to an end. However, this model does not account for softening and requires longer computational time, compared to the other models.

B.5 Hoek-Brown model

Material behaviour of rocks differs from that of soils. Mainly it is the fact that the rocks are stiffer and stronger, and that the stiffness of the rock does not depend on the stress levels, which are negligible. Contrarily, the stiffness on the rock depends largely on the shear strength. Therefore, in intact and not jointed rock, the Mohr-Coulomb model may be inefficient. In general, this failure criterion can be expressed as a relationship between the principal stresses as:

$$\sigma_1' = \sigma_3' - |\sigma_{ci}| \left(m_b \frac{-\sigma_3'}{\sigma_{ci}} + s \right)^a \tag{B.65}$$

Where the auxiliary constants s and a, along with the reduced value m_b, of the intact rock parameter m_i, depend on the Geological Strength Index GSI and the Disturbance factor D, are calculated as:

$$
\begin{aligned}
m_b &= m_i e^{\left(\frac{GSI-100}{28-14D}\right)} \\
s &= e^{\left(\frac{GSI-100}{9-3D}\right)} \\
a &= \frac{1}{2} + \frac{1}{6}\left(e^{\left(\frac{GSI}{15}\right)} - e^{\left(\frac{-20}{3}\right)}\right)
\end{aligned} \tag{B.66}
$$

The uni-axial compressive and tensile strength of the specific rock is found using the expressions B.67 below based on the intact rock uni-axial compressive strength, σ_{ci}.

$$
\begin{aligned}
\sigma_c &= |\sigma_{ci}| s^a \\
\sigma_t &= \frac{s|\sigma_{ci}|}{m_b}
\end{aligned} \tag{B.67}
$$

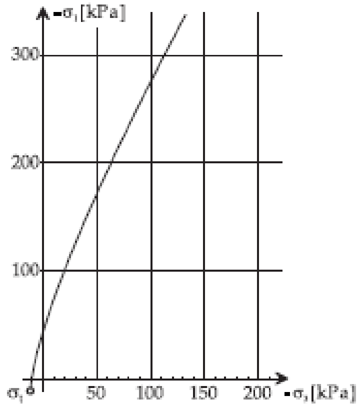

Figure B.14: The Hoek-Brown failure criterion in principal stress axes [**Plaxis**]

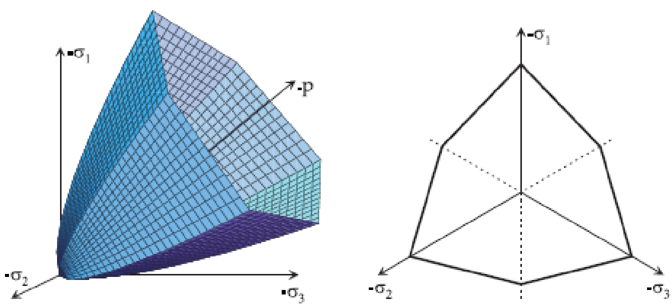

Figure B.15: The Hoek-Brown failure criterion in principal stress space [**Plaxis**]

Much like with the Mohr-Coulomb criterion, more than one equation is needed to express failure, due to the corners of the yield surface. Assuming $\sigma_1' < \sigma_2' < \sigma_3'$ failure criterion can be written as:

$$f_{HB,13} = \sigma_1' - \sigma_3' + \overline{f}(\sigma_3') \qquad where: \qquad \overline{f}(\sigma_3') = |\sigma_{ci}|\Big(m_b \frac{-\sigma_3'}{|\sigma_{ci}|} + s\Big)^a \tag{B.68}$$

$$f_{HB,12} = \sigma_1' - \sigma_2' + \overline{f}(\sigma_2') \qquad where: \qquad \overline{f}(\sigma_2') = |\sigma_{ci}|\Big(m_b \frac{-\sigma_2'}{|\sigma_{ci}|} + s\Big)^a$$

Besides the failure functions, two plastic potential functions.

$$g_{HB,13} = S_1 - \Big(\frac{1+\sin\psi_{mob}}{1-\sin\psi_{mob}}\Big)S_3 \tag{B.69}$$

$$g_{HB,12} = S_1 - \Big(\frac{1+\sin\psi_{mob}}{1-\sin\psi_{mob}}\Big)S_2$$

Where the transformed stresses, S_i are expressed by:

$$S_i = \frac{-\sigma_1}{m_b|\sigma_{ci}|} + \frac{s}{m_b^2} \qquad for \qquad i = 1,2,3 \tag{B.70}$$

B.5.1 Parameters of the Hoek-Brown model

The Hoek-Brown material model consists of 8 parameters. These are more common in mining and geological industries, rather than the geotechnical field. This and the more empirical nature of the model in comparison to the Mohr-Coulomb, create some uncertainties. Therefore it is advised to be used with care and based on extensive individual experience.

Rock Mass Young's Modulus, E_{rm}

Young's modulus is calculated based on the axial compression tests performed on intact rock. This does not realistically represent the in-situ stiffness. Therefore, Hoek-Brown model uses a reduced value E_{rm}. This is calculated as:

$$E_{rm} = E_i\Big(0.02 + \frac{1-D/2}{1+e^{((60+15D-GSI)/11)}}\Big) \tag{B.71}$$

Poisson's Ratio, ν

This is an elastic parameter, and would usually a value between 0.1 and 0.2 for rock masses.

Intact rock parameter, m_i

An empirical model parameter which is derived from the rock type, with general values for different rocks given in a table.

Geological Strength Index, GSI

GSI parameter shows how intact the rock is. In general $GSI = 100$ is the equivalent to intact rock, whereas $GSI = 0$ expresses soil like material.

Disturbance factor, D

Expresses the disturbance of the rock mass due to processes such as blasting or excavation using machinery or a tunnel boring. A disturbance factor of $D = 0$ means no disturbance, where $D = 1$ expresses severe disturbance.

Uni-axial compressive strength of intact rock, σ_{ci}

The uni-axial strength of a rock that is completely intact, or in other words $GSI = 100$ and $D = 0$. Only testing in laboratories, much like for soil materials, determines this value exactly.

Dilatancy, ψ and σ_ψ

Rocks exhibit dilatant behaviour only during shearing with low confining stress. With higher stresses this behaviour diminishes. This is modelled with a specific value for ψ at $\sigma_\psi = 0$ which linearly decreases until $\psi = 0$ at a certain stress expressed by σ_ψ. A representation of this can be seen in figure B.16 below.

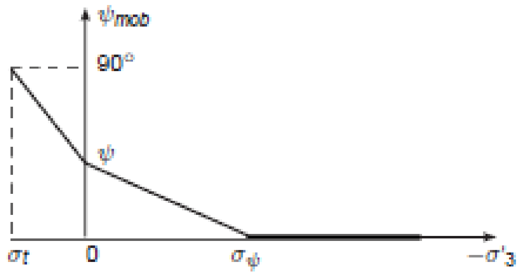

Figure B.16: Development of mobilised dilatancy angle ψ [**Plaxis**]

The relationships shown in figure B.16 above are expressed by the following equations, where the dilatancy is decreasing until 0 at stress equalling σ_ψ, whereas dilatancy is artificially increased in the tensile region to allow plastic expansion.

$$\psi_{mob} = \frac{\sigma_\psi + \sigma'_3}{\sigma_\psi}\psi \qquad for \qquad (0 > \sigma'_3 > \sigma_\psi) \tag{B.72}$$

$$\psi_{mob} = \psi + \frac{\sigma'_3}{\sigma_t}(90^\circ - \psi) \qquad for \qquad (\sigma_t > \sigma'_3 > 0)$$